COMPARISONS BETWEEN CONSTANT PRESSURE MIXING (CPM) AND CONSTANT RATE OF MOMENTUM CHANGE (CRMC) EJECTORS ON PERFORMANCES OF STEAM EJECTOR REFRIGERATION SYSTEMS

BY

BORIRAK KITRATTANA

A DISSERTATION SUBMITTED IN PARTIAL FULFILLMENT OF THE REQUIREMENTS FOR THE DEGREE OF DOCTOR OF PHILOSOPHY (ENGINEERING AND TECHNOLOGY)
SIRINDHORN INTERNATIONAL INSTITUTE OF TECHNOLOGY
THAMMASAT UNIVERSITY
ACADEMIC YEAR 2022

THAMMASAT UNIVERSITY
SIRINDHORN INTERNATIONAL INSTITUTE OF TECHNOLOGY

DISSERTATION

BY

BORIRAK KITRATTANA

ENTITLED

COMPARISONS BETWEEN CONSTANT PRESSURE MIXING (CPM) AND CONSTANT RATE OF MOMENTUM CHANGE (CRMC) EJECTORS ON PERFORMANCES OF STEAM EJECTOR REFRIGERATION SYSTEMS

was approved as partial fulfillment of the requirements for
the degree of Doctor of Philosophy (Engineering and Technology)

on April 26, 2023

Chairperson T. Sriveerakul
(Associate Professor Thanarath Sriveerakul, Ph.D.)

Member and Advisor
(Professor Satha Aphornratana, Ph.D.)

Member
(Assistant Professor Thunyaseth Sethaput, Ph.D.)

Member
(Associate Professor Bundit Limmeechokchai, D.Eng.)

Member Maroay P.
(Maroay Phlernjai, D.Eng.)

Director
(Professor Pruettha Nanakorn, D.Eng.)

Dissertation Title	COMPARISONS BETWEEN CONSTANT PRESSURE MIXING (CPM) AND CONSTANT RATE OF MOMENTUM CHANGE (CRMC) EJECTORS ON PERFORMANCES OF STEAM EJECTOR REFRIGERATION SYSTEMS
Author	Borirak Kitrattana
Degree	Doctor of Philosophy (Engineering and Technology)
Faculty/University	Sirindhorn International Institute of Technology/ Thammasat University
Dissertation Advisor	Professor Satha Aphornratana, Ph.D.
Academic Years	2022

ABSTRACT

An ejector refrigeration system can efficiently convert low grade heat to useful refrigeration. The system is relatively simple compared to other heat-powered refrigeration systems. Its system performance depends mainly on the performance of the ejector used. The most widely used design model of the ejector is the one-dimensional compressible flow theory. In this theory, mixing in the mixing chamber occurs at constant pressure. The major compression effect is created by a normal shock. Ejectors designed based on this model are known as CPM ejectors (constant pressure mixing). However, the shock presents very high thermodynamic losses. To increase efficiency, the constant rate of momentum change (CRMC) design model was purposed by I. W. Eames in 2002, aiming to eliminate the shock wave from the flow process. It was claimed that CRMC ejector provided superior performance over the conventional ejector (CPM ejector). However, there are a limited number of publications associated with performance comparison between these two ejectors and only a few are experimental studies.

According to the design criteria for the CRMC ejector, based on the same input data (designed working conditions), the CRMC ejector provides a smaller ejector throat diameter. This results in producing significantly different ejector area ratios between the two ejectors. It is well known that using ejectors with different area ratios yields a significant difference in ejector performance (trade-off between the mass entrainment ratio (Rm) and the critical condenser pressure (P_{cri}) as supported by many researchers.

With the difference between the two design models, there is a lack of the experimental work to prove the improvement potential of the CRMC ejector compared to the conventional ejector (CPM). The study of Eames in 2002 showed that the CRMC ejector outperforms the CPM ejector. However, such studies were implemented under different experimental units which might not reflect the real improvement potential via the CRMC ejector.

In this dissertation, a CRMC ejector was experimentally investigated and compared with the widely used CPM ejector under the same ejector area ratio. The impact of the boiler temperature, evaporator temperature, and primary nozzle size on the performance of both the CRMC and CPM ejectors were studied. The experimental results revealed that at the same ejector area ratio, the CRMC ejector always produced a higher mass entrainment ratio compared to that of the CPM ejector. However, the critical condenser pressure was still identical. The entrainment ratio of the CRMC ejector was, on average, 18.9% higher than that of the CPM ejector. A compression shock wave was still found in the flow process of the CRMC ejector and observed from the transparent sight of the ejector.

This shows that the improvement potential of the CRMC ejector is not the result of the elimination of the compression shock wave as proposed in the design theory. The key improvement is suggested to be its ability to produce a lower momentum loss during the mixing process. A simulation work based on computational fluid dynamics (CFD) revealed that the compression shock wave was indeed still present in the CRMC ejector and not eliminated from the mixing process of the ejector as suggested by the theory. The mixing processes within the mixing chamber of the two ejectors (CRMC and CPM) were found to be very similar, both experimentally and in the simulation, since the major compression effect was created by a shock wave. The difference between the two ejectors was that the curved profile mixing chamber of the CRMC ejector provided a lower momentum loss and consequently higher mixing chamber efficiency. This is suggested to be the main reason for the superior performances of the CRMC ejectors over those of the conventional CPM ejectors.

Keywords: Ejector, Ejector refrigeration system, Refrigeration system, Heat powered refrigeration system

ACKNOWLEDGEMENTS

I am grateful to many people who have supported me throughout my dissertation journey. First and foremost, I would like to express my deepest appreciation to my dissertation advisor, Prof. Dr. Satha Aphornratana, for his valuable comments, feedback, and unwavering support. His expertise and guidance have been instrumental in shaping this dissertation.

I would also like to extend my gratitude to the members of the dissertation examination committee: Asst. Prof. Dr. Thunyaseth Sethaputand, Assoc. Prof. Dr. Bundit Limmeechokchai, and Dr. Maroay Phlernjai. Their insightful feedback and constructive criticism have been incredibly helpful in improving the quality of this dissertation.

Furthermore, I would like to thank everyone who was involved in the project, particularly Dr. Tongchana Thongtip, Mr. Nikom Meedet, and Mr. Pongpak Lap-Arparat, for their invaluable guidance, support, and contributions. Their dedication and hard work have been critical to the success of this project.

Last but not least, I would like to express my heartfelt appreciation to my parents for their unwavering love, support, and encouragement. Your unconditional support has been a constant source of strength and motivation for me. Thank you for always being there for me.

Borirak Kitrattana

TABLE OF CONTENTS

LIST OF TABLES

LIST OF FIGURES

LIST OF SYMBOLS/ABBREVIATIONS

Symbols/Abbreviations	**Terms**
A	Area (m^2)
AR	Ejector area ratio
CAM	Constant area mixing
COP	Coefficient of Performance
C_p	Specific heat capacity (J/kg·K)
CPM	Constant pressure mixing ejector
$C_{primary}$	Primary fluid expansion coefficient
CRMC	Constant rate of momentum change ejector
D	Diameter (mm)
g	gravitational acceleration (m/s^2)
h	Specific enthalpy (kJ/kg)
k	specific heat ratio
L	Length (m)
M	Mach number
M_o	Momentum (kg·m/s)
$\dot{m}$	Mass flow rate (kg sec^{-1}, kg min^{-1})
η	Efficiency
NXP	Nozzle Exit Position (mm)
P	Absolute pressure (kpa,mbar)
PR	Pressure ratio
$\dot{Q}$	Heat rate (W)
R	gas constant (kJ/kg·K)
ρ	Density (kg/m^3)

Rm	Mass entrainment ratio of an ejector
T	Temperature (°C)
V	Velocity (m/s)
$\dot{w}$	Work rate (W)
x	Distant along x- axis (m)
Z	Elevation (m)

Subscripts

boiler	condition for the boiler
con	condition for the condenser
cri	critical condition
D	diffuser
e	ejector exit
evap	condition for the evaporator
i	condition at the mixing chamber inlet
isen	isentropic process
max	maximum
mix	condition at the ejector mixing
nozz-exit	condition at the primary nozzle exit
nozz-isen	condition when nozzle being operated as the isentropic process
nozzle	condition for the primary nozzle
o	total or stagnation
p	primary fluid condition
pump	condition for the pump
rec	recovery

s	secondary fluid condition
t	condition at the primary nozzle throat
T	condition at the mixing chamber throat
upstream	condition at the upstream of the ejector

CHAPTER 1
INTRODUCTION

1.1 Introduction

Currently, global warming is a major problem of the world. The origin of it is a result of a rapid increase in the average global temperature (due to releasing the greenhouse gases (GHG) emission) which is due to human activities. Hence, reducing GHG emissions is a major objective to relieve the global warming. According to a published work (Bian, 2020), the overall temperature rise was mainly a result of releasing industrial waste heat to the environment. Thus, utilizing waste heat could be the way to solve this problem.

Waste heat is a by-product produced as a result of doing work that uses thermal energy. The waste heat is inevitable according to laws of thermodynamics. Due to the lower temperature of the waste heat compared to the original heat source, waste heat is often released to the environment. However, it is still usable. In a cold climate country, it can be directly used to warm up the building. However, in a hot climate country, Thailand, for example, cooling or air conditioning is needed instead of heating.

Heat powered refrigeration systems can utilize waste heat to produce useful cooling purposes. An absorption refrigeration system is commonly used in this situation. However, the drawback of the absorption refrigeration system is the complexity and cost of the system (installation and maintenance cost). Another alternative heat powered refrigeration system is an ejector refrigeration system or jet refrigeration system. This system is much simpler since it uses only one working fluid, while the absorption refrigeration system needs at least two working fluids (refrigerant and absorbent). Moreover, an ejector refrigeration system is the only refrigeration system that can use only water as a working fluid. Water is the most environmentally friendly and cheapest fluid. Even if the ejector refrigeration system seems to have advantages over the absorption refrigeration systems, the main disadvantage is the system efficiency. The coefficient of performance (COP) of the ejector refrigeration system is generally lower than that of the absorption refrigeration system. This might be the reason which hinders the ejector refrigeration system from being widely used.

With a higher COP, the ejector refrigeration system will be more feasible and might be competitive with the absorption refrigeration system. The COP of the system strongly depends on the efficiency of the ejector used. Many researchers have studied and tried to improve the performance of the ejector. One of the design methods to improve the ejector performance purposed by Eames (2002) is the Constant Rate of Momentum Change (CRMC). This design method provides a variable flow area ejector in contrast with the conventional Constant Pressure Mixing (CPM) design method. The intention of the CRMC design method is to eliminate a normal shock wave that occurs inside the ejector. The shock wave causes the major loss in the flow process. Without the shock wave, the efficiency of the ejector will be higher, which results in a higher system COP.

According to the design criteria for the CRMC ejector (Eames, 2002) and CPM ejector (Eames et al., 1995) based on the same input data (designed working conditions), the CRMC ejector has a smaller ejector throat diameter. This results in producing significantly different ejector area ratios between the two ejectors (ratio of area of ejector throat to area of primary nozzle throat). It is well known that using ejectors with different area ratios yields a significant difference in ejector performance (trade-off between the mass entrainment ratio (Rm) and the critical condenser pressure (P_{cri})) as supported by many researchers (Ariafar et al., 2014; Liu et al., 2017; Yapıcı et al., 2008). The previous study of Eames (2002) on a CRMC steam ejector refrigeration system has shown that at the same working condition, the CRMC ejector provides higher entrainment ratio and the critical condenser pressure. However, the CRMC and CPM ejectors in his study were tested under different ejector area ratios and experimental test units. This may be the cause of the deviation in the results since some of the control variables might not be the same. Moreover, the experimental results were still limited to the specified working conditions.

Previous studies on CRMC ejector confirmed that the CRMC design method could improve performance of the ejector and its refrigeration cycle (Chandra & Ahmed, 2014; Kumar et al., 2013). However, almost all of these studies have experimentally tested and compared the CRMC ejector with the CPM ejector directly (under different ejector area ratios). In the original work of Eames, the tested results of Worall (2001) based on the CRMC ejector were compared with Aphornratana (1995)'s results based on the CPM ejector. The result showed that at the same operating conditions, the CRMC ejector provided higher entrainment ratio and critical condenser pressure. Chandra and Ahmed (2014) experimentally and numerically compared CPM and CRMC ejectors. Their results also showed that the CRMC method could enhance performance of an ejector. They claimed that the enhancement was due to the elimination of shock wave as purposed by Eames (2002). However, there was no evidence that demonstrates the absent of the shock wave via the CRMC method. Moreover, in these two studies, the CPM ejector and the CRMC ejector were compared under different ejector area ratio. This might be inadequate to indicate the improvement potential of the CRMC ejector since it was well known that, the ejector with identical area ratio should perform with the same performances. In order to compare these two ejector design methods, it is more reasonable to compare CPM and CRMC ejectors with the same ejector area ratio. However, there is still a lack of work in this research area.

From all of the reasons mention earlier, this dissertation focuses on an experimental study of the CRMC and the CPM ejectors on steam ejector refrigerator performance. The CRMC and the CPM ejectors were tested and compared with each other on the same experimental testing unit. All of the operating conditions tested on this steam ejector refrigerator were controlled to study the effect of using the CRMC and the CPM ejectors on various operating conditions. The results of the CRMC ejectors were then compared to those of the CPM ejectors with identical ejector area ratio and operating conditions. The aim of this study is to prove that the CRMC ejector can really outperform the CPM ejector given the same controlled environmental variables. Then the results were analysed by means of computational fluid dynamics (CFD). The CFD technique was used as a tool to provide a better understanding of the flow processes of the ejector with the filled contour and quantitative data of the flow. The understanding of the flow process of the CRMC and CPM ejector could help in design and optimization of the ejector.

1.2 Scope of the study

- The CRMC and CPM design methods were used to design the ejectors for using with steam-water.

- The CRMC and the CPM ejectors were tested and compared on the experimental steam ejector refrigerator with various operating conditions
- CFD analysis was used to enhance understanding of the CRMC and the CPM ejectors

1.3 Dissertation organization

This dissertation describes and evaluates comparison studies of CPM and CRMC ejectors' performances experimentally and numerically by mean of Computational Fluid Dynamics (CFD). The literature was evaluated to establish the state of the art, and is described in Chapter 2. Theories and mathematical models for both CPM and CRMC ejectors were developed and are described in Chapter 3. Designs and calculations of the experimental ejectors are provided. The details of developing the experimental steam ejector refrigerator is provided in Chapter 4. In Chapter 5, the experimental results are provided and discussed. To explain and analyse the results in Chapter 5, CFD simulation was used, and the results are provided in Chapter 6. Chapter 7 presents the general conclusion, discussion, and recommendations of future research.

CHAPTER 2
LITERATURE REVIEW AND BACKGROUND THEORY

Ejectors have been used and developed for many applications application such as refrigeration, pumping and evacuation systems. Since this dissertation is mainly focused on performance of CPM and CRMC ejectors in refrigeration systems, the literature review will be mainly focused on refrigeration applications and CRMC ejectors. A brief history and fundamental working principles are also provided in this section.

2.1 The history

Henry Giffard invented the condensing injector in 1858 in order to refill the reservoir of the steam engine boiler. The detail of Giffard's injector invention was provided by Kranakis (1982). Giffard's injector utilized high-pressure steam from the boiler itself as a motive fluid to feed water into the boiler. This had advantages over a mechanical pump since there were no moving parts and no mechanical power was required. The primary nozzle used in Giffard's injector and other designers in that period was the converging nozzle. Giffard's concept was to create a high speed jet of steam which would induce a partial vacuum inside the injector. Liquid water was drawn in to the injector and mixed with the steam. The high-speed mixture of condensed steam and water was then slowed down and pressurized as it was flown through a diverging duct diffuser prior to feeding into the boiler.

Since the primary nozzle used with Geffard's injector was a converging duct type, maximum speed of the jet stream was limited at sonic speed. The vacuum produced was limited. In 1869, a converging-diverging nozzle was first introduced by Schau. This was long before De Laval's experimental supersonic nozzle in 1890. The converging-diverging nozzle could produce a supersonic jet stream and therefore a much lower vacuum could be created compared with a converging type nozzle. In 1901, Sir Charles Persons invented a steam ejector which was used to remove air and non-condensable gases from a condenser of a steam turbine engine. Since then, steam ejectors were widely used to produce vacuum environments in many industrial applications. In 1908, Maurice Leblanc, a French engineer, applied a steam ejector to his first steam ejector refrigeration cycle

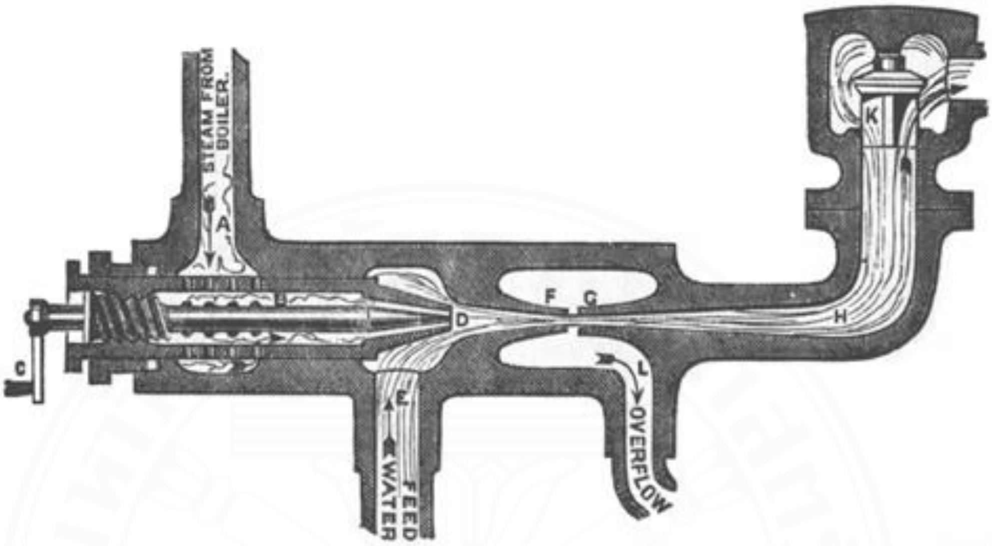

Figure 2.1 Giffard’s injector

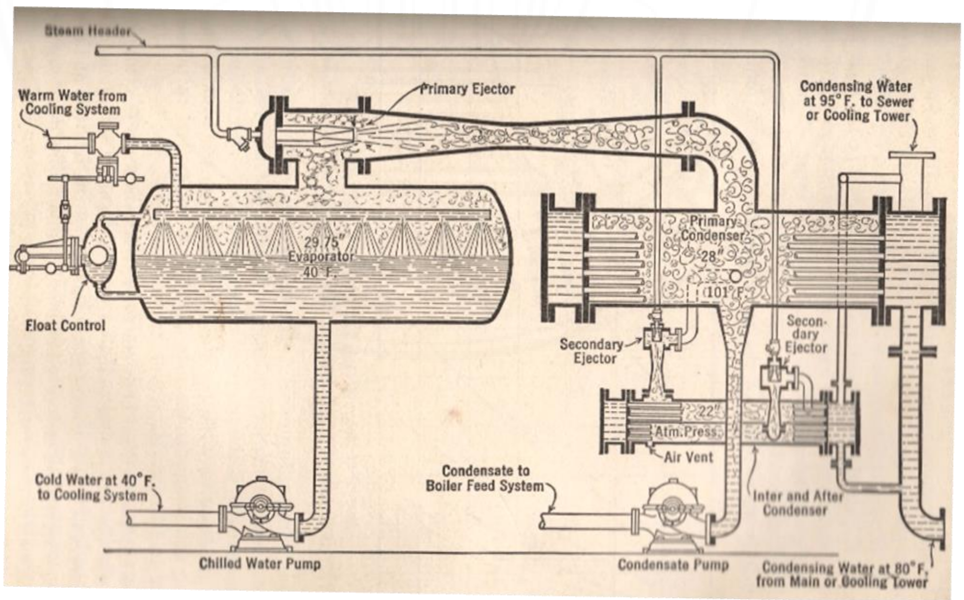

Figure 2.2 Steam ejector refrigeration cycle (Macintire & Hutchinson, 1950)

A steam ejector refrigeration cycle was first commercially available in 1909. At that time, refrigerants used with conventional refrigeration machine were ammonia, sulphur dioxide, methyl chloride, and propane which could result in fatal accidents when they leaked. The only safe refrigerant was water. There was a strong possibility that a steam ejector refrigeration system might find a field of operation in special applications. For example, the system could be used to cool the passenger coaches or in some industries that require chilled water for processing work and have a plentiful supply of medium pressure steam. The steam ejector refrigeration system was also used as an air conditioner for large buildings. These buildings were supplied with steam from district heating plants. The system had the lowest operating cost since the steam consumption is low in summer. The steam ejector refrigeration systems of Maurice Leblanc were first used successfully during the early decades of the 20th century. However, after development of high-speed compressors and new type of refrigerants (CFC refrigerants in 1928), the steam ejector refrigeration systems were supplanted by systems using mechanical compressors.

In the last thirty years, the ejector refrigeration systems have regained popularity and have interested many researchers as can be seen from the number of research publications. This may be the results of the fossil fuel crisis and the emission of greenhouse gases. Ejector refrigeration systems are simpler and easier to operate compared with absorption refrigeration systems, the most widely used heated power refrigeration systems. They can be driven with low grade thermal energy which is normally wasted from industrial processes. Apart from steam-water, organic refrigerants such R245fa, R134a, or R141b can also be used as working fluids. The use of these organic refrigerants allows the ejector refrigeration system to be driven with wasted heat with temperature below 100°C.

2.2 Ejector process and 1-D theories

The first one-dimensional ejector theory was first introduced in 1941 by Flügel (1941). In 1942, Keenan and Neumann (1942) performed a theoretical and experimental study of air ejectors and classified them into two categories according to position of the primary nozzle: Constant-Area Mixing (CAM) and Constant-Pressure Mixing (CPM). For the CAM ejector, the primary nozzle exit plane was located within the ejector constant-area section and the mixing process of the primary and the secondary fluid occurred inside this constant area section as shown in figure 2.3. The position of the primary nozzle exit plane of the CPM ejector was located within the converging entertainment section and the mixing process occurred at constant pressure, and then flowed to the constant area section. According to Keenan et al. (1950), the CPM ejector had better performance than the CAM ejector. Moreover, Keenan also provided the one-dimensional ejector theory which showed good agreement with the experimental results. This theory has been used as the fundamental of ejector analysis since then. However, Keenan's theory could not predict the choking phenomenon of secondary fluid which commonly occurred. To take this phenomenon to account, Munday and Bagster (1977) proposed a theory to describe secondary fluid choking effects. It was assumed that after the secondary fluid was entrained into the mixing chamber, it reached sonic speed and choked at some section, called "an effective area", which is an annulus area formed between the primary fluid jet core and the mixing chamber wall. This area was believed to be constant and independent from the backpressure of the ejector.

Eames et al. (1995) conducted experimental studies of a small-scale steam-jet refrigerator and also introduced a theoretical model. This model introduced adiabatic efficiencies of the primary nozzle, the mixing process, and the diffuser. However, this model did not consider the choking of secondary flow. They suggested that, calculation results from 1-D ejector theory was the performance at the critical operation or when the ejector was operated at the critical condenser pressure.

The idea of effective area and secondary flow choke was reassessed by Huang et al. (1999). They further developed Keenan's model by adding the choke flow of secondary fluid into the process. This model showed a good agreement with the experimental result of the R141b ejector refrigerator.

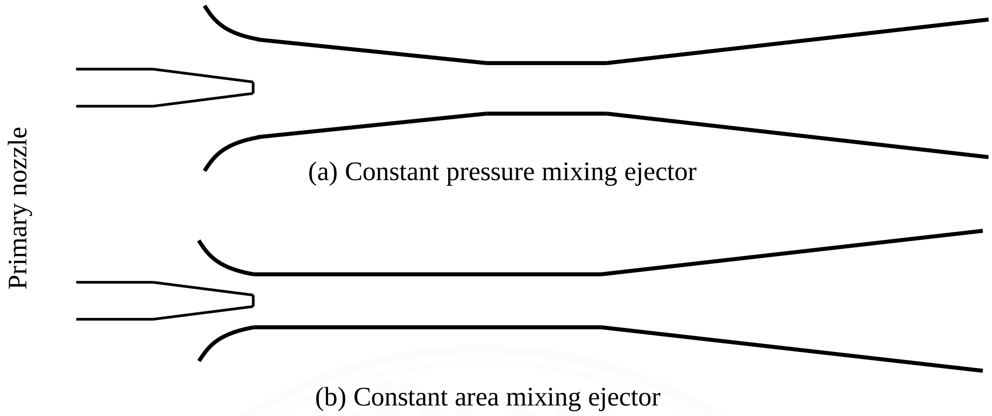

Figure 2.3 Geometries of each type the ejector

Figure 2.4 shows the flows process according to the Munday and Bagster (1977) theory. As a high-pressure fluid (P), known as “a primary fluid”, expands and accelerates through a converging-diverging primary nozzle, it fans out with supersonic speed and creates a very low pressure at the nozzle exit plane (1). A low-pressure vapour, known as “a secondary fluid” (S), is then entrained into the mixing chamber (process S-1). The secondary fluid accelerates, then reaches sonic speed and is choked at some cross section known as “an effective area”. The effective area is an annulus area formed between the primary jet core and the mixing chamber wall. Then the primary and secondary fluids are mixed in the mixing chamber at a constant pressure (process1-2). The mixing process is completed by the end of the throat section (2’). Speed of the mixed fluid is lower than speed of the primary fluid at the exit plane but still higher than sonic speed. The supersonic flow normally experiences shock wave when it flows to high pressure downstream of the ejector. The shock wave is assumed to be a normal shock which causes a sudden drop in the speed from supersonic to subsonic speed and sudden increase in static pressure, static temperature and static density (process 2’-3). Then, the subsonic mixed fluid stream (3) is further compressed as its speed is reduced to almost stagnation state at the diffuser exit plane (process 3-e).

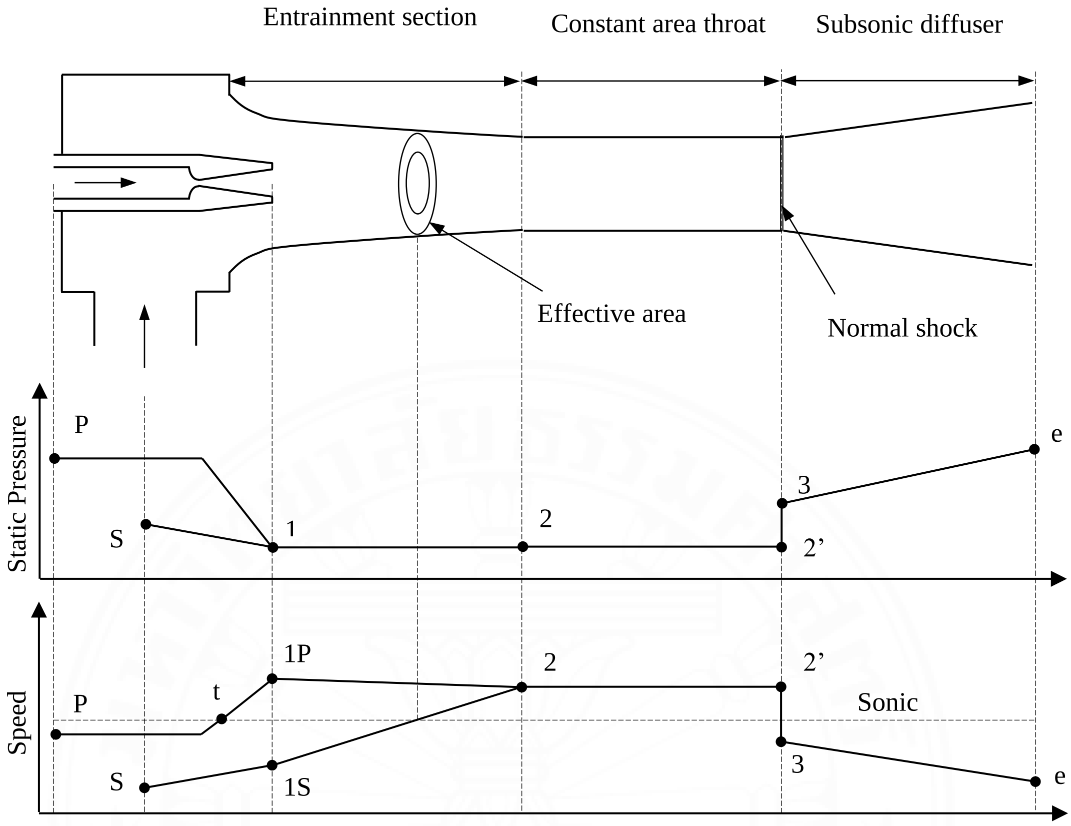

Figure 2.4 Schematic of ejector and plot of pressure and speed along the ejector

The ejector performance is described by “a mass entrainment ratio” which is the ratio between the mass flow rates of secondary fluid to the mass flow rate of primary fluid.

$$\mathrm{Rm} = \frac{\text{mass flow rate of secondary fluid}}{\text{mass flow rate of primary fluid}} \tag{2.1}$$

The mass entrainment ratio of ejector is an important parameter which is strongly related to the coefficient of performance (COP) of the ejector refrigeration system.

2.3 Flow phenomenon of the ejector operation

In previous works (Besagni et al., 2021; Chandra & Ahmed, 2014; Sriveerakul et al., 2007a), it has been demonstrated that the CFD model can be used for predicting flow inside the ejector. Hence, the graphic contour of the relevant parameters obtained from simulations can later be used as a tool to discuss the ejector performance improvement via using the CRMC and CPM ejectors. In this section, the flow phenomenon occurring inside the steam ejector is explained. The purpose is to provide the background of the streams flowing through the ejector. The explanation can be used as the background to understand the flow process. It will further be used to discuss the ejector performance influenced by different working conditions and ejector geometries. The typical contour of Mach numbers which is used for demonstration is shown in figure 2.5.

From figure 2.5, as the primary fluid is expanded and accelerated through the primary nozzle, its speed increases along the converging part of the nozzle until it reaches sonic level at the nozzle's throat. This results in the choke flow of the primary fluid (1) at the nozzle throat. The supersonic flow of the primary stream is achieved as the fluid is further expanded and accelerated through the diverging part of the nozzle. At the nozzle's exit plane, primary fluid fans out with supersonic speed (2) and experiences free boundary pressure within a mixing chamber. This results in the presence of the expansion wave or shock train (3), (Ruangtrakoon et al., 2013; Shigeru et al., 2012; Sriveerakul et al., 2007b). The presence of the expansion wave indicates that the primary flow speed is further accelerated to achieve a higher Mach number. This may be called the shock-expansion wave by some researchers (Ruangtrakoon et al., 2013; Shigeru et al., 2012; Sriveerakul et al., 2007b).

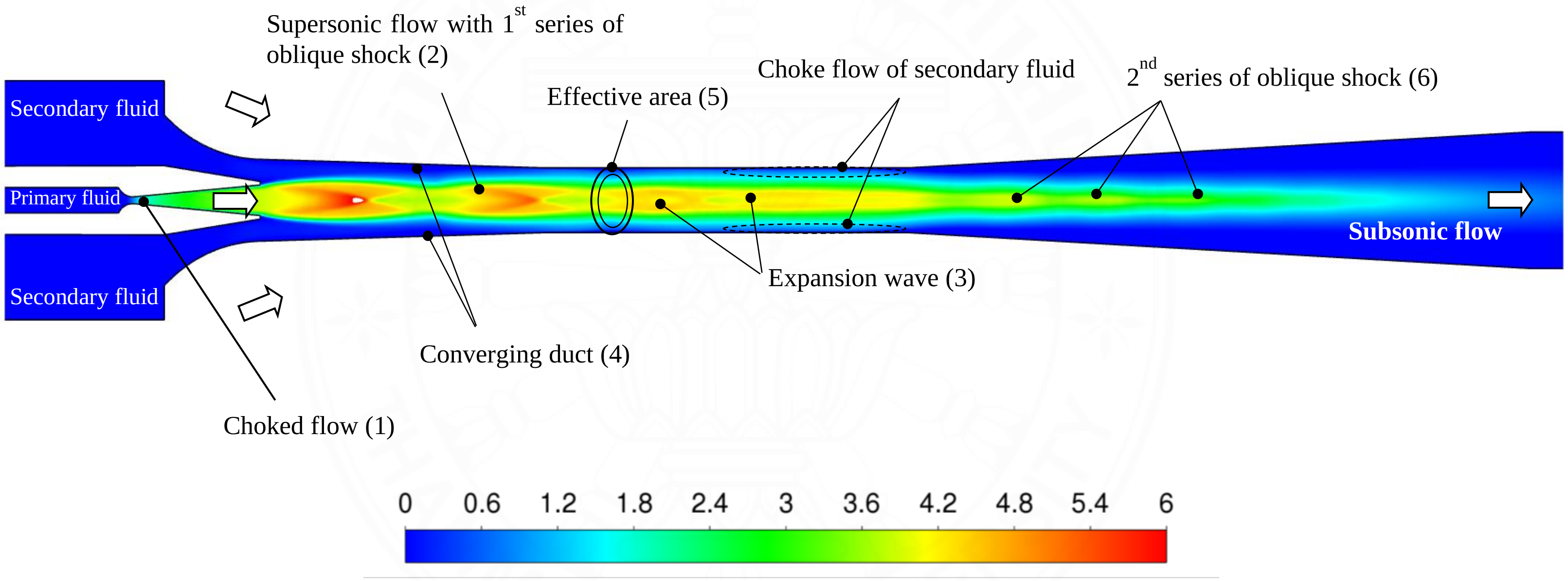

Figure 2.5 The filled contour of Mach number representing the flow inside the steam ejector

Normally, from the ejector operation, there are three types of the expanded states of the expansion wave: under-expanded state, over-expanded state, and perfectly-expanded state as typically shown in figure 2.6. They are classified by "the primary fluid expansion coefficient" (Thongtip & Aphornratana, 2021) which is defined as:

$$C_{primary} = \frac{PR_{upstream}}{PR_{nozz\text{-}isen}} \tag{2.2}$$

Where $PR_{upstream}$ and $PR_{nozzle\text{-}iser}$ are:

$$PR_{upstream} = \frac{P_{boiler}}{P_{evap}} \tag{2.3}$$

$$PR_{nozz\text{-}isen} = \frac{P_{boiler}}{P_{nozz\text{-}exit}} = \left[1+\left(\frac{k\text{-}1}{2}\right)\cdot M^2\right]^{\frac{k}{k\text{-}1}} \tag{2.4}$$

Where P_{boiler} and P_{evap} are the boiler pressure and the evaporator pressure which can be measured directly. However, it is hard to measure the pressure at the primary nozzle exit plane ($P_{nozz\text{-}exit}$). Therefore, Mach number may be used to calculate $PR_{nozz\text{-}isen}$ which can be calculated from:

$$\frac{A_{nozz\text{-}exit}}{A_t} = \frac{1}{M}\left[\left(\frac{2}{k+1}\right)\left(1+\frac{k\text{-}1}{2}\cdot M^2\right)\right]^{\frac{k+1}{2\cdot(k\text{-}1)}} \tag{2.5}$$

Where $\frac{A_{nozz\text{-}exit}}{A_t}$ is the area ratio of the primary nozzle exit to the throat section.

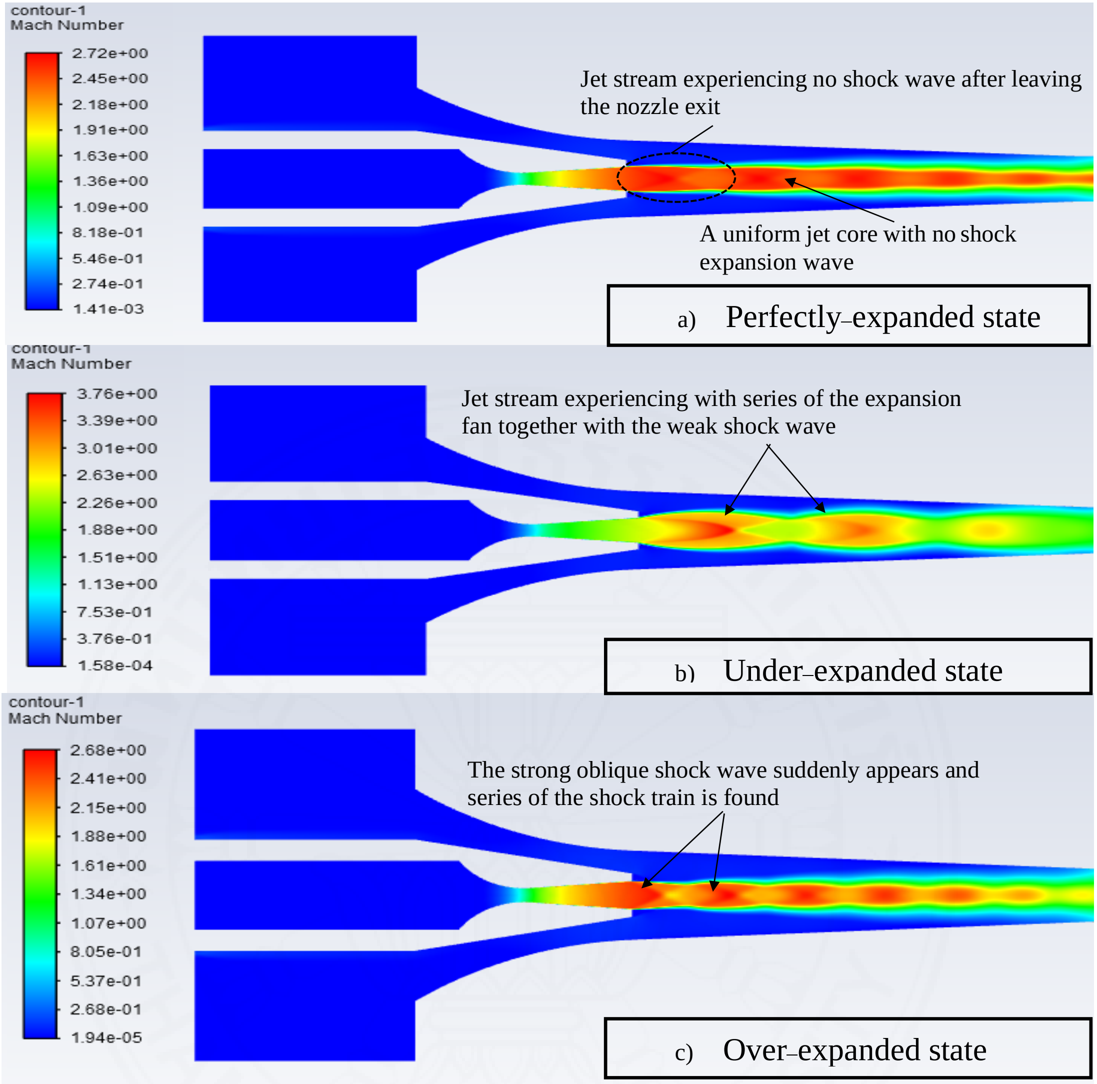

Figure 2.6 The typical expanded state of the expansion wave

It is recommended that the $PR_{upstream}$ for the ejector operation should approximately be equal or close to the $PR_{nozz\text{-}isen}$ or $C_{primary} \approx 1$. This is so that the primary fluid expansion wave experiences no shock train along the jet core as typically shown in figure. 2.6a. Therefore, it provides less impact of shock expansion wave due to the flow being closer to isentropic flow. This results in a lower thermodynamic loss and total momentum loss.

If the $PR_{upstream}$ is higher than the $PR_{nozz\text{-}isen}$ ($C_{primary} > 1$), an under-expanded state of the expansion wave is formed. This formation comes with a series of expansion fans (Ruangtrakoon et al., 2013; Shigeru et al., 2012; Sriveerakul et al., 2007b) which results in further increasing the Mach number combined with the weak oblique shock wave formation as shown in figure 2.6b. For this case, the nozzle exit pressure is higher than the mixing chamber pressure. The impact of the expansion fan and weak oblique shock mitigates the ejector performance due to thermodynamic loss and total momentum loss. Thus, during the entrained process, the secondary stream is disturbed by the expansion fan and shock wave formation. However, there are some advantages for operating the ejector at an under-expanded state. First, it helps to better convey the secondary stream because there is a further increasing of the Mach number of the primary stream after leaving the primary nozzle. This causes greater potential for producing a better shear-mixing process. Second, the supersonic jet core is more stable than that operated with an over-expanded state; therefore, it is flexible for operating the ejector within a wider range of working conditions.

If the $PR_{upstream}$ is lower than the $PR_{nozz\text{-}isen}$ ($C_{primary} < 1$), an over-expanded state of the expansion wave is found. The static pressure at the nozzle exit is lower than the mixing chamber. As a result of producing the over-expanded state, the primary jet core is formed with the series of oblique shock train as shown in figure 2.6c. Since the shock wave cannot be considered as the isentropic process due to the flow separation and boundary layers, a higher thermodynamic loss and total momentum loss of the mixed stream are the result. For operating the ejector in the over-expanded state, variations in the evaporator pressure have a great impact on the shear-mixing process between primary and secondary streams. This is because the jet core is not strong enough to perform its best shear-mixing process. Furthermore, the impact of the shock train may disturb the flow of the secondary stream during the momentum transfer process. If the evaporator saturation temperature is too high, the primary jet stream will not sustain long enough to perform the shear-mixing process and, therefore, the secondary fluid stream cannot reach its choked condition.

As the expansion wave is being formed, the mixing chamber pressure further drops. This causes the secondary fluid to be drawn into the mixing chamber. The secondary flow is accelerated by shear force at the interface of the two streams, due to the large difference in the velocities of the streams. It is obvious that the flow area for the secondary fluid is decreased as it flows through the mixing chamber section. Therefore, the "converging duct" is formed for secondary entrained fluid (4). Along this converging duct, the secondary flow speed is increased until it reaches sonic value, resulting in the choked flow of secondary fluid. The flow area where the secondary fluid is choked is commonly called an "effective area" (5). It is seen that the effective area is the annulus area formed between the expansion wave and mixing chamber's wall and, therefore, its area depends significantly on the expansion state of the primary stream. In such a case, as the over–expanded state is promoted, it yields a larger effective area. A higher amount of the secondary fluid can be entrained and vice versa.

As the secondary flow is being choked, the mixing process of the two fluid streams begins. The location where the mixing process occurs is varied along the ejector's throat, depending on the working condition. During the mixing process, the momentum transfer between the two fluids is implemented. This causes the reduction in primary stream momentum as seen in figure 2.5 at which point the expansion wave gradually disappears. Along the ejector's throat, the mixed stream experiences high downstream discharge pressure. This results in the presence of the second series of oblique shock which is called "2nd shock" (6). The 2nd shock is classified as the compression shock wave whose speed is changed from supersonic to subsonic. Thus, the pressure recovery process is made possible. The location where the 2nd shock takes place is varied, either at the ejector's throat or at beginning of the subsonic diffuser, depending upon the working conditions. Across the series of the oblique shock waves, its flow form gradually changes from supersonic to subsonic. As a result, its static pressure is increased gradually. The pressure recovery process is further achieved as the mixed stream flows through the subsonic diffuser section. The flow process of the two streams is considered to be finished after leaving the subsonic diffuser.

2.4 Ejector refrigeration cycle

Figure 2.7 shows a schematic diagram of an ejector refrigeration cycle. The cycle consists of a condenser, an evaporator, and an expansion valve similar to a vapour compression refrigeration cycle. However, the ejector refrigeration cycle uses an ejector, a boiler, and a circulating pump to elevate pressure of the vapour refrigerant instead of a mechanical compressor.

The boiler receives heat from a high temperature thermal source to generate a high pressure and high temperature refrigerant vapour which is used as the primary fluid for the ejector. The primary fluid then flows to the ejector to create a low-pressure region at the suction port which is connected to the evaporator. This generates low pressure inside the evaporator which allows the fluid to evaporate at low temperature and create a refrigeration effect. The low-pressure vapour refrigerant from the evaporator is drawn into the ejector as the secondary fluid. At the ejector outlet, pressure of the fluid is increased to be higher than evaporator pressure. Then it is condensed to liquid in the condenser by releasing heat to the environment. Part of the liquid refrigerant is pumped back to the boiler by a boiler feed pump and the remainder is returned to the evaporator via a throttling valve.

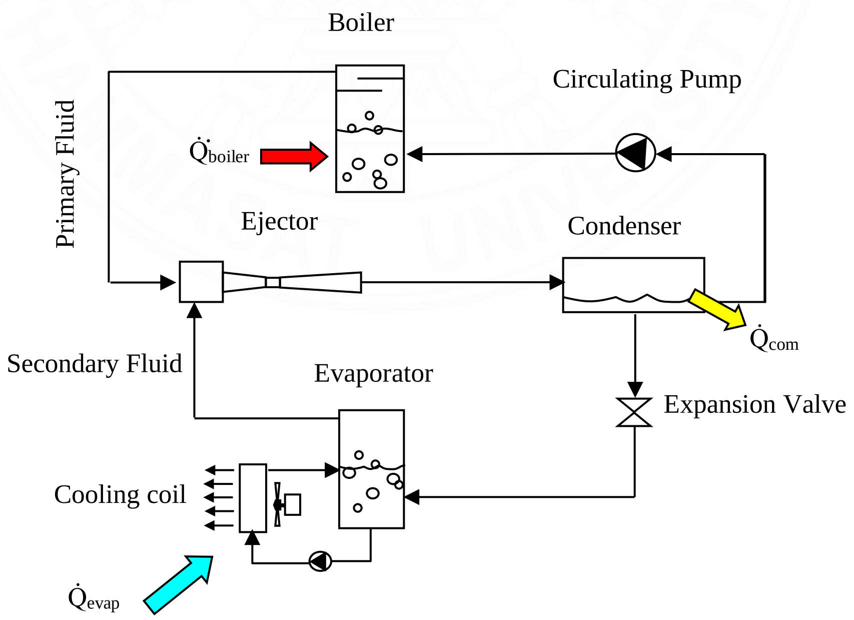

Figure 2.7 Schematic of the ejector refrigeration cycle or jet refrigeration cycle

The ejector refrigeration cycle is powered mainly by thermal energy at the boiler while using a small amount of mechanical work to circulate the refrigerant. Coefficient of performance (COP) of the ejector refrigeration cycle is defined as:

$$COP = \frac{\left|\dot{Q}_{evap}\right|}{\left|\dot{Q}_{boiler}\right| + \left|\dot{W}_{pump}\right|} \tag{2.6}$$

Where $\dot{Q}_{evap}$ is cooling load absorbed by evaporator (kW)

$\dot{Q}_{boiler}$ is thermal energy transfer to boiler (kW)

$\dot{W}_{pump}$ is mechanical work for driving the circulating pump (kW)

Thermal energy transfer to the boiler and cooling load transfer to the evaporator are calculated from:

$$\dot{Q}_{boiler} = \dot{m}_P (h_{g@T_{boiler}} - h_{f@T_{con}}) \tag{2.7}$$

$$\dot{Q}_{evap} = \dot{m}_S (h_{g@T_{evap}} - h_{f@T_{con}}) \tag{2.8}$$

Where $h_{g@T_{boiler}}$ is specific enthalpy of the primary fluid which is equal to enthalpy of saturated vapour at the boiler saturation temperature (kJ/kg)

$h_{g@T_{evap}}$ is specific enthalpy of the secondary fluid which is equal to enthalpy of saturated vapour at the evaporator saturation temperature (kJ/kg)

$h_{f@T_{con}}$ is specific enthalpy of the working fluid at the boiler and evaporator inlets which is equal to enthalpy of saturated liquid at the condenser saturation temperature (kJ/kg)

Normally the mechanical power required for driving the boiler feed pump is relatively low compared to the thermal energy input at the boiler and at the evaporator. Thus, coefficient of performance can be simplified as:

$$COP = Rm \cdot \frac{(h_{g@T_{evap}} - h_{f@T_{con}})}{(h_{g@T_{boiler}} - h_{f@T_{con}})} \tag{2.9}$$

At the operating condition which has low temperature, it can be assumed that the $h_{g@T_{boiler}} \approx h_{g@T_{evap}}$ COP can be assumed as:

$$COP \approx Rm \tag{2.10}$$

2.5 Performance Characteristic of an ejector refrigerator

Performance of the ejector refrigeration system is usually described by a performance curve as shown in figure 2.8. To create the performance curve, the boiler saturation temperature and the evaporator saturation temperature are fixed while the condenser pressure is varied. The mass entrainment ratio is determined with variation of condenser pressure. By doing this, the critical condenser pressure is determined. The critical condenser pressure is the highest possible condenser pressure at which the ejector refrigerator can operate at the desired condition (choked flow of secondary fluid).

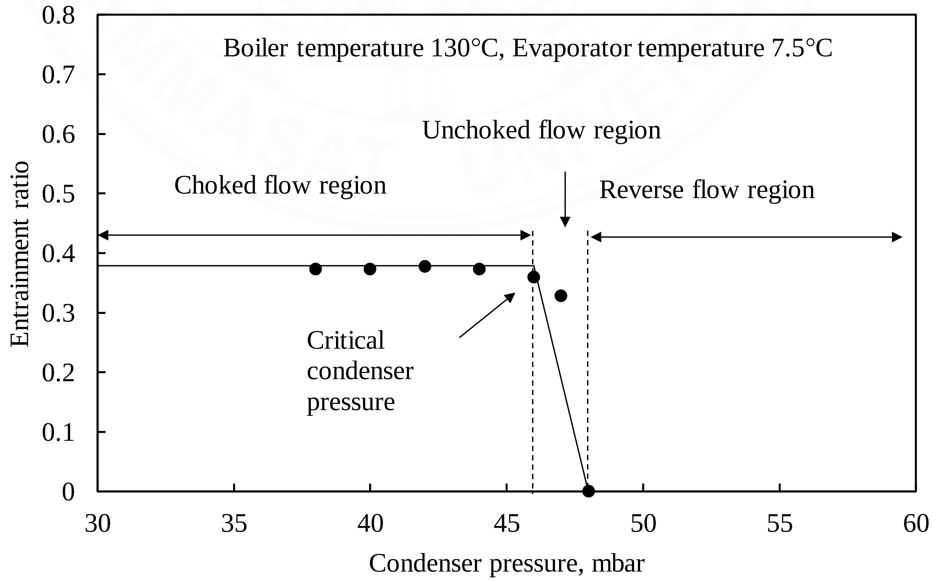

Figure 2.8 Typical performance curve of ejector refrigeration system

The performance curve can be divided into three regions. In the first region, entrainment ration is constant and independent from the condenser pressure. This region is called the *Choked flow region*. The second region is the region in which the entrainment ratio rapidly decreases with increasing of the condenser pressure. This region is called the *Unchoked flow region*. In the final region, the working fluid flows back into secondary fluid port. This region is called the *Reversed flow region*.

In the *Choked flow region,* the entrainment ratio is constant and independent from the variation of the condenser pressure. Since the boiler saturation temperature is fixed throughout the experiment and the primary nozzle is a convergent-divergent type, the primary fluid is accelerated to supersonic speed at the primary nozzle outlet. At the primary nozzle throat, the primary fluid is choked at the sonic speed (M= 1). As a result, mass flow rate of the primary fluid is constant throughout the experiment. The entrainment ratio is constant due to the ejector entraining a constant amount of the secondary fluid. This is because the secondary fluid is choked in the mixing chamber as mentioned in section 2.2.

When the ejector is operated in this region, the shock wave presents either in the constant area throat or the subsonic diffuser for the CPM ejector. The position of the shock wave depends on the condenser pressure. By decreasing the condenser pressure, the shock wave is moved downstream to the ejector outlet and vice versa (Ruangtrakoon et al., 2013). The impact of the shock wave doesn't interfere with the entertainment of secondary fluid which allows the secondary fluid to be choked throughout.

When the condenser pressure is increased to a certain value, the entrainment ratio begins to drop. This condenser pressure is known as "critical condenser pressure" (P_{cri}). If the condenser pressure is further increased beyond this critical value, the entrainment ratio is rapidly decreased. This region is called the *unchoked flow region*. The name "unchoked flow" is due to the secondary fluid no longer being choked in this region. In this region, the condenser pressure is high enough to force the shock wave to move toward the primary nozzle and interfere with the mixing process and entrainment process.

When the condenser pressure is increased to one particular value, the ejector is not be able to entrain secondary fluid and the entrainment ratio is zero. This point is called the *break down point*. If the condenser pressure is further increased, the primary fluid will flow back to evaporator. This operating range is called the *reversed flow region*.

2.6 Effect of operating conditions on ejector performance

Figure 2.9 shows the effect of operating condition on the performance curve. The boiler temperatures are 130°C and 140°C, and the evaporator temperatures are 5°C and 10°C. At constant evaporator temperature of 5°C, increasing the boiler saturation temperature from 130°C to 140°C causes the primary fluid pressure to also increase. This causes a higher primary fluid flow rate. However, the secondary fluid flow is slightly decreased which results in a lower entrainment ratio. With a higher primary flow, the momentum of the mixed fluid is higher which allows the ejector to operate at a higher condenser pressure. As a result, the critical condenser pressure is higher and the entrainment ratio is lower. By doing this, the ejector can operate at a higher condenser pressure but the overall COP of the system is lower.

If the evaporator temperature is increased from 5°C to 10°C while the boiler saturation temperature remains constant at 130°C, the entrainment ratio increases and the ejector can also operate at a higher condenser pressure. Since the boiler temperature is fixed, mass flow rate of the primary fluid is also constant. On the other hand, increasing evaporator temperature results in a higher secondary fluid pressure which is the upstream pressure of the mixing chamber. This not only results in a higher secondary fluid mass flow rate, but also allows the ejector to operate at a higher critical condenser pressure due to the higher momentum of the mixed fluid. Moreover, more cooling load can be absorbed by increasing evaporator temperature. With higher evaporator temperature, it seems to provide better performance. However, higher evaporator temperature, sometimes, may not be desirable since a curtain cooling temperature is required in the refrigeration application.

By changing operating conditions, the performance of the ejector is not improved. It is just a trade-off between entrainment ratio, critical condenser pressure, and the cooling temperature.

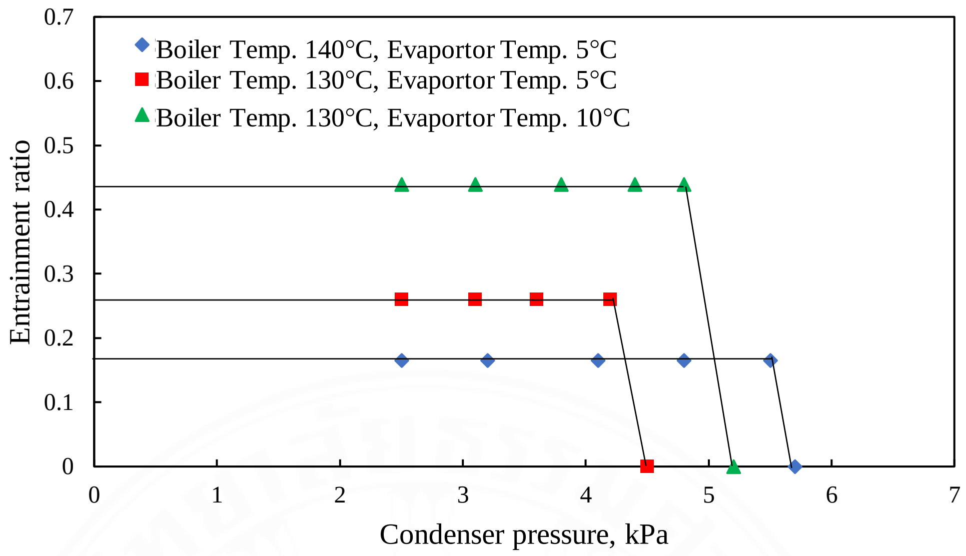

Figure 2.9 Effect of operating condition on system performance

Another way to represent the performance of the ejector is to plot the performance map as shown in figure 2.10. The performance map is plotted for the critical point of operations with various boiler and evaporator temperatures. The figure shows a performance map with boiler temperatures of 130°C, 135°C, and 140°C and evaporator temperatures of 5°C, 7.5°C, and 10°C. The performance map shows the overall performance of the ejector with different operating conditions. This can be used to compare the performance of the ejector. The ejector is considered to be performing better when the map is shifted up or to the right, or both. If the map shifts up, this means the ejector can operate at the same critical condenser pressure but provides higher entrainment ratio at the same operating condition. If the map shifts to the right, the ejector can operate at higher condenser pressure with the same entrainment ratio. If the map shifts up and right, the ejector provides higher both entrainment ratio and critical condenser pressure.

As was seen previously, there is a trade-off between the entrainment ratio and the critical condenser pressure; i.e., as the entrainment ratio increases, the critical condenser pressure decreases. This causes difficulty in comparing ejector performance based on these parameters. For example, ejector A has a higher entrainment ratio but lower critical condenser pressure than ejector B. In this case, it cannot be concluded that one ejector has better performance than the other. Therefore, the ejector efficiency is introduced to indicate the performance of the ejector by taking both entrainment ratio and critical condenser pressure into account. The ejector efficiency is the ratio of expansion work rate recovered by the ejector to the maximum possible expansion work rate recovery potential (Elbel & Hrnjak, 2008) which is described as follows:

$$\eta_{ejector} = \frac{\dot{w}_{rec}}{\dot{w}_{rec\text{-}max}} \tag{2.11}$$

Where $\dot{w}_{rec}$ is expansion work rate recovered by the ejector (W)

$\dot{w}_{rec\text{-}max}$ is the maximum possible expansion work rate recovery potential (W)

From the definition, it can be derived as

$$\eta_{ejector} = Rm \cdot \frac{h_{s\text{-}isen} - h_s}{h_p - h_{p\text{-}isen}} \tag{2.12}$$

Where h_s is the specific enthalpy of the secondary fluid inlet (suction port inlet) (kJ/kg)

$h_{s,isen}$ is the specific enthalpy for an assumed isentropic compression from the secondary fluid inlet to ejector exit (P_s to P_e) (kJ/kg)

h_p is the specific enthalpy of primary fluid at the primary nozzle inlet (kJ/kg)

$h_{p,isen}$ is the specific enthalpy for an assumed isentropic expansion from the primary nozzle inlet to ejector exit (P_p to P_e) (kJ/kg)

For the ejector refrigeration cycle, P_p is the primary fluid or the boiler saturation pressure, P_s is the secondary fluid or the evaporator saturation pressure, and P_e is the ejector exit or the condenser saturation pressure. Therefore, $h_{s.isen}$ depends on the secondary fluid specific entropy and the ejector outlet pressure P_e., and $h_{p.isen}$ depends on the primary fluid specific entropy and the ejector outlet pressure P_e.. Each state is shown in figure 2.11.

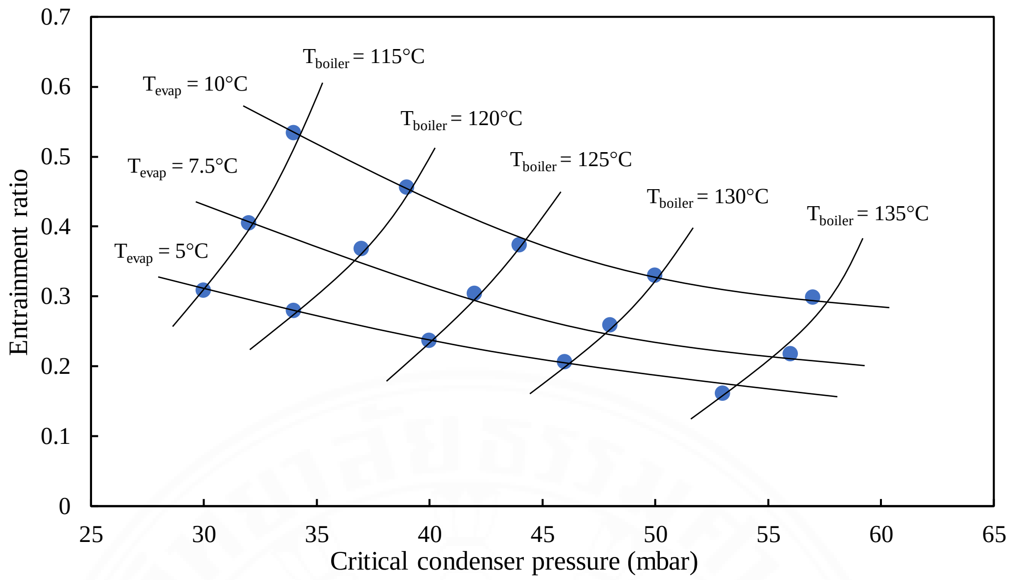

Figure 2.10 Typical performance map of the steam ejector

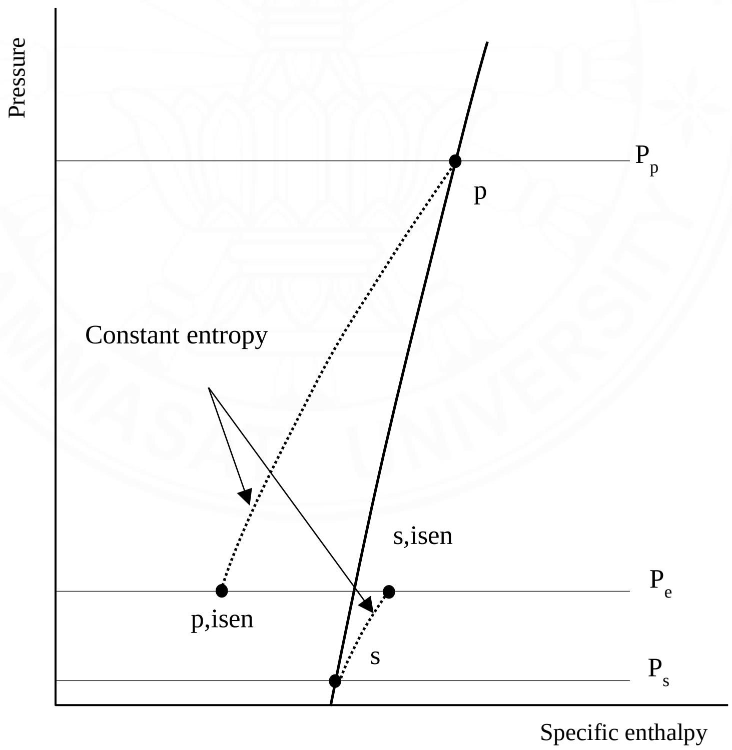

Figure 2.11 The state using for calculate ejector efficiency

2.7 Effect of geometries on ejector performance

In the studies of Keenan et al. (1950), Hoggarth (1970), Eames et al. (1999) and Aphornratana and Eames (1997), it was found that the ejector performance, i.e., entrainment ratio and critical condenser pressure of an ejector can be varied by changing the position of the primary nozzle. Retracting the nozzle into the mixing chamber causes the entrainment ratio to increase at some expense to critical condenser pressure. However, retracting the primary nozzle to curtain point causes the ejector to no longer entrain the secondary fluid. On the other hand, moving the primary nozzle into the mixing chamber causes a lower entrainment ratio and a higher condenser pressure. The optimum position of the primary nozzle exit varies with operating condition and the particular ejector.

Experimental studies of the effect of ejector area ratio were conducted (Ariafar et al., 2014; Liu et al., 2017; Yapıcı et al., 2008). The ejector area ratio is defined as follows:

$$AR_{ejector} = \frac{A_T}{A_t} \tag{2.13}$$

Where $AR_{ejector}$ is area ratio of the ejector
A_T is the cross-sectional area of throat section of the mixing chamber
A_t is the cross-sectional area of throat section of the primary nozzle

The influence of using a high area ratio is similar to that of decreasing the boiler saturation temperature where the entrainment ratio increases and the critical condenser pressure decreases. The higher area ratio can be achieved by increasing the mixing chamber throat diameter or decreasing the primary nozzle throat diameter. The ejector area ratio is an important parameter and previous studies by Eames et al. (1999), Chunnanond and Aphornratana (2004) and Chen et al. (2014) show that at the same ejector area ratio and operating condition, the ejector should perform identically.

The area ratio of the primary nozzle also affects the performance of the ejector. The primary nozzle area ratio is defined as:

$$AR_{nozzle} = \frac{A_{nozz\text{-}exit}}{A_t} \tag{2.14}$$

Where AR_{nozzle} is the area ratio of the primary nozzle

$A_{nozz\text{-}exit}$ is the cross-sectional area of primary nozzle exit

A_t is the cross-sectional area of throat section of the primary nozzle

The primary nozzle area ratio affects the exit Mach number of the nozzle. Higher primary nozzle area ratios cause higher primary nozzle exit Mach numbers. In general, a relatively high Mach number is more desirable, but the nozzle with a higher Mach number is limited by the nozzle's exit diameter and the minimum boiler pressure required (Ruangtrakoon et al., 2011). The primary nozzle with high area ratio (high exit Mach number) requires higher minimum boiler pressure to dive the primary nozzle.

2.8 Constant Rate of Momentum Change ejector (CRMC)

As mentioned earlier, the conventional design of an ejector is the Constant-Pressure Mixing (CPM) ejector as shown in figure 2.3. The main disadvantage of this ejector design is the normal shock process inside the ejector, which produces a major compression effect. Normal shock is highly irreversible and causes a significant loss of stagnation pressure. Eames (2002) purposed a new method to design an ejector with the intention of eliminating the normal shock process inside the ejector. The design method is called the Constant Rate of Moment Change (CRMC) method. As the name suggests, the new design method assumes that the momentum of fluid flow inside the ejector changes at a constant rate along the ejector's mixing chamber and diffuser. The flow profile of the ejector design using this method is gradually changed, which allows the flow to gradually slow down and reach the sonic speed (M=1) at the throat section of the mixing chamber. Figure 2.12 shows the profiler of the CRMC ejector from Eames (2002) study. Shock wave is expected to be absent in the CRMC ejector. Without the shock wave, the high stagnation pressure loss associated with the shock wave is also minimized, which results in the ejector operating at a higher back pressure.

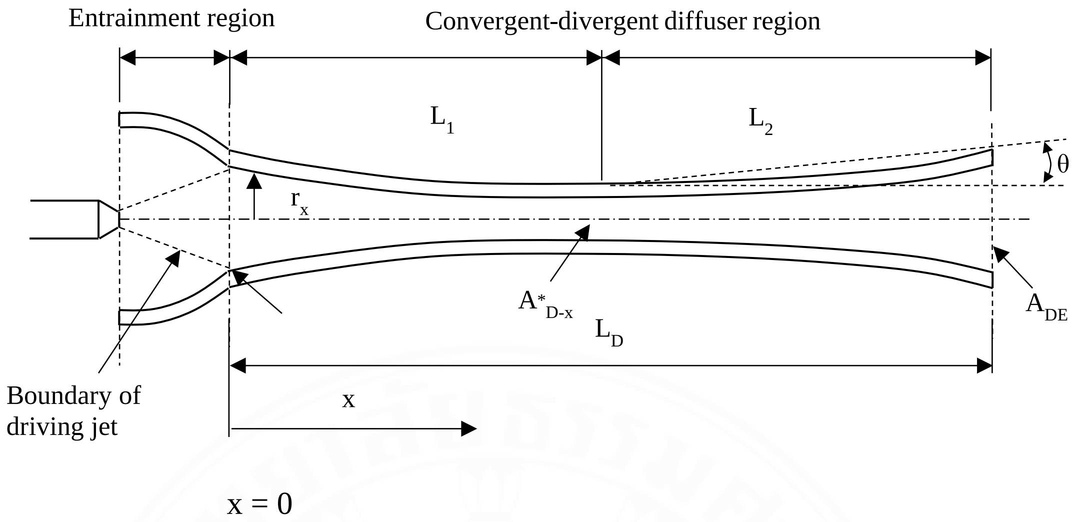

Figure 2.12 The profile of the CRMC ejector by Eames (2002)

In the study of Eames (2002), the CRMC ejector was compared experimentally with the CPM ejector. The result of CRMC ejector from Worall (2001) was compared to the results form Aphornratana (1995). They showed that the CRMC ejector provided both higher entrainment ratio and critical condenser pressure at the same boiler and evaporator saturation temperatures.

Worall (2001) conducted an experiment on a CRMC steam ejector. The results showed variations and fluctuations in entrainment ratio with condenser pressure. There was no constant entrainment ratio in the result as shown in figure 2.13. The author explained that the secondary fluid was not choked as there was no constant entrainment ratio region in the performance curve.

Chandra and Ahmed (2014) conducted experimental work and CFD simulation on CPM and CRMC ejectors working with steam. The CRMC and CPM ejectors from their study were designed using the same input design parameters which provided different mixing chamber throat diameters. The CRMC ejector had a mixing chamber throat of 12.81 mm while that of the CPM ejector was 20 mm. It was found that under the same input data for design, the CRMC ejector had a smaller throat diameter which resulted in a much different ejector area ratio between the two ejectors. Their experimental results showed that the CRMC ejector produced a higher entrainment ratio and critical condenser pressure than the CPM ejector at the same boiler temperature as shown in figure 2.14. The authors claimed that the performance improvement was due to the shock wave being completely eliminated.

Eames et al. (2013) performed an experimental and numerical study of an ejector used for an air conditioning application as shown in figure 2.15. Refrigerant R245fa was used and the ejector was designed using the CRMC method. There were significant differences between the theoretical results produced by the simulation model and those measured experimentally.

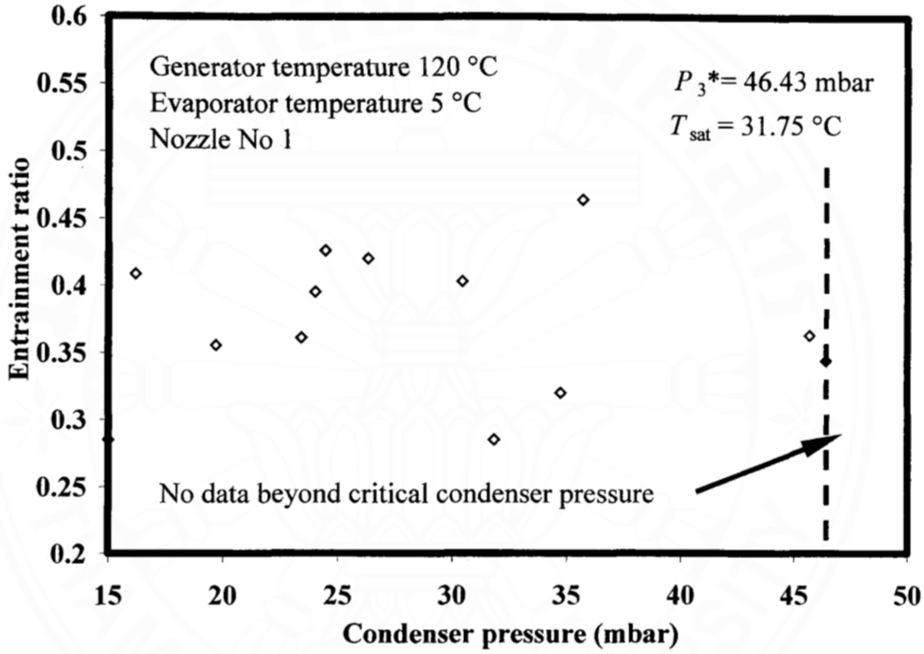

Figure 2.13 Performance of CRMC ejector by Worall (2001)

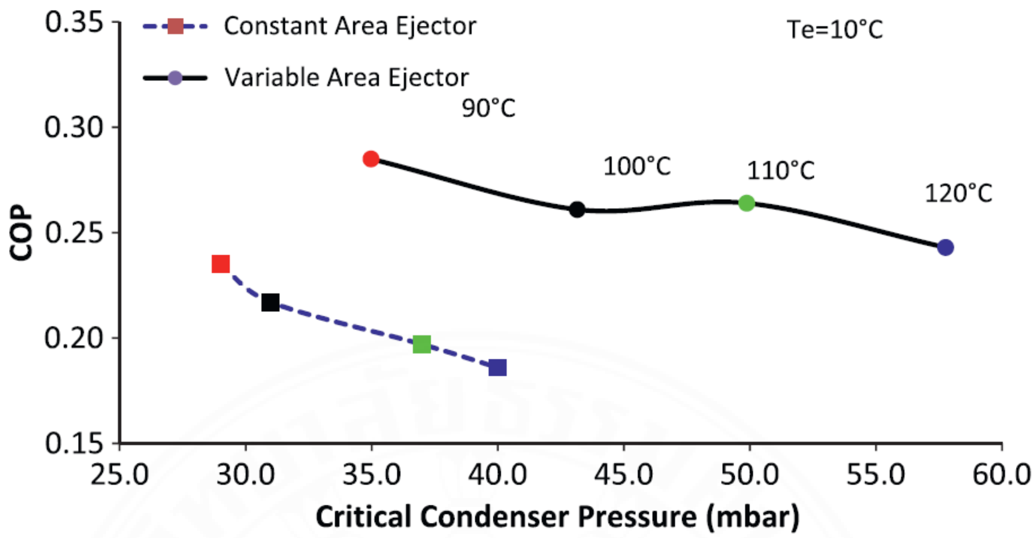

Figure 2.14 Performance comparison of CPM and CRMC ejectors at different boiler temperatures from work of Chandra & Ahmed (2014)

The CRMC design method also used in the study of Milazzo et al. (2014) and Mazzelli and Milazzo (2015). Refrigerant R245fa was used in these studies. In the first study, three CRMC ejectors were designed and tested. The geometries of ejectors used in these studies are shown in figure 2.16. The COPs of the first two ejectors were relatively low. Therefore, the third ejector was designed by using CFD technique to improve the design of the ejector. The third ejector from this study was used again in the study by Mazzelli and Milazzo (2015). The study also included the friction losses inside the ejector to the model. According to this study, such losses had a minor influence on the entrainment ratio in the choked flow region (condenser lower than the critical value), but did have a significant influence on the entrainment ratio at the unchoked flow region (condenser pressure higher than the critical value).

Alsafi (2017) performed an experimental CFD and flow visualization of the air CRMC ejector. The results of the CRMC ejector in this study were compared with the previous experimental result of a CPM ejector. The CRMC achieved higher entrainment ratio and critical back pressure. However, the evidence of shock wave elimination was not found.

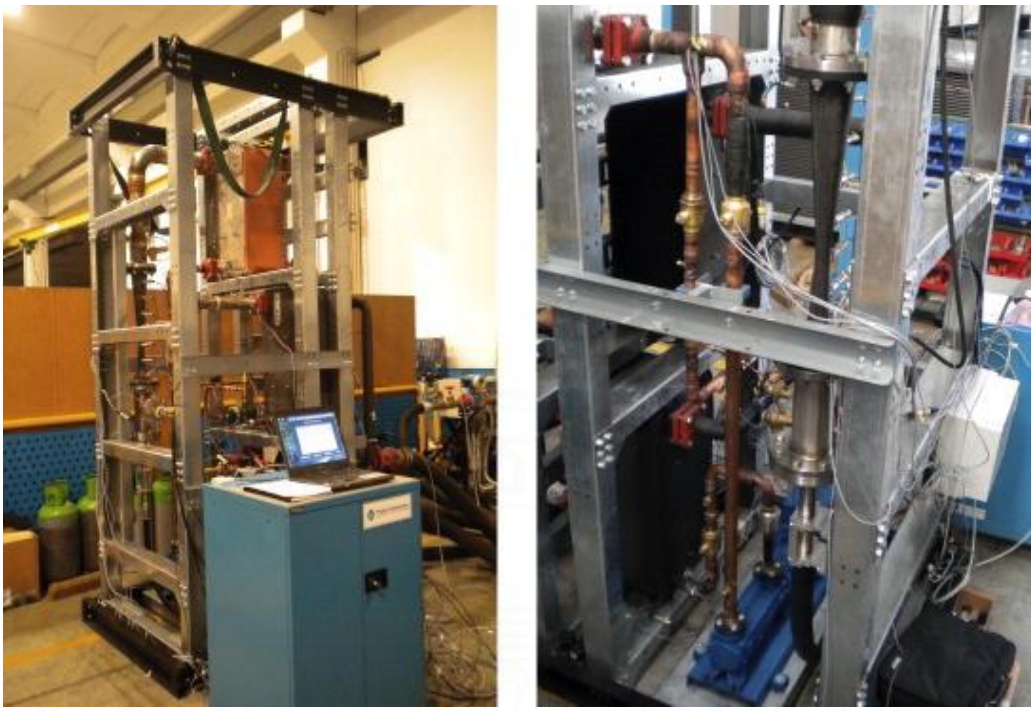

Figure 2.15 A R245fa ejector refrigerator operated as a chiller machine developed Eames et al. (2013)

Bumrungthaichaichan et al. (2022) studied the performance of CRMC and CPM ejectors applied in refrigeration under equivalent ejector geometry by CFD simulation. The study used the CFD technique to analyse the flow process of the CPM and CRMC ejector under the same ejector area ratio and length. The working fluid used was water. The results show that at the same working condition, the CRMC ejector provided higher entrainment ratio than the CPM ejector with almost identical critical condenser pressure. The authors claimed that the flow of mixed fluid after the shock wave inside the CRMC ejector has higher speed which might come from less momentum loss for the flow.

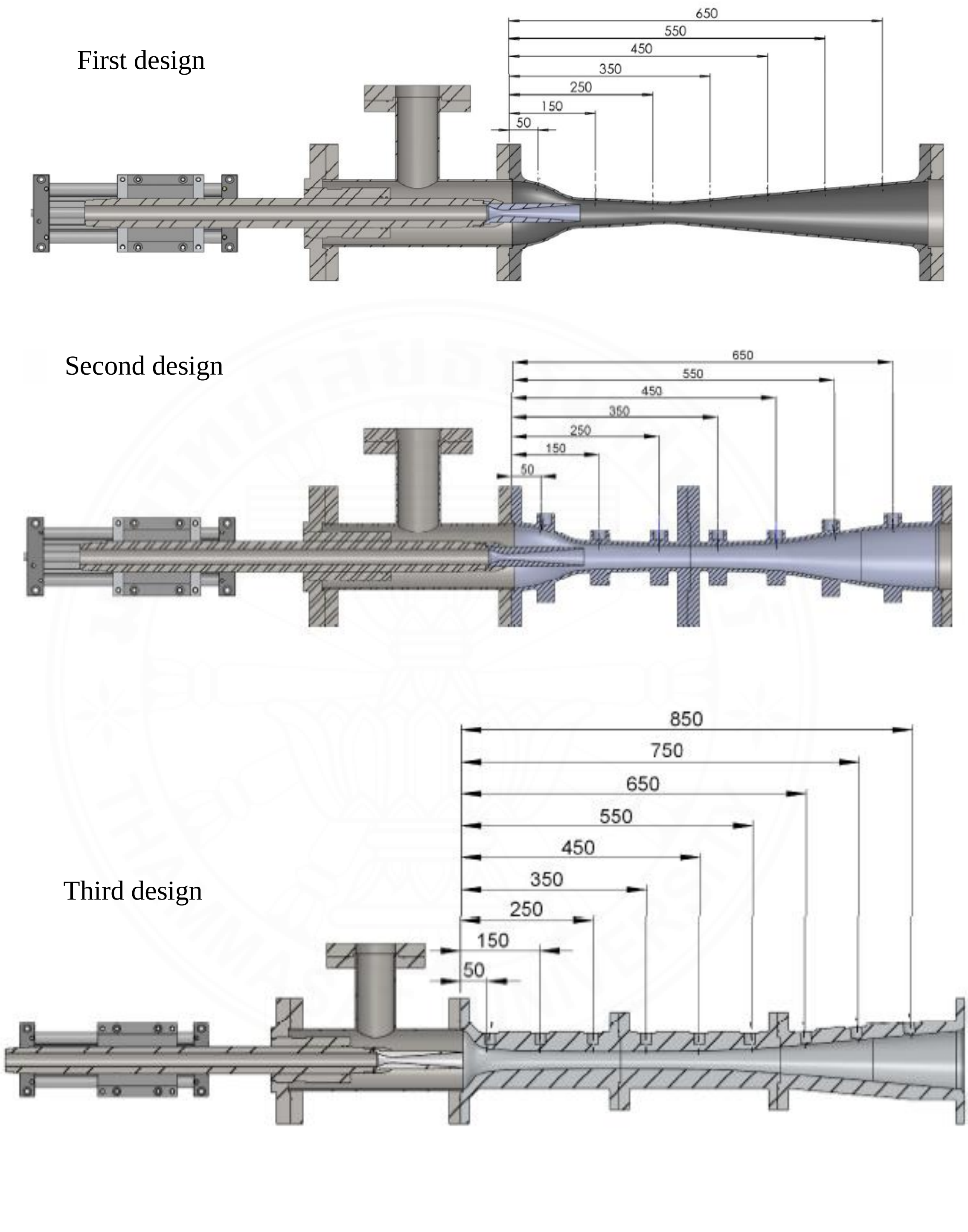

Figure 2.16 Geometry of the ejectors using in Milazzo et al. (2014) study

Theories and past researches on ejector refrigeration cycle were provided in this chapter. There were a handful of literatures which were related to the CRMC ejector.

They showed that the CRMC design method could improve the performance of the ejector. However, only a limited number were conducted experimentally, especially for comparison of CPM and CRMC ejectors. Moreover, in previous studies, comparisons between these two ejector designs were obtained from the ejectors with different area ratios. This may oppose the theory which suggests that the ejector with the same ejector area ratio should have a similar critical performance. Therefore, the CRMC and CPM ejectors should be compared under the same ejector area ratio. Thus, the comparative performance between these two types of ejectors is more comparable and provides a different perspective into the problem of ejector performance improvement.

2.9 Conclusion

This chapter provided the background theory and the literature review of the ejector. The literature review shows that CRMC ejector can be used in ejector refrigeration application and can enhance the performance of the system. However, there is still a lack of experimental data on the CRMC performance improvement over the CPM ejector. Moreover, the explanation of the improvement of CRCM ejector is needed. This led to the study of the comparison of CPM and CRMC in this dissertation to provide more information on the CRMC ejector which can be a useful tool for the improvement of the ejector refrigeration system.

CHAPTER 3
DESIGN OF STEAM EJECTOR

This chapter provides the design theories of the CPM and CRMC ejectors. These theories are used to design the steam ejectors used in this dissertation. Both theories are based on one-dimensional fluid flow. The CPM ejector's theory was first purposed by Keenan et al. (1950). The original Keenan's theory was then modified by many researchers (Aphornratana & Eames, 1997; Huang et al., 1999; Munday & Bagster, 1977). For the CPM ejector, the modified Keenan's theory by Ruangtrakoon and Aphornratana (2019), which included efficiencies at the primary nozzle, the mixing chamber and the diffuser, was used in this dissertation. For the CRMC ejector, the theory by Eames (2002) was used.

In this chapter design methods for both CPM and CRMC ejectors are provided. Example of calculations are also given. The results show that performance of the CRMC ejector is far superior to that of the CPM ejector.

3.1 Development of ejector models

Figure 3.1 shows variation for static pressure and flow speed of the primary and the secondary fluids for both CPM and CRMC ejectors. For both ejectors, the high-pressure primary (P) is expanded through a converging-diverging nozzle to supersonic speed (1). At the nozzle exit (1), a low-pressure region is created. This allows the secondary fluid (S) to be drawn. The primary and the secondary fluids are then mixed together with constant pressure of P_1 in the mixing chamber. The flow is assumed to be completely mixed at (2). From the figure, it can be seen that the mixing processes are assumed to occur at constant pressure for both the CPM and CRMC model ($P_1 = P_2$). This implies that the calculations for both models are identical until the fluids are completely mixed (2). The difference between the CPM and the CRMC occurs downstream after the two fluids are completely mixed as shown in figure 3.1. For the CPM model, a normal shock wave with zero thickness is assumed to be induced in the constant area section causing a sudden increase in static pressure and a rapid drop in speed of the mixed flow (3). The shock wave causes the flow to change from supersonic region (M>1) to subsonic region (M<1). Then the flow is further compressed in the diverging subsonic diffuser to raise it to equal back pressure at the diffuser outlet (e). On the other hand, for the CRMC model, after the two fluids are completely mixed (2), it is assumed that the momentum of the flow is changed at a constant rate which allows the flow to gradually slowdown from supersonic region to subsonic region without the normal shock.

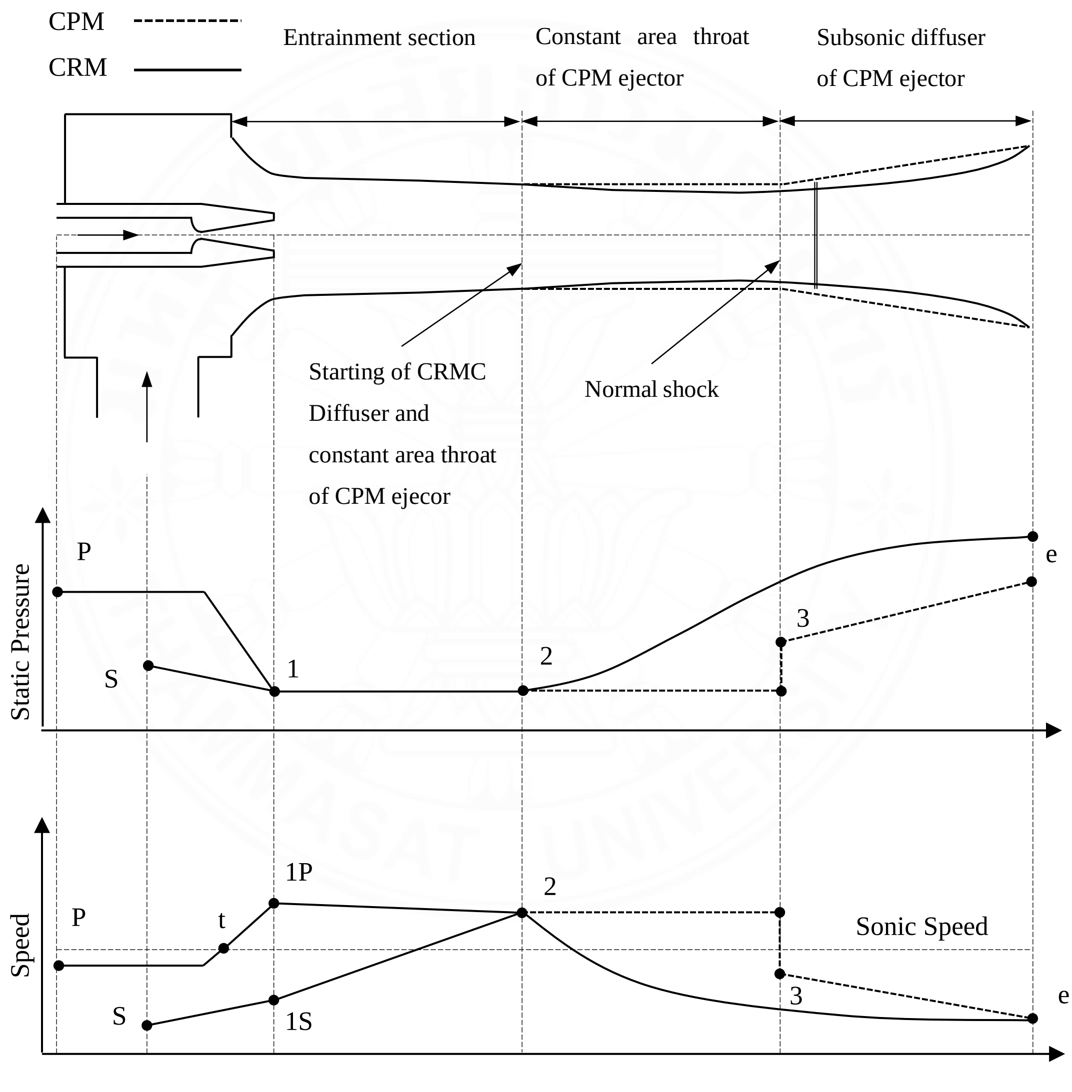

Figure 3.1 Schematic view of CPM and CRMC ejector and pressure-speed variation along the ejector

It can be said that for a CPM ejector, the major compression effect is created by a normal shock which is in contrast to the CRMC ejector of which the compression effect is created by gradually reducing the flow speed of the mixed fluids. The normal shock induced in the CPM ejector is highly irreversible and causes significant loss in stagnation pressure compared with a gradual decrease in flow speed from supersonic to subsonic in the CRMC ejector. If the process in the CRMC ejector is isentropic, the stagnation pressure is preserved. Therefore, it was believed that the CRMC ejector should provide better performance for both the mass entrainment ratio and the critical discharge pressure.

Before the mathematical models for the CPM and the CRMC ejectors can be developed, and for simplicity, the following assumptions are made:

- The fluid is ideal gas.
- Primary and secondary fluids are the same gas.
- The flow is adiabatic.
- The entrainment and mixing process are carried out under constant pressure (P1=P2).
- The mixing pressure is 70% of secondary fluid pressure (P1=0.7Ps).

It must be noted that upstream of section 2 (the section in which the two fluids are assumed to be completely mixed), processes for both CPM ejector and CRMC ejector are identical. The differences between them begin downstream of this section.

3.2 Governing equations for compressible flow of ideal gas

For both models, steam and water vapour are assumed to be ideal gases. Relationships of temperature, pressure and density can be determined from the ideal gas equation:

$$P = \rho \cdot R \cdot T \tag{3.1}$$

Where P is absolute pressure (kPa)

T is absolute temperature (K)

R is gas constant (kJ/kg·K)

ρ is density (kg/m^3)

Energy conservation equation is also applied:

$$\dot{Q} = \dot{W} + \sum \dot{m}_e \left(h_e + \frac{V_e^2}{2} + g \cdot Z_e\right) - \sum \dot{m}_i \left(h_i + \frac{V_i^2}{2} + g \cdot Z_i\right) \tag{3.2}$$

When applying the energy conservation equation to the ejector without change in potential energy, heat transfer to the environment and mechanical work input, the energy conservation equation becomes

$$\sum \dot{m}_e \left(h_e + \frac{V_e^2}{2}\right) = \sum \dot{m}_i \left(h_i + \frac{V_i^2}{2}\right) \tag{3.3}$$

or

$$\sum \dot{m}_e \cdot h_{o-e} = \sum \dot{m}_i \cdot h_{o-i} \tag{3.4}$$

Where h_{o-e} and h_{o-i} are total enthalpy or stagnation enthalpy which is a combination of kinetic energy and enthalpy, therefore

$$h_o = h + \frac{V^2}{2} \tag{3.5}$$

The stagnation temperature and pressure can be obtained from

$$T_o = T + \frac{V^2}{2 \cdot C_p} \tag{3.6}$$

$$\frac{P_o}{P} = \left[\frac{T_o}{T}\right]^{\frac{k}{k-1}} \tag{3.7}$$

Where T_o is total temperature or stagnation temperature of the fluid (K)

T is static temperature of the fluid (K)

$\frac{V^2}{2 \cdot C_p}$ is dynamic temperature of the fluid (K)

P_o is total pressure or stagnation pressure of the fluid (kPa)

P is static pressure of the fluid (kPa)

Another parameter that is widely used in ideal gas analysis is the Mach number which is a ratio between fluid speed and sonic speed of the fluid:

$$M = \frac{V}{V_{sound}} = \frac{V}{\sqrt{k \cdot R \cdot T}} \tag{3.8}$$

Where V_{sound} is velocity of sound or sonic velocity (m/s)

All of these governing equations are used as fundamental equations for calculating properties of each stage throughout the flow process.

3.3 Ejector performance calculation

This method was first proposed by Keenan et al. (1950). Recently, this theory was modified by Ruangtrakoon and Aphornratana (2019) to make it easier to understand and use. These modifications are also applied to Eames (2002) CRMC theory. To calculate performance of the ejector, all the governing equations mentioned previously are applied. Isentropic efficiencies of the primary nozzle, mixing chamber, and subsonic diffuser are included. As mentioned earlier, the processes in the primary nozzle, entrainment, and mixing process are identical for both models. Thus, both models use the same calculation procedure until the mixing process (2). Then the calculations are different for each model.

3.3.1 Primary nozzle

The primary nozzle used is a converging-diverging or De-Laval type supersonic nozzle. The hot and high-pressure steam accelerates from a stagnation stage to supersonic speed at the outlet of the nozzle. Figure 3.2 shows a schematic and speed diagram of the primary nozzle.

Primary fluid (P) with high pressure, high temperature, and low speed or in stagnation stage is accelerated and expanded in the convergent section until it reaches sonic speed $(M_t = 1)$ at the throat which also causes static temperature and static pressure of the fluid to decrease. Then, fluid is further accelerated until it reaches supersonic speed in the divergent section. At the exit plane of the primary nozzle, the speed of the primary fluid reaches supersonic speed $(M_{1P} > 1)$. At the nozzle exit, the supersonic primary fluid jet stream has low pressure and low temperature.

If the expansion process in the primary nozzle is isentropic, the energy conservation equation becomes

$$\dot{m}_P \cdot (h_P + \frac{V_P^2}{2}) = \dot{m}_P \cdot (h_{1P'} + \frac{V_{1P'}^2}{2}) \tag{3.9}$$

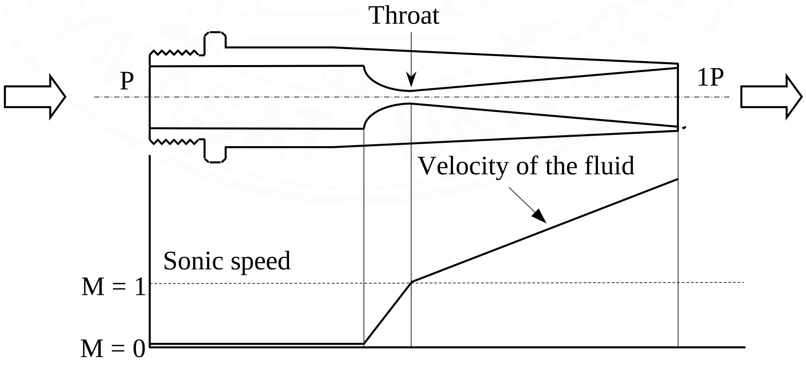

Figure 3.2 Schematic and speed variation of the primary nozzle

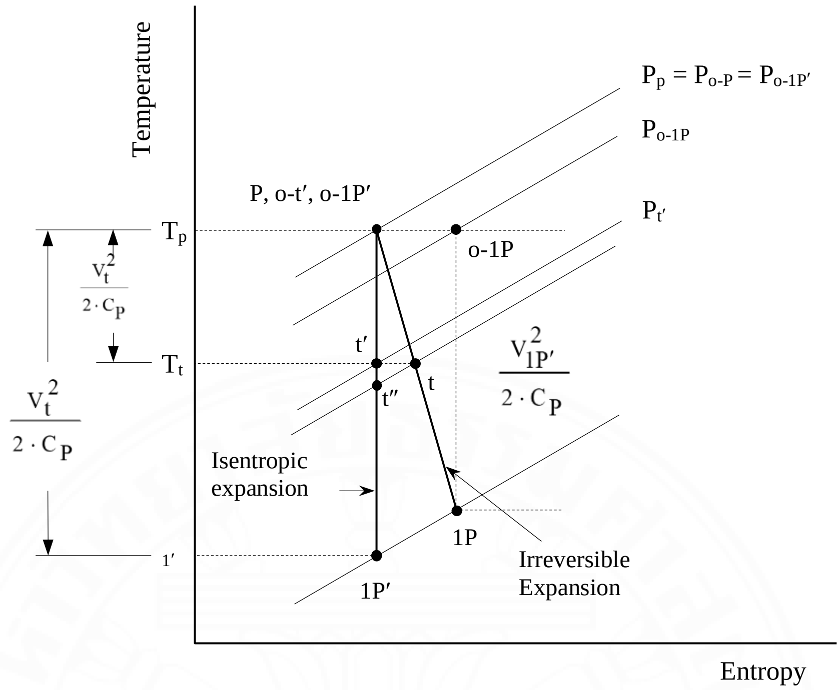

Figure 3.3 Expansion process of the fluid in the primary nozzle on temperature-entropy (T-S) diagram

Thus, $h_{o\text{-}P} = h_{o\text{-}1P'}$ and $T_{o\text{-}P} = T_{o\text{-}1P'}$. When isentropic expansion is assumed, there is no loss in stagnation pressure:

$$P_{o\text{-}P} = P_P = P_{o\text{-}t'} = P_{o\text{-}1P'} \tag{3.10}$$

Static pressure of the fluid at the nozzle exit and in the mixing chamber are assumed to be the same $(P_1 = P_2)$. According to Ruangtrakoon and Aphornratana (2019), static pressure at the nozzle exit plane is approximately 70% of the secondary fluid pressure $(P_1 \approx 0.7P_s)$. Therefore, if the expansion process in the nozzle is isentropic, static temperature of the primary fluid at the exit plane is calculated from

$$\frac{T_{1P'}}{T_P} = \left(\frac{P_1}{P_P}\right)^{\frac{k-1}{k}} \tag{3.11}$$

The speed of the primary fluid at the nozzle outlet is equal to

$$V_{1P'} = \sqrt{2 \cdot C_P \cdot (T_P - T_{1P'})} \tag{3.12}$$

In reality, there is a friction between the fluid and the nozzle's wall, so the expansion process in the primary nozzle is not isentropic. Hence, the velocity of the primary fluid decreases. Nozzle isentropic efficiency is described as

$$\eta_{nozzle} = \frac{V_{1P}^2/2}{V_{1P'}^2/2} \tag{3.13}$$

Nozzle isentropic efficiency is the ratio of the kinetic energy of the actual expansion process to the kinetic energy of the isentropic expansion process:

$$\eta_{nozzle} = \frac{T_P - T_{1P}}{T_P - T_{1P'}} \tag{3.14}$$

Normally, converging-diverging nozzle efficiency is approximately 90% to 95%. Thus, the actual velocity is

$$V_{1P} = \sqrt{2 \cdot C_P \cdot (T_P - T_{1P})} \tag{3.15}$$

And the Mach number is

$$M_{1P} = \frac{V_{1P}}{\sqrt{k \cdot R \cdot T_{1P}}} \tag{3.16}$$

When the expansion process in the nozzle is irreversible, there is a stagnation pressure loss $(P_{o\text{-}1P} < P_{o\text{-}P})$. If the mass flow rate of the primary fluid is known, the cross-sectional area of the nozzle exit plane is

$$A_{1P} = \frac{\dot{m}_P}{\frac{P_{1P}}{R \cdot T_{1P}} \cdot V_{1P}} \tag{3.17}$$

From figure 3.2, at the primary nozzle throat, where the fluid is at sonic velocity (M=1), whether isentropic expansion process or irreversible process, velocity and temperature of the fluid are equal (M_t=$M_{t'}$), but at different static pressure. The nozzle with isentropic expansion process has a higher static pressure at the throat $(P_{t'} > P_t)$. The velocity of the fluid at the throat from both processes is equal to sonic velocity, so

$$V_{t'} = V_t = \sqrt{k \cdot R \cdot T_t} \tag{3.18}$$

Static temperature is

$$T_{t'} = T_t = T_P - \frac{k \cdot R \cdot T_t}{2 \cdot C_P} \tag{3.19}$$

Static pressure for isentropic process is

$$\frac{P_{t'}}{P_P} = \left(\frac{T_{t'}}{T_P}\right)^{\frac{k}{k-1}} \tag{3.20}$$

Static pressure for irreversible process is

$$\frac{P_t}{P_P} = \left(\frac{T_{t''}}{T_P}\right)^{\frac{k}{k-1}} \tag{3.21}$$

And $T_{t''}$ is calculated from

$$\eta_{nozzle} = \frac{T_P - T_t}{T_P - T_{t''}} \tag{3.22}$$

The cross-sectional area of the throat is calculated from

$$A_t = \frac{\dot{m}_P}{\frac{P_t}{R \cdot T_t} \cdot V_t} \tag{3.23}$$

3.3.2 Secondary fluid at mixing chamber inlet

Since pressure at the primary nozzle outlet is slightly less than the evaporator pressure, the secondary fluid is accelerated and flows into the mixing chamber. To reduce complexity in calculation, isentropic expansion is assumed. Thus, static temperature of secondary fluid is calculated from

$$\frac{T_{1S}}{T_S} = \left(\frac{P_1}{P_S}\right)^{\frac{k-1}{k}} \tag{3.24}$$

Secondary fluid velocity is

$$V_{1S} = \sqrt{2 \times C_P \times (T_S - T_{1S})} \tag{3.25}$$

The cross-sectional area of secondary fluid at the mixing chamber inlet, which is the area formed between the mixing chamber wall and the primary nozzle exit, is calculated from

$$A_{1S} = \frac{\dot{m}_S}{\frac{P_{1S}}{R \cdot T_{1S}} \cdot V_{1S}} \tag{3.26}$$

Total area of mixing chamber inlet is

$$A_1 = A_{1P} + A_{1S} \tag{3.27}$$

3.3.3 Mixing process

In the mixing chamber, the supersonic primary fluid mixes with low velocity secondary fluid. This process is assumed to occur at a constant pressure. The mixing process is completely finished at the throat (2) before the normal shock is induced for case of CPM ejector. If the mixing chamber is considered as a control volume, the momentum equation becomes

$$(P_1 \cdot A_1 - P_2 \cdot A_2) = (\dot{m}_P + \dot{m}_S) \cdot V_2 - (\dot{m}_P \cdot V_{1P} + \dot{m}_S \cdot V_{1S}) \tag{3.28}$$

Since pressure in the mixing chamber is assumed to be constant, the value on the left hand side of equation is zero. Moreover, in reality, primary and secondary fluid might not be completely mixed. This results in reduced velocity of the mixing fluid. To make the calculation result more realistic, mixing efficiency is added to the calculation:

$$V_2 = \eta_{mix} \cdot \frac{\dot{m}_P \cdot V_{1P} + \dot{m}_S \cdot V_{1S}}{\dot{m}_P + \dot{m}_S} \tag{3.29}$$

From the experimental data, mixing efficiency is approximately, $\eta_{mix} = 95\%$ (Ruangtrakoon et al., 2011). When velocity of mixing fluid is determined, static temperature of mixed fluid is calculated from

$$T_2 = T_{o-2} - \frac{V_2^2}{2 \cdot C_P} \tag{3.30}$$

Where T_{o-2} is stagnation temperature of mixing fluid which can be determined from the energy equation

$$(\dot{m}_P + \dot{m}_S) \cdot h_{o-2} = \dot{m}_P \cdot h_P + \dot{m}_S \cdot h_S \tag{3.31}$$

and from $\Delta h = C_P \cdot \Delta T$:

$$\dot{m}_P \cdot C_p \cdot (T_{o-2} - T_P) = \dot{m}_S \cdot C_P \cdot (T_S - T_{o-2}) \tag{3.32}$$

Mach number of the mixed fluid:

$$M_2 = \frac{V_2}{\sqrt{k \cdot R \cdot T_2}} \tag{3.33}$$

The cross-sectional area of the mixing chamber throat:

$$A_2 = \frac{\dot{m}_P + \dot{m}_S}{\frac{P_2}{R \cdot T_2} \cdot V_2} \tag{3.34}$$

The calculations of CPM and CRMC methods are identical until this point. Downstream of this point, a normal shock is assumed to be induced for the CPM method while the velocity of the mixed fluid is gradually decreased for the CRMC method.

3.3.4 Normal Shock wave in the constant area throat section for CPM ejector

Figure 3.4 shows the process across the normal shock wave in the throat section. The normal shock wave is irreversible and causes velocity of the fluid to instantly drop to subsonic velocity. Since adiabatic process is assumed, kinetic energy is converted to enthalpy, resulting in instant increases in static pressure, static temperature, and static density: $h_{o\text{-}2} = h_{o\text{-}3}$ and $T_{o\text{-}2} = T_{o\text{-}3}$

For irreversible process, stagnation pressure of the fluid decrease: $P_{o\text{-}3} < P_{o\text{-}2}$ even $P_3 > P_2$

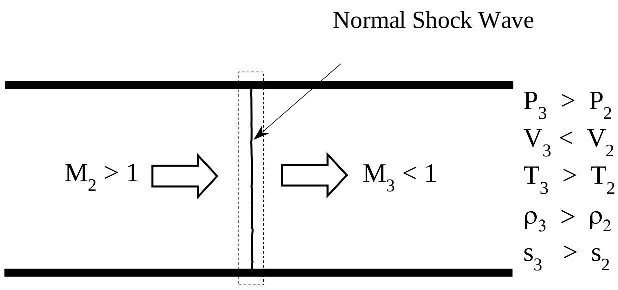

Figure 3.4 Normal shock wave in the mixing chamber throat

To calculate properties of the mixed fluid after a normal shock wave, the energy conservation equation, mass conservation equation, and momentum conservation equation are used:

$$h_2 + \frac{V_2^2}{2} = h_3 + \frac{V_3^2}{2} \tag{3.35}$$

From the mass conservation equation

$$\rho_2 \cdot V_2 = \rho_3 \cdot V_3 \tag{3.36}$$

And the momentum conservation equation

$$(P_2 - P_3) = \rho_2 \cdot V_2 (V_3 - V_2) \tag{3.37}$$

To determine velocity, temperature, and pressure of the fluid after normal shock, these three equations need to be solved. From the energy conservation equation and adiabatic condition, stagnation temperature is constant, thus

$$\frac{T_3}{T_2} = \frac{1 + M_2^2 \cdot (k-1)/2}{1 + M_3^2 \cdot (k-1)/2} \tag{3.38}$$

From the mass conservation equation, the ratio of static pressure becomes

$$\frac{P_3}{P_2} = \frac{M_2}{M_3} \cdot \frac{\sqrt{T_3}}{\sqrt{T_2}} \tag{3.39}$$

The Mach number becomes

$$M_3^2 = \frac{M_2^2 + \frac{2}{k-1}}{\frac{2 \cdot k}{k-1} \cdot M_2^2 - 1} \tag{3.40}$$

When static temperature, static pressure, and Mach number upstream of the normal shock wave are known, properties of the fluid downstream of the normal shock wave can be determined.

3.3.5 Subsonic diffuser for CPM ejector

After the normal shock wave, the mixed fluid is slowed down to subsonic velocity and the static pressure is increased. However, there is still some kinetic energy left. If velocity of the fluid is further decreased until almost the stagnation stage, kinetic energy will convert back to enthalpy. The pressure is further recovered. Figure 3.5 shows the compression process at the diffuser on a temperature-entropy diagram.

If fluid is slowed down isentropically until stagnation stage (o-3), pressure of the fluid will be equal to stagnation pressure $(P_{o\text{-}3})$ which is the highest possible pressure. To do that, a diffuser with very large outlet is needed. In practice, velocity of the fluid at the diffuser outlet (V_4) is approximately 30 to 50 m/s. Moreover, the compression process in the diffuser might not be a reversible process because of friction and loss in the diffuser. The diffuser efficiency is defined as

$$\eta_{\text{diffuser}} = \frac{T_{4'} - T_3}{T_{o-3} - T_3} \tag{3.41}$$

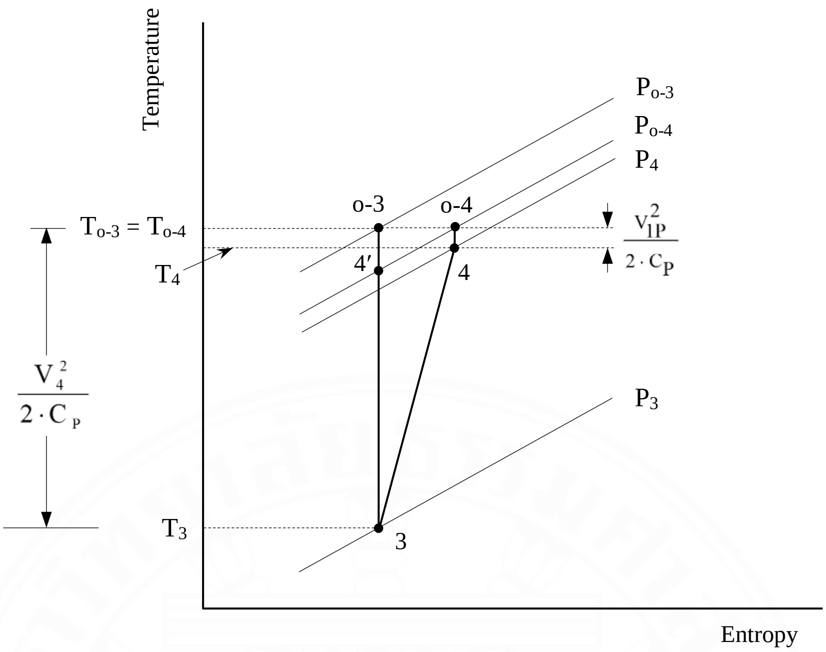

Figure 3.5 Compression process in diffuser on temperature-entropy (T-S) diagram

The diffuser isentropic efficiency has a value of around 90 to 95%, (Çengel & Boles, 1994). $T_{o\text{-}3} - T_3$ represents the kinetic energy of the fluid at the diffuser inlet which can convert to the possible highest pressure $(P_{o\text{-}3})$. Whereas, $T_{4'} - T_3$ represents the kinetic energy of the fluid which can be converted isentropically to the actual stagnation pressure at the diffuser outlet. Stagnation temperature of the fluid at the diffuser outlet is

$$T_{o-3} = T_{o-4} = T_3 + \frac{V_3^2}{2 \cdot C_P} \tag{3.42}$$

From Thus, $P_{o\text{-}4} = P_{4'}$ is calculated by

$$\frac{P_{4'}}{P_3} = \left(\frac{T_{4'}}{T_3}\right)^{\frac{k}{k-1}} \tag{3.43}$$

Since $T_{o-4} = T_{o-3}$ and the velocity of the fluid at diffuser outlet is known, T_4 can be calculated from

$$T_4 = T_{o-4} - \frac{V_4^2}{2 \cdot C_P} \tag{3.44}$$

Static pressure at the diffuser outlet can also be determined:

$$\frac{P_4}{P_{o-4}} = \left(\frac{T_4}{T_{o-4}}\right)^{\frac{k}{k-1}} \tag{3.45}$$

Cross-sectional area of the diffuser outlet is

$$A_4 = \frac{\dot{m}_P + \dot{m}_S}{\frac{P_4}{R \cdot T_4} \cdot V_4} \tag{3.46}$$

3.3.6 Supersonic diffuser for CRMC ejector

The method of performance calculation of the CRMC ejector is also based on the same governing equations provided in section 3.2. The calculation and design of the primary nozzle, secondary fluid inlet, and mixing process also the same and were provided in sections 3.3.1 to 3.3.4, respectively. By the end of the entrainment region (section 2), the fluid is assumed to be completely mixed. Then, the supersonic mixed fluid is gradually slowed in the converging-diverging diffuser unlike the CPM method in which the normal shock is induced at the throat of the mixing chamber in order to create the major compression effect. However, for the CRMC method, the supersonic mixed fluid is gradually slowed down to almost stagnation state. This allows the fluid pressure to be recovered almost isentropically. The CRMC method creates the geometry and profile of the supersonic diffuser (converging part) and subsonic diffuser (diverging part) with unity Mach number at the throat. This is believed to eliminate thermodynamic shock process within the diffuser at the design-point operating condition. This can be achieved by letting the momentum of fluid flow to change at a constant rate along the ejector. This allows the static pressure to increase gradually and eliminates the total pressure loss associated with the normal shock.

The geometry of the CRMC ejector is shown in figure 3.6. The CRMC method is used to calculate performance and cross-sectional area of the converging-diverging diffuser of the CRMC ejector. The cross-sectional area of the CRMC diffuser is gradually changed allowing the velocity of the fluid to progressively decrease from the supersonic section (L_1) to the subsonic section (L_2). The CRMC method can be described by the following equation:

$$\frac{d\dot{M}_o}{dx} = (\dot{m}_p + \dot{m}_s)\frac{dV}{dx} = C \tag{3.47}$$

Where M_o is momentum of the mixed fluid (kg·m/s)

x is distance along the diffuser (x = 0 at diffuser inlet)

C is constant value

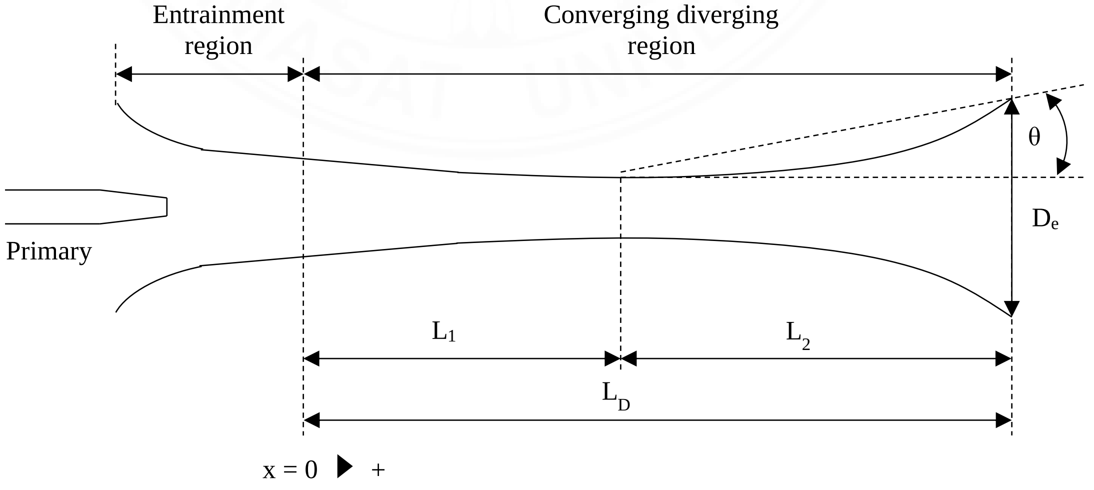

Figure 3.6 Geometry of the CRMC ejector

Referring to figure 3.6 the boundary conditions of equation (3.47) are

$V = V_2$ at x = 0 and $V = V_e$ at $x = L_D$

Using the above boundary condition to solve equation (3.47)

$$V_x = V_2 - \frac{(V_2 - V_e)}{L_D} \cdot x \quad \text{for } 0 \le x \le L_D \tag{3.48}$$

Where V_2 is velocity of the mixed fluid at the diffuser inlet (m/s) and is obtained from equation (3.29)

V_e is velocity of the mixed fluid at diffuser exit (m/s)

L_D is length of the diffuser section (m)

The value of V_2, which is velocity of fluid at the mixing region exit plane, can be achieved from equation (3.29). The value of L_D can be determined by using a semi-empirical method provided in next section. In order to determine the cross-sectional area at any distance (x) along the diffuser, both static pressure and temperature should be determined:

$$T_x = T_{o\text{-}2} - \frac{V_x^2}{2Cp} \tag{3.49}$$

$$P_x = P_{o\text{-}2}\left(\frac{T_x}{T_{o\text{-}2}}\right)^{\frac{k}{k-1}} \tag{3.50}$$

The density of fluid at distance x is

$$\rho_x = \frac{T_x}{RT_x} \tag{3.51}$$

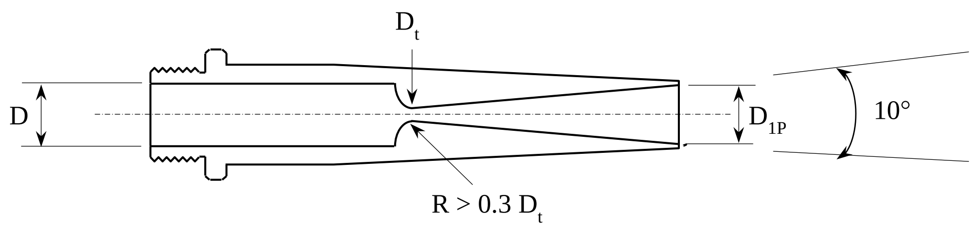

Figure 3.7 Design of primary nozzle

From mass continuity, the diameter of CRMC diffuser at distance x is

$$D_x = 2\sqrt{\frac{\dot{m}_p(1+Rm)RT_x}{\pi P_x V_x}} \tag{3.52}$$

3.4 Design of ejector

The ejector performance calculation and the cross-sectional areas of the ejector are provided in section 3.3. In this section, a typical design of the ejector is provided including lengths of each section and angles of converging and diverging ducts.

3.4.1 Primary nozzle

Figure 3.7 shows the schematic of the primary nozzle. Normally, a convergent-divergent nozzle is designed for saturated vapour or superheat vapour at high pressure with velocity less than 50 m/s at the nozzle inlet. The converging duct is curved with a radius less than 30% of the throat diameter $(R > 0.3D_t)$. This also prevents boundary layer formation at the throat which causes mass flow rate to be less than the calculated result. The diverging duct is flared out at approximately 10°. If the angle is less than this, the nozzle will be too long and create more friction. If the angle is more than this, there might be separation between fluid and nozzle wall which decreases efficiency of the nozzle.

3.4.2 Mixing chamber for CPM ejector

Figure 3.8 shows the typical design of the CPM ejector. Geometry of the mixing chamber inlet affects efficiency of the ejector. Not only diameter of the throat and of the mixing chamber inlet, but length and angle of the mixing chamber are also important. If the mixing chamber is too short, primary and secondary fluid will not be completely mixed before the normal shock is induced. If the mixing chamber inlet is too long, there will be high friction loss in the mixing chamber. From experiment investigations, the appropriate length of the entrainment section to constant area section, measured from the primary nozzle outlet plane, should be 5 to 10 times the throat diameter. Length of the constant area throat should be 2 to 4 times the throat diameter. The angle of the entrainment section is approximately 2° to 10°. The inlet is a bell mouth to reduce friction. This design is to make sure that the fluid is completely mixed before normal shock wave is induced.

Position of the primary nozzle also affects the ejector efficiency which can be determined from experiments or computational fluid dynamics (CFD). Normally, the primary nozzle outlet is located inside the mixing chamber by a distance 0.5 to 1.0 times of the constant area throat diameter. If the primary nozzle is moved into the mixing chamber, mass flow rate of the secondary fluid will decrease, but pressure at the diffuser outlet will increase. If the primary nozzle is moved out from the mixing chamber, mass flow rate of the secondary fluid will increase, but pressure at the diffuser outlet will decrease. Position of the primary nozzle should be adjusted by experimentation.

Normally, the diffuser is flared out with an angle of 3° to 5°. If the diffuser is more obtuse, separation might occur. The diffuser outlet should have a cross-sectional area approximately 5 times the cross-sectional area of the throat.

3.4.3 Supersonic diffuser for CRMC ejector

This section describes the method of calculating the length of the CRMC diffuser, L_D. Referring to figure 3.6, the CRMC diffuser is divided into two parts at the diffuser throat: supersonic part (L_1) and subsonic part (L_2). Length of the supersonic part (L_1) can be calculated from

$$L_1 = L_D \frac{(V_2 - V_x^*)}{(V_2 - V_e)} \tag{3.53}$$

Where V_x^* is velocity of the mixed fluid at diffuser throat (m/s)

From figure 3.6, $L_D = L_1 + L_2$; substitute this in to equation (3.53)

$$L_1 = \frac{L_2\left(\dfrac{V_2 - V_x^*}{V_2 - V_e}\right)}{1-\left(\dfrac{V_2 - V_x^*}{V_2 - V_e}\right)} \tag{3.54}$$

Length of the CRMC diffuser subsonic part (L_2) can be calculated from the geometry of the CRMC diffuser. From figure 3.6, the angle θ is assumed to be 4° to 5° to prevent separation of the fluid and diffuser wall similar to the subsonic diffuser of the CPM ejector. Thus, the length L_2 is

$$L_2 = V_x^* \frac{\left(\dfrac{V_e}{V_x^*} - 1\right)}{2\tan\theta} \tag{3.55}$$

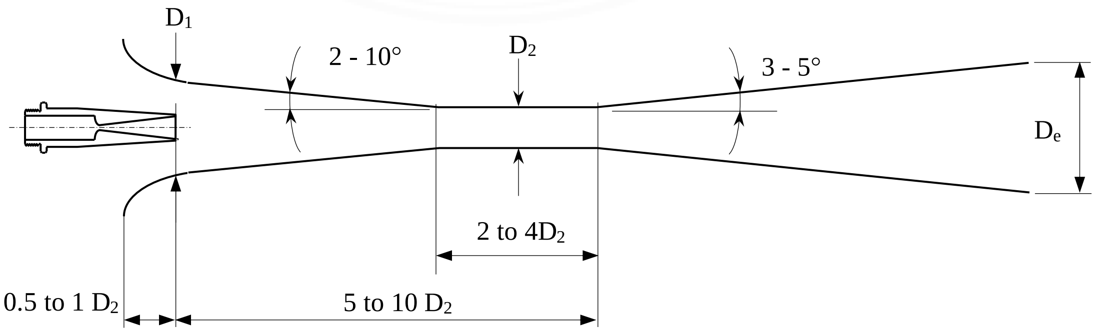

Figure 3.8 Design of mixing chamber of the ejector

Since the Mach number at the throat section is unity, the ratio of exit diameter to the throat diameter, $\frac{V_e}{V_x^*}$, can be calculated from

$$\frac{V_e}{V_x^*} = \frac{1}{\sqrt{M_e}}\left(\frac{2+(k-1)M_e^2}{k+1}\right)^{(k+1)/4(k-1)} \tag{3.56}$$

The Mach number at the diffuser exit plane is approximately equal to

$$M_e \cong \frac{V_e}{\sqrt{kRT_{o-2}}} \tag{3.57}$$

3.5 Calculated result of CPM vs CRMC

This section shows the example of calculated results using equations provided in the previous section to compare the CPM and the CRMC design methods. The calculation input parameters are listed in table 3.1. The calculation results are listed in tables 3.2 to 3.4. The calculated results of the mixing processes are listed in table 3.2. The mixing process of the CPM and the CRMC ejector are identical since the assumption of the mixing process for both design methods is the same. Table 3.3 shows the calculated result of the shock process and compression process in the sub sonic diffuser of the CPM ejector. The calculated stage of the mixed fluid after the mixing process of the CRMC ejector is listed in table 3.4. This table shows the stage at different positions (x) along the CRMC diffuser. It is noted that the stagnation temperature and pressure of CRMC diffuser are constant throughout. Figure 3.9 shows the calculated geometry of the CPM and CRMC diffuser. The CMRC method provides a gradual change converging-diverging profile along the ejector. On the other hand, the profile of the CPM method is parallel, and then changes to the straight-sided conical subsonic diffuser. The inlet of the CRMC diffuser and CPM diffuser have the same diameter. However, the throat section of the CRMC diffuser is smaller than the CPM diffuser. This is because the CRMC assumed the flow to gradually slowdown from supersonic velocity at section 2 to 30-50 m/s at ejector outlet. Thus, the diffuser should be converging-diverging with unity Mach number at the throat in the same manner as the primary nozzle, but in the opposite way.

Table 3.1 Parameters using for calculation

Parameter	Symbol	Value
Primary fluid total temperature, (°C)	T_{o-p}	130
Primary fluid total pressure, (kPa)	P_{o-p}	270
Secondary fluid temperature, (°C)	T_{o-s}	5
Secondary fluid pressure, (kPa)	P_{o-s}	0.873
Primary fluid mass flow rate, (kg/hour)	m_p	3.32
Entrainment ratio	Rm	0.4
Diffuser Exit velocity (m/s)	V_e	30
Diffuser included angle (for CRMC) (degree)	θ	8
Gas constant (J/kg·K)	R	461.5
Specific heat capacity at constant pressure (J/kg·K)	C_p	1872
Ratio of Specific heat value	k	1.327

Table 3.2 Calculated results of mixing process of CPM and CRMC ejector

Stage	T_o (K)	T (K)	P_o (kPa)	P (kPa)	V (m/s)	M	A (m^2)	D (mm)
t	403.00	346.35	252.95	136.79	460.55	1.00	2.537×10^{-6}	1.80
1P		105.48	139.32	0.61	1055.43	4.15	7.561×10^{-5}	9.81
1S	278.00	254.61	0.873		295.93	0.75	0.401×10^{-3}	-
1	-	-	-		-	-	$A_{1S}+A_{1P}$	24.63
2	367.29	208.37	6.10		771.36	2.10	0.286×10^{-3}	19.00

Table 3.3 Calculated results of process after the mixing process of CPM ejector

Stage	T_o (K)	T (K)	P_o (kPa)	P (kPa)	V (m/s)	M	A (m^2)	D (mm)
3	367.29	350.45	3.82	3.16	250.58	0.54	0.286×10^{-3}	19.00
e		367.05	3.79	3.78	30	0.06	1.725×10^{-3}	46.8

Table 3.4 Calculated results of process after the mixing process of CPM ejector

x (mm)	T_o (K)	T (K)	P_o (kPa)	P (kPa)	V (m/s)	M	A (m^2)	D (mm)
0	367.29	208.37	6.1	0.611	771.36	2.16	0.286×10^{-3}	19.07
20		228.77		0.893	720.14	1.92	0.23×10^{-3}	17.11
40		247.77		1.234	668.93	1.72	0.194×10^{-3}	15.72
60		265.37		1.630	617.72	1.53	0.17×10^{-3}	14.73
80		281.57		2.074	566.50	1.36	0.155×10^{-3}	14.05
100		296.37		2.553	515.29	1.21	0.146×10^{-3}	13.62
120		309.76		3.054	464.08	1.07	0.141×10^{-3}	13.41
140		321.76		3.563	412.86	0.93	0.141×10^{-3}	13.42
160		332.35		4.064	361.65	0.80	0.146×10^{-3}	13.64
180		341.55		4.540	310.44	0.68	0.157×10^{-3}	14.12
200		349.34		4.975	259.23	0.56	0.175×10^{-3}	14.93
220		355.73		5.355	208.01	0.45	0.206×10^{-3}	16.21
240		360.72		5.666	156.80	0.33	0.262×10^{-3}	18.28
260		364.31		5.899	105.59	0.22	0.378×10^{-3}	21.94
280		366.50		6.044	54.37	0.11	0.721×10^{-3}	30.30
292		367.14		6.087	23.59	0.05	1.652×10^{-3}	45.87

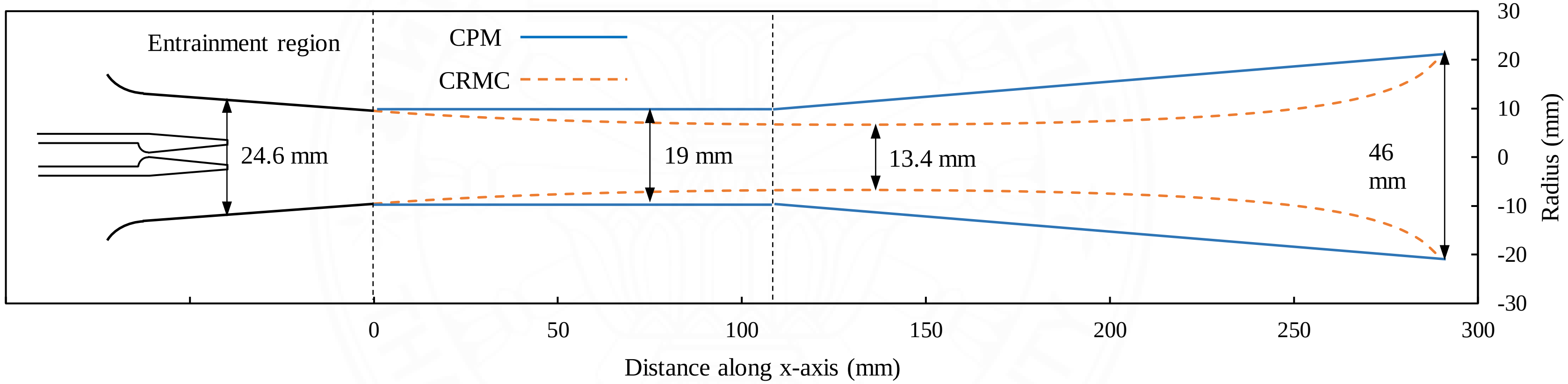

Figure 3.9 Radius of CPM and CRMC ejector along x-axis

Figures 3.10 and 3.11 show the plot of static pressure and velocity along the diffuser, respectively. Since there is no shock process in the CRMC diffuser, there is no sudden drop in velocity and sudden increase in pressure. The pressure gradually increases while the velocity decrease linearly along the diffuser in contrast to the CPM diffuser. The linearity of velocity profile is due to assumption of CRMC method of constant rate of momentum change. Since the momentum is a product of mass and velocity, with the constant mass flow, the velocity change is at constant rate. Moreover, due to no loss from the shock process, the pressure at the diffuser outlet of the CRMC diffuser is higher than the CPM diffuser for the same entrainment ratio. This calculation result implies that, theoretically, the CRMC ejector should capable to operate at a higher critical condenser pressure with the same entrainment ratio compared to CPM ejector.

If the shock wave disappears from the flow process inside the mixing chamber of an ejector based on the assumption of the CRMC method (Eames, 2002), the ejector operation can be simplified to a simple thermodynamics model in which an isentropic turbine and an isentropic compressor are being operated simultaneously as shown in figure 3.12. The expansion process of the primary fluid ($\dot{m}_p$) across the primary nozzle may be considered as an isentropic turbine. Pressure at the turbine outlet is equal to that of the secondary fluid (evaporator pressure). The primary fluid from the turbine outlet (turbine's exhaust) is then mixed with the secondary fluid ($\dot{m}_s$). The pressure recovery process of the mixed stream is achieved via the compression process across the isentropic compressor which is coupled to the turbine's shaft. Ideally, this ejector model is reversible, and, thus, performance of an ejector designed based on the CRMC method may be closer to a reversible ejector (no loss in stagnation pressure). Therefore, the CRMC ejector is expected to provide much better performance than the CPM ejector. Unfortunately, there is no evidence or current research to indicate that the CRMC ejector can really eliminate the shock wave. This is one of the research gaps of the CRMC ejector which is still needs investigation.

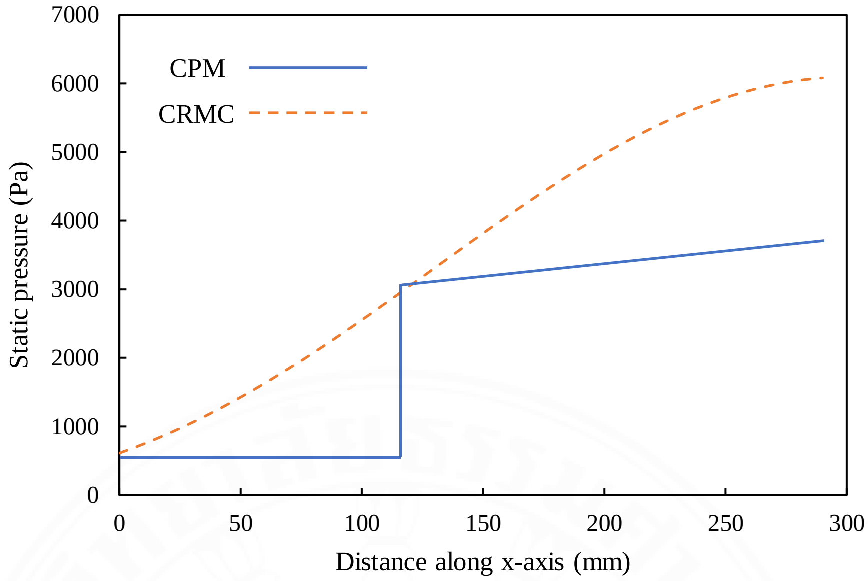

Figure 3.10 Static pressure along x-axis

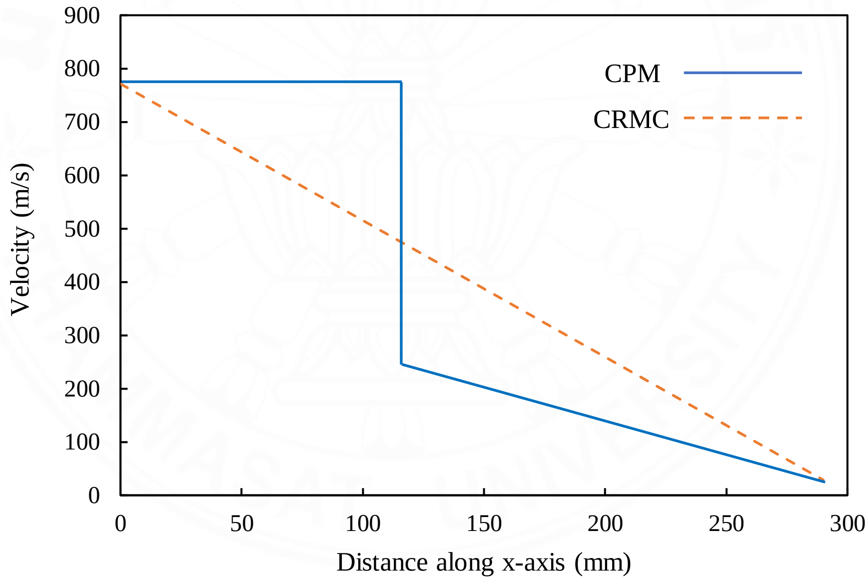

Figure 3.11 Velocity along x-axis

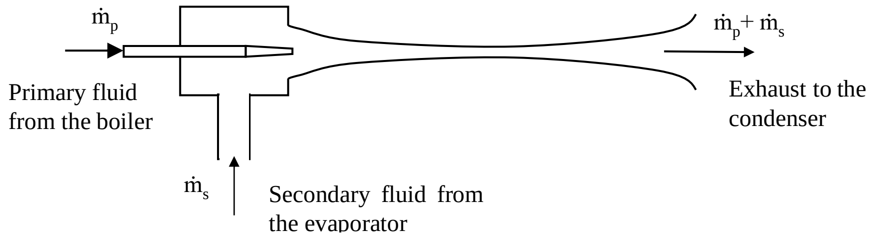

(a) Schematic view of CRMC ejector

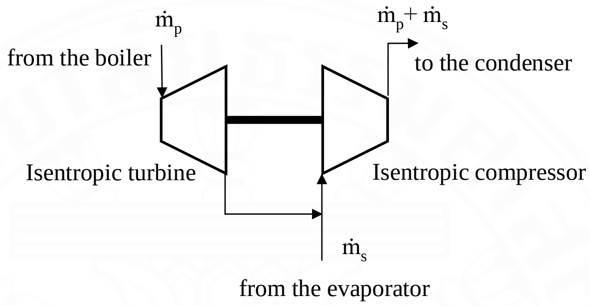

(b) Schematic of turbine-compressor model

Figure 3.12 CRMC ejector as a thermodynamic cycle

3.6 Conclusion

The performance calculation and design of CPM and CRMC ejector are described in this chapter. Both types of ejectors use the same mathematical model on the primary nozzle and entrainment process. The mixing processes are assumed to be at constant pressure. However, a shock wave is assumed to occur in the constant area throat in the CPM design method. The subsonic diffuser of the CPM ejector is a conical diverging duct. On the other hand, the CRMC method aims to eliminate the shock wave by letting the rate of the momentum change to be constant throughout the diffuser. Unlike the CPM design method, this method generates the smooth converging-diverging curve profile diffuser. This allows the velocity of the fluid to decrease gradually from supersonic to almost stagnation state at the diffuser outlet. However, the throat of CRMC ejector is smaller than CPM ejector at the same design parameters. This provides a different ejector area ratio which theoretically provides much different performance.

CHAPTER 4
EXPERIMENTAL STEAM EJECTOR REFRIGERATION SYSTEM

This chapter explains how an experimental steam ejector refrigerator was designed, constructed and tested. Both CPM and CRMC ejectors were tested. Two CPM mixing chambers and two CRMC mixing chambers together with four primary nozzles were used. The evaporator provided cooling capacity up to 1 kW. The cooling load was supplied using electrical heaters. The electrical heated steam boiler was 10 kW. The use of electrical heaters as heat sources for both the evaporator and the boiler provided ease of control and measurement. The condenser was cooled by water provided from a 15-kW water chiller. The used of the water chiller allowed the temperature of cooling water to be varied down to 20°C as required. Therefore, the saturation pressure in the condenser could be controlled precisely.

A schematic view and a photograph of the experimental steam ejector are shown in figures 4.1 and 4.2, respectively. The ejector refrigerator was designed so that the ejector could be replaceable, so the CRMC and CPM ejector could be tested on the same testing unit. The main components of the experimental steam ejector refrigerator were a steam boiler, an evaporator, a condenser, an ejector, a circulating pump, and measuring devices.

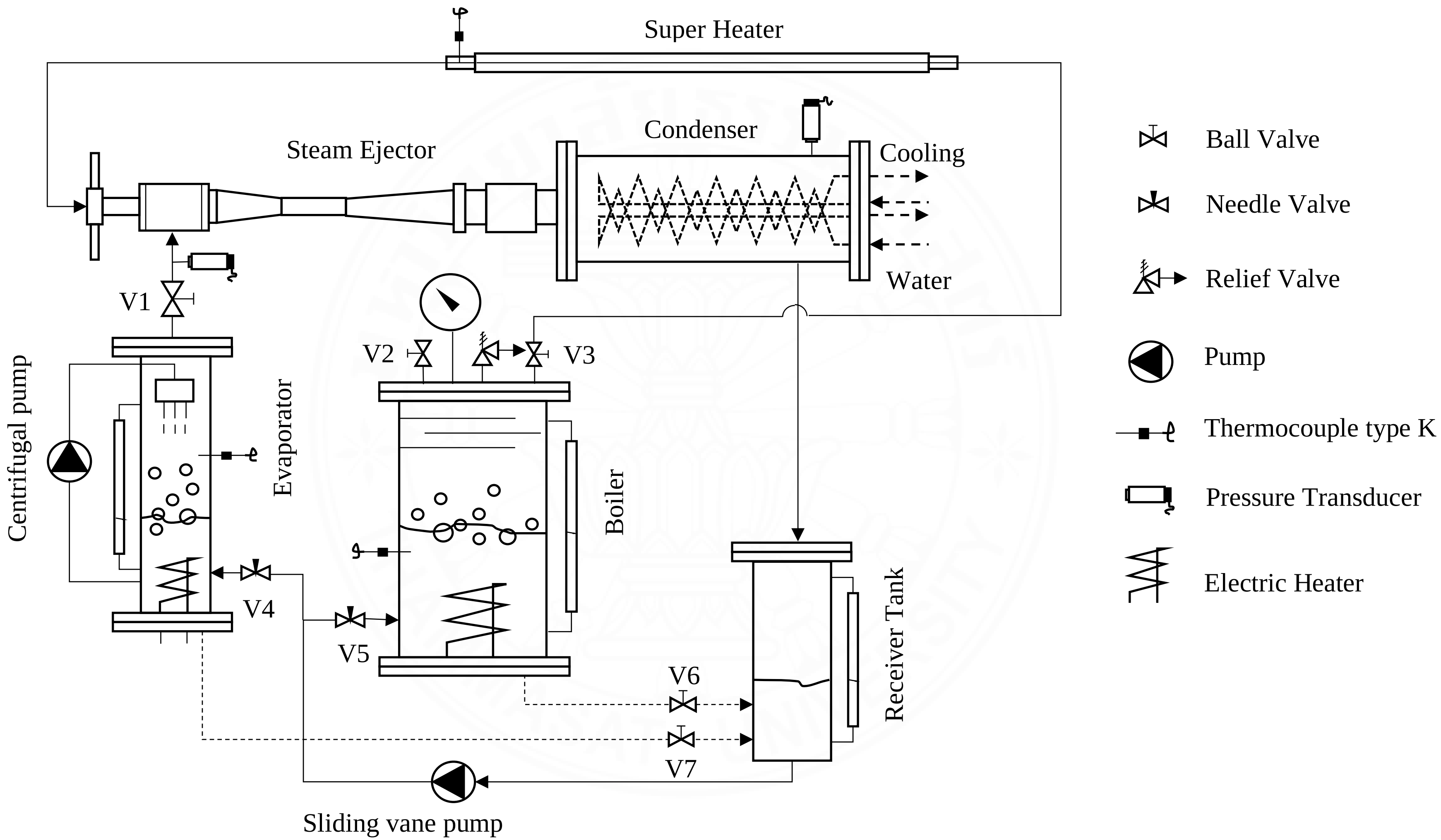

Figure 4.1 Schematic of the experimental steam ejector refrigerator

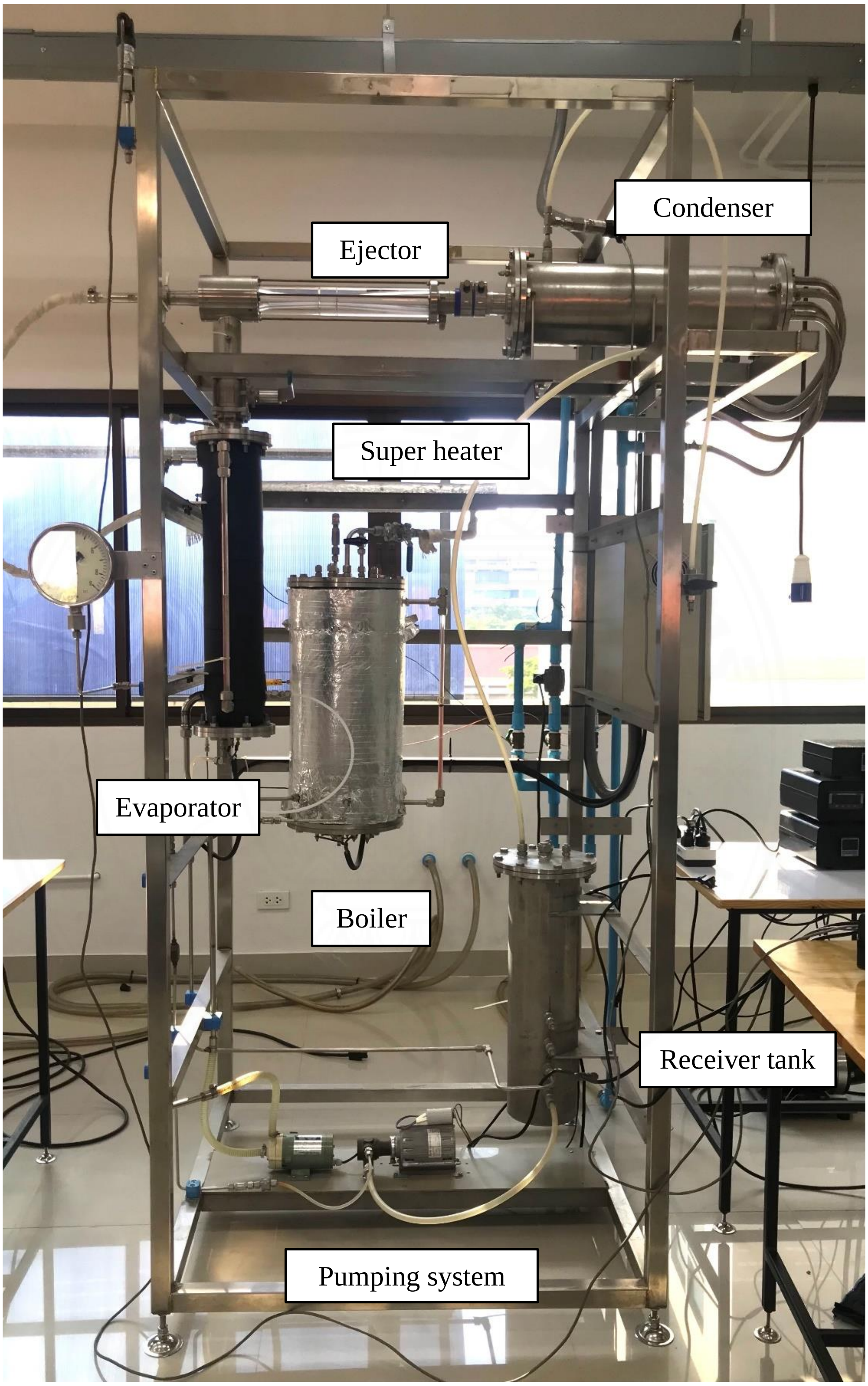

Figure 4.2 Photograph of the experimental steam ejector refrigerator

4.1 The steam boiler

The steam boiler was constructed from 8-inch schedule 40 (ID = 210.9 mm and OD = 219.08 mm), SUS 304 stainless steel pipe with flanges welded on both ends. The total length of the boiler shell was 60 cm. To monitor saturation pressure inside the boiler, a pressure gauge with range of -1 to 9 bar was installed. For safety, a pressure relief valve was installed at the top of the boiler with the pre-set pressure of 10 bar. Three baffle plates were installed at the top part in the boiler in order to prevent liquid droplets from being carried with the steam to the ejector. A glass tube level indicator was installed along the boiler length for observing liquid water level in the boiler. A 10-kW immersion electric heater was installed at the bottom end for simulating heat source supplied to the system. The boiler was insulated with fiberglass wool insulator to prevent heat loss to environment.

4.2 The superheater

The superheater was installed to ensure that the steam entering the primary nozzle was dry steam and no droplets were entering the primary nozzle. The saturated steam from the boiler was heated up to 1-2°C above the saturation temperature. The superheater was 500W electric heater inserted along the 1-inch schedule 10 (ID = 31.75 mm), stainless steel pipe. The power of the super heater was controlled by adjusting voltage across the super heater using voltage dimmer. The superheater was also insulated with fiberglass wool insulator.

4.3 The evaporator

The evaporator was designed based on a spray column. The shell was constructed from a 3-inch furniture grade 304 stainless steel tube (ID = 72 mm and OD = 73.78 mm) with length of 60 cm. Both ends were welded to stainless steel flanges. A glass tube level indicator was installed along the length of the evaporator to observe the liquid level inside. A shower head was installed at the top part inside the evaporator. The liquid water at the bottom part of the evaporator was circulated through the shower head via the circulating pump (15 W magnetic couple pump). This was to promote the refrigeration effect by increasing the surface area of water for the evaporation process.

A 3-kW immersion electric heater was installed at the bottom part and used as a simulated cooling load. To prevent the unwanted heat gain from surroundings, the evaporator was well insulated with 30 mm thickness EPDM insulator.

4.4 The condenser

The condenser was a shell and coil water cooled type heat exchanger. The shell was constructed from a 6-inch schedule 10 (ID = 164.88 mm and OD = 168.28 mm), SUS 304 stainless steel pipe with a length of 52 cm. Two sets of copper coils were installed in the condenser. The cooling coils were rolled from 20 meters of 1/2 inch annealed copper tube. The reason for using two sets of coils was to prevent fluctuation of condenser pressure. The cooling water flowed continuously in one coil, while flow of cooling water in another coil was controlled by a solenoid valve. The cooling water was supplied from a 15-kW vapour-compression chiller. The advantage of using of a water chiller instead of a cooling tower was that the temperatures of the cooling water could be adjusted precisely even at temperatures lower than the environment. The experimental refrigerator could be tested even at saturation temperatures as low as 20°C. Therefore, this allowed the experimental refrigerator to be tested with a wide range of condenser saturation temperatures and pressures.

4.5 The receiver tank

During each test, V4, V5, and the pump were all closed in order to allow the primary fluid and the secondary fluid to be boiled or evaporated out from the boiler and the evaporator, respectively. This was in order to determine the flow rate of the two fluid streams. Then, all the fluids were condensed to liquid at the condenser and accumulated in the receiver tank. When the test was finished, the liquid accumulated in the receiver tank was pumped back to boiler and the evaporator for the next test.

The receiver tank was constructed from a 6-inch schedule 10 (ID = 164.88 mm and OD = 168.28 mm), SUS 304 stainless steel pipe with the length of 60 cm. Both ends were welded with flanges. A glass tube level indicator was installed along the length of the receiver tank to observe the liquid level inside.

4.6 The steam ejector

Figures 4.3 and 4.4 show a photograph and a drawing of the experimental ejector. It consisted of the suction chamber, the NXP adjuster, the mixing chamber, and the primary nozzle. The suction chamber was machined from a billet stainless steel bar. It was welded perpendicularly (not tangential) with 1½ inch schedule 10 SUS304 stainless steel pipe which was also connected to the evaporator and used as the secondary fluid suction duct. The body was designed so that the mixing chambers and the primary nozzle could be easily interchanged. The NXP adjuster was a hollow threaded shaft to which the primary nozzle was mounted at the end. It allowed the primary nozzle exit position (NXP) to be adjusted as required. It this dissertation, the NXP was fixed at 23 mm.

Figure 4.3 Photograph of the experimental steam ejector

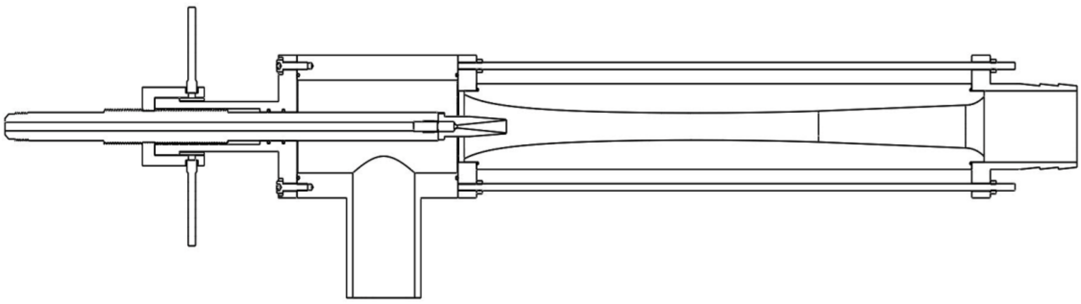

Figure 4.4 Schematic of the experimental steam ejector

Four mixing chambers were used. Two were constant pressure mixing chambers with throat diameters of 19.0 mm (CPM19.0) and 13.4 mm (CPM13.4), and the other two were constant rate momentum change mixing chambers with throat diameters of 19.0 mm (CRMC19.0) and 13.4 mm (CRMC13.4). They were designed based on the method provided in chapter 3. The drawings of the mixing chambers are shown in figure 4.5. The design parameters using for designing the ejectors are listed in table 4.1.

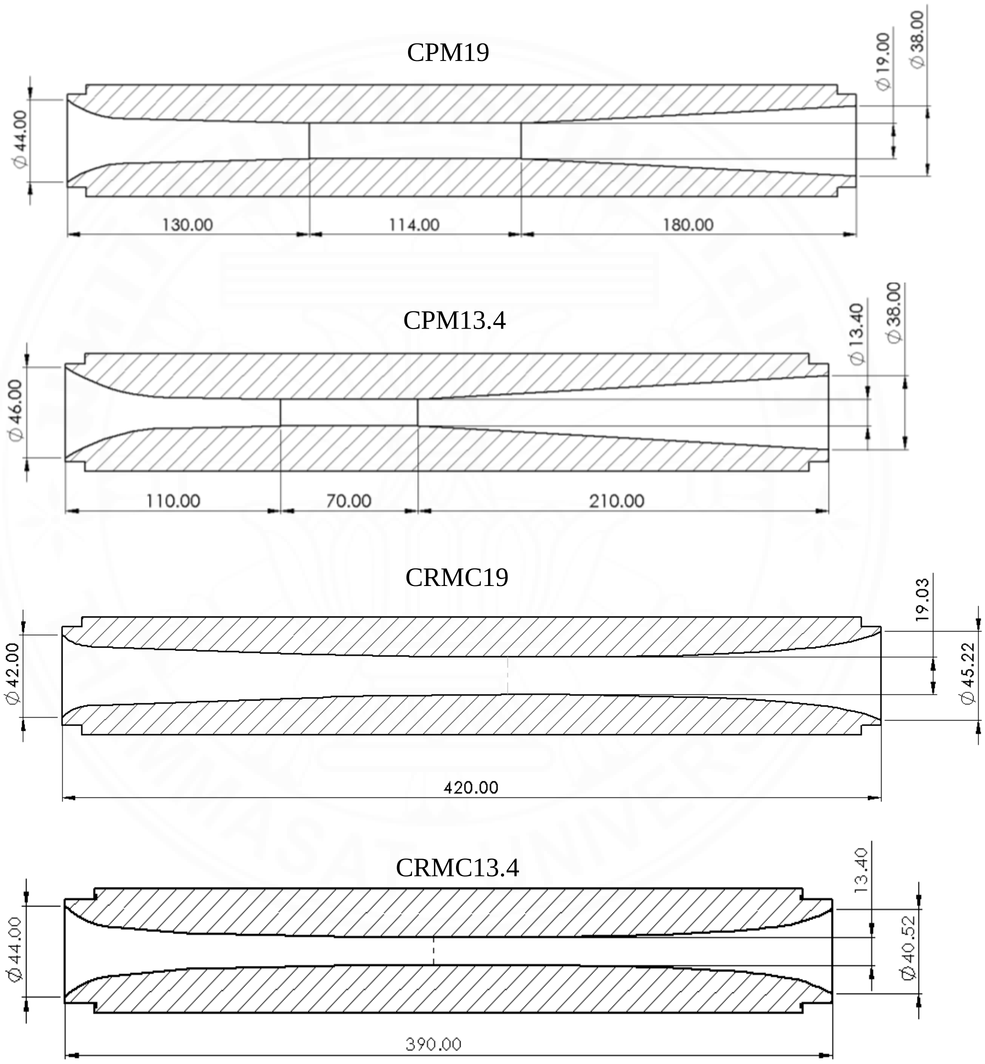

Figure 4.5 Drawings of the mixing chambers

Table 4.1 Parameters using for calculation

Parameter	Symbol	CPM19 &CRMC13.4	CPM13.4	CRMC19
Primary fluid total temperature, (°C)	$T_{o\text{-}p}$	130	110	140
Primary fluid total pressure, (kPa)	$P_{o\text{-}p}$	270	143.4	361.5
Secondary fluid temperature, (°C)	$T_{o\text{-}s}$		5	
Secondary fluid pressure, (kPa)	$P_{o\text{-}s}$		0.873	
Primary fluid mass flow rate, (kg/hour)	m_p	3.32	1.95	4.77
Entrainment ratio	Rm	0.4	0.3	0.64
Diffuser Exit velocity (m/s)	V_e		50	
Diffuser included angle (for CRMC) (degree)	θ		8	
Gas constant (J/kg·K)	R		461.5	
Specific heat capacity at constant pressure (J/kg·K)	Cp		1872	
Ratio of Specific heat value	k		1.327	

These four mixing chambers were designed to be a single piece in order to eliminate any unsmooth connection between each section. It was not possible to machine the mixing chambers in single pieces since they had a high ratio between depth and throat diameter. Moreover, it was very hard to directly machine the curved profile of the CRMC mixing chamber. It was much easier to machine the mould and then cast the mixing chamber from the mould. Figure 4.6 shows the mould used for casting the mixing chambers. The moulds were machined by a Computer Numerical Control (CNC) machine to get the precise profile of the designed ejectors. The moulds were separated into two pieces with a screw connection at the middle so that the mould could be removed from the casted resin. Clear polyester resin was used because it was easy to cast and didn’t deform with high temperature. With a clear mixing chamber, flow inside the mixing chamber could be observed. Figure 4.7 shows a drawing of the mould assembly during the casting process. After the resin was fully cured and set, it was removed from the mould. It was then machined and polished on the lathe in order to get exact dimensions and full transparency.

Figure 4.6 Photograph of the mould of CRMC13.4 ejector

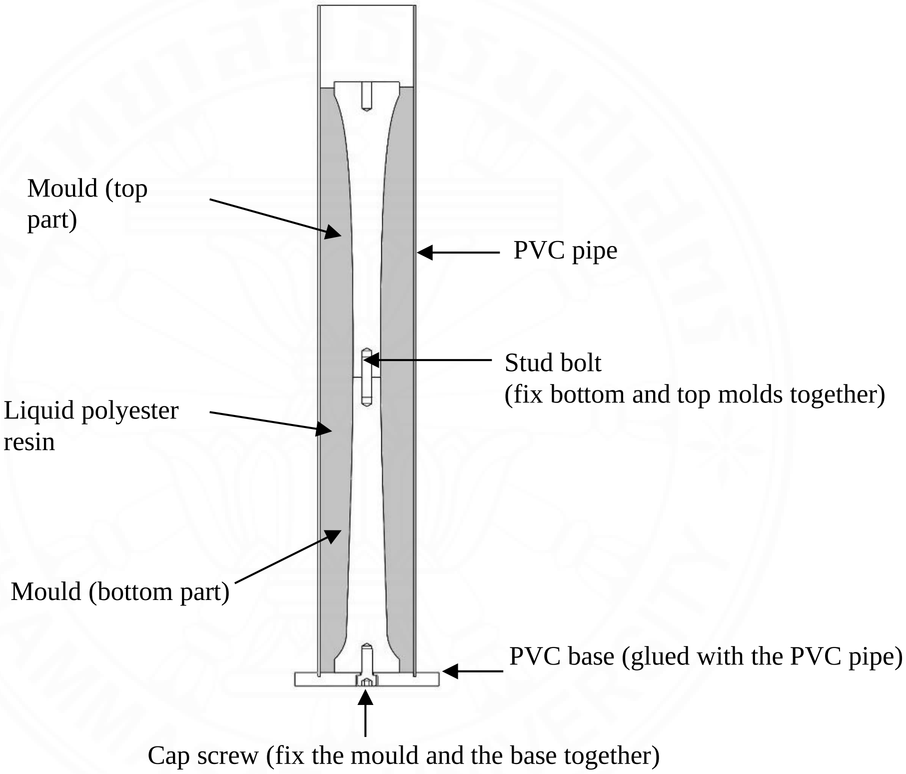

Figure 4.7 Drawing of the mould assembly during the casting process

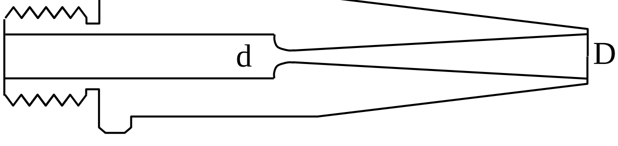

Figure 4.8 Schematic of primary nozzle

Table 4.2 Dimensions of the primary nozzle

Nozzle	d (mm)	D (mm)	Nozzle's area ratio (A_{exit}:A_{throat})	Calculated exit Mach number
D1.4	1.4	6.3	20:1	4
D1.7	1.7	7.6		
D2.0	2.0	8.9		
D2.4	2.4	10.7		

Four primary nozzles were used in this work. All of the primary nozzles were machined from billet brass. They were machined on a lathe to obtain exact outer dimensions. For the converging-diverging profile inside, an Electrical Discharge Machining (EDM) technique was used in order to achieve high precision. Diameters of the primary nozzles' throats were 1.4mm, 1.7mm, 2.0mm and 2.4mm, respectively, as listed in figure 4.8 and table 4.2. The calculated exit Mach number of the primary nozzles was 4.0. Throughout the investigation, NXP (nozzle exit position) was placed at +23 mm for all of the tests. NXP was equal to zero when the nozzle exit plane was located at the mixing chamber inlet plane. NXP had a positive value when the nozzle exit plane moved inside the mixing chamber and vice versa.

4.7 Pumping system

In this system, two types of mechanical pump were used: a magnetic coupling centrifugal pump and a sliding vane pump. As mention earlier, for the evaporator, the magnetic coupling centrifugal pump was used to circulate water from the bottom part of the evaporator and spray it down at the top part of the evaporator column. Another pump was used to feed water from the receiver tank to the boiler and the evaporator. The water at low pressure had low viscosity, and was almost a saturated liquid which was prone to be cavitated. Therefore, the use of a piston pump or diaphragm pump was not possible since they are equipped with an inlet check valve which causes the pressure to drop resulting in cavitation. Moreover, a positive displacement pump like a magnetic couple gear pump is very expensive. It was found that a sliding vane pump, which was designed to be used with a large commercial coffee machine, was relatively cheap and worked well for this situation. Figure 4.9 shows photographs of the evaporator recirculating pump and the boiler feeding pump.

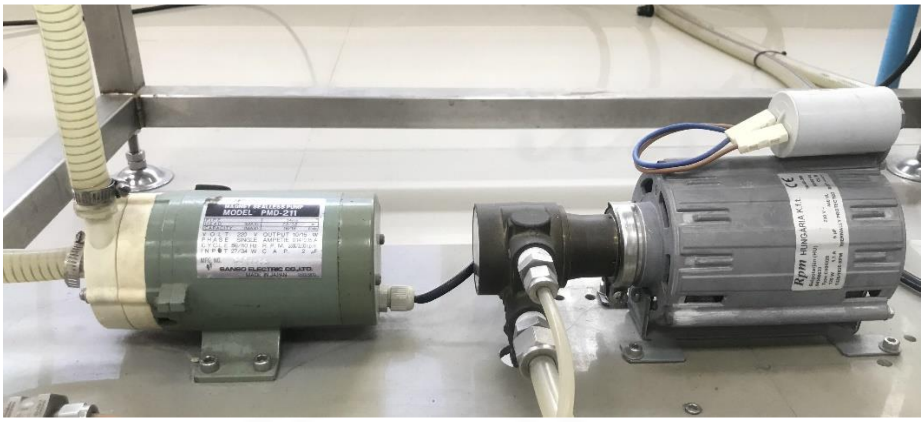

Figure 4.9 The evaporator recirculating pump and the boiler feeding pump

4.8 Leak proof and purging system

Even the system was operated with moderate pressure at the boiler and under vacuum condition (or negative pressure) in other components. For safety reason, all vessels were hydrostatic pressure tested to 15 bar. Then they were pressurized to 7 bar with compressed air in order to ensure that there was no leak of air or non-condensable gases into the system for the component under negative pressure (the evaporator, the condenser, and the receiver tank) or no leak of high-pressure steam for the component under positive pressure (the boiler).

A feature of the system was that it could be easily dismantled for modification. This resulted in the use of many removable joints, gaskets, and O-ring seals. Perfect leak tightness was therefore, impossible. As most of the components were under vacuum condition, air or non-condensable gases slowly and continuously accumulated in the system. A vacuum pump was used to evacuate air and all non-condensable gases from the system before starting an experiment. A leak rate below 0.01 mbar/min was measured. This might resulted the overall condenser pressure, which was the ejector’s discharge pressure, to be higher than the saturation pressure of the water vapour. This should not affect value of the critical condenser pressure obtained since the condenser pressure was maintained automatically at the set point value.

4.9 Instrumentation and control

In order to analyse the performances of the experimental steam ejector, temperatures, pressures and mass flow rates of the working fluid were measured. The measuring devices were installed at the relevant positions to obtain necessary data. Type-K thermocouples with uncertainty of ±0.5°C were installed at the points of interest as shown in figure 4.1. All of the thermocouple probes were calibrated with a precision mercury thermometer.

The saturation pressures within the condenser and the evaporator were measured by absolute pressure transducers (0-250 mbar-abs) with uncertainty of ±0.25%. All of the pressure transducers were calibrated. A double-stage high vacuum pump was employed to provide absolute zero pressure reference while the positive pressure was calibrated with a mercury manometer. A precision mercury barometer was used for barometric pressure

Digital PID temperature controllers were used to control saturation temperatures at the boiler and the evaporator. The controller sent signals to turn on/off the electric heaters to heat up the water to the desired value. The saturation pressure of the condenser was controlled by adjusting the cooling water flow rate via a flow control valve and a solenoid valve. The solenoid valve was on/off controlled by a digital pressure controller operating with a pressure transducer installed at the condenser. Moreover, the use of a water chiller for supplying the cooling water allowed the temperature to be adjusted as required.

Liquid water levels in all vessels (the boiler, the evaporator, and the receiver tank) were observed from attached sight-glasses. To feed water to the boiler and evaporator, valve V5 and valve V4 should be open, respectively. This allows the circulating pump to feed water from the receiver tank to the boiler and evaporator.

If the evaporation rates of the water inside the boiler and the evaporator were needed, valve V5 and valve V4 were closed. This allowed the liquid level in both vessels to drop over a time interval. The dropping rate of water level in the boiler and the evaporator was then converted to the mass flow rate of the primary fluid and the secondary fluid, respectively. To ensure the accuracy of the mass flow rate obtained from this method, volume and level of liquid within the boiler and the evaporator were carefully calibrated and measured using volumetric flasks and measuring cylinders. By performing error analysis, the error of 3.25% on entrainment ratio is obtained.

4.10 Experimental procedure

- Fill the boiler and the receiver tank with deionized water to approximately 1/3 of the way up a sight glass or to a sufficient amount to immerse the electric heater.
- A double-stage high vacuum pump was used to remove all air and non-condensable gases.
- Close valves V2, V3, V5 and V6 according to figure 4.1 to isolate the boiler from the rest of the system.
- Switch on the boiler heater and set the desired temperature at the digital PID temperature controller and wait until the pre-set temperature is reached.
- Turn on the cooling water system to maintain the pressure of the condenser and set the desired condenser pressure at the digital pressure controller. The cooling water flow was then regulated by an on/off solenoid valve which controlled by the digital controller
- Open valve V3 to allow the high-pressure steam to flow to the primary nozzle of the ejector.
- Switch on the superheater to avoid wet steam at the primary nozzle. Electric power input to the super heater was adjusted in order to superheat the saturated steam by 1 or 2°C before entering the primary nozzle to ensure that the primary steam remains dry.
- Turn on the magnetically coupled centrifugal pump to circulate the water within the evaporator from the bottom to the shower head at the top of the evaporator column.
- Open valve V1 to allow fluid from the evaporator to flow to the mixing chamber.
- Turn on the evaporator's electric heater and set the desired evaporator temperature at the digital PID temperature controller as the saturation temperature of the water in the evaporator continues to drop. Therefore, the water temperature in the evaporator could be maintained constant at the pre-set value.

- Flow rate of primary fluid and secondary fluid was obtained by measuring the decreasing rate of the water level via the attached sight glass during certain time intervals in steady operation.
- During this test, the make-up water was turned off by closing valves V4 and V5. This allows the evaluation of the ejector entrainment ratio at the particular operating condition.
- The critical condenser pressure was measured when the steam ejector was operated in critical operating condition.

4.11 Conclusion

This chapter provides the details of design and construction of the experimental steam ejector refrigeration system. The system was designed to provide a cooling capacity of up to 1 kW. Four mixing chambers and four primary nozzles were used. The details of ejectors and all components were provided. The instrumentation control and experimental procedure, which indicate the accuracy of the results, were also provided in detail.

CHAPTER 5
EXPERIMENTAL RESULT AND DISCUSSION

In this chapter, both CPM and CRMC ejectors were tested on the experimental steam ejector refrigerator. First, the CPM and the CRMC mixing chambers with the same design conditions were tested. Then the CPM and CRMC ejectors with the same ejector area ratios were tested and compared.

5.1 CPM and CRMC ejectors under the same design condition

This section aims to provide preliminary comparison of the experimental performance of the CRMC ejectors and the CPM ejectors under the same design input data. To investigate this, experimental results obtained from the conventional CPM ejector with throat diameter of 19 mm (CPM19.0) were used for discussion. The CRMC ejector with throat diameter of 13.4 mm (CRMC13.4) was used. The designed input data of CPM19 and CRMC13.4 were the same (boiler saturation temperature, evaporator saturation temperature, and the primary fluid critical mass flow rate). The design methods of both ejectors were provided in chapter 3. The two ejectors were tested with the same primary nozzle with throat diameter of 1.7 mm (D1.7). Hence, the CRMC ejector had an ejector area ratio of 62 while the CPM ejector had an ejector area ratio of 125. These two ejectors were tested under a fixed boiler and evaporator temperatures of 130°C and 7.5°C, respectively. The condenser pressure was varied in order to determine the critical point of operation. The results are shown in figure 5.1.

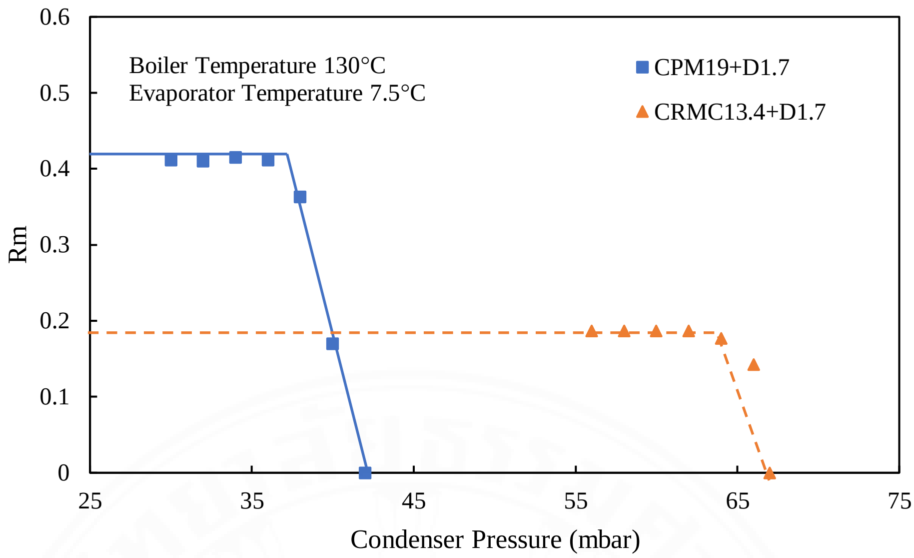

Figure 5.1 Performance of CPM19.0 and CRMC13.4

It can be seen from figure 5.1 that the CPM ejector produced a much higher entrainment ratio throughout the choked flow region compared to the CRMC ejector. However, the CRMC ejector produced a much higher critical condenser pressure than the CPM ejector. It was obvious that there was a trade-off between the entrainment ratio and the critical condenser pressure when they were compared under the different ejector area ratios. Therefore, it cannot be concluded that the CRMC ejector (CRMC13.4) is better than the CPM ejector (CPM19.0). This phenomenon commonly occurs when two ejectors are tested with different ejector area ratios even when they are the same design (Ariafar et al., 2014; Liu et al., 2017; Yapıcı et al., 2008). Performance of the ejector is considered to be improved only when the entrainment ratio or the critical condenser pressure increases, while another parameter remains the same or both of them increase. To eliminate this effect, the two ejectors must be compared under the same ejector area ratio which will provide a reasonable comparison. This will be presented in the next section.

5.2 Comparative performance of CPM and CRMC ejectors under the same ejector area ratio

5.2.1 Same area ratio via different primary nozzles throat diameters and mixing chamber ejector throat diameters

The previous section has shown that comparative performance between CRMC and CPM ejectors should not be implemented based on different ejector area ratios. This is because their performance is not comparable due to having the trade-off between the mass entrainment ratio and the critical condenser pressure. Further comparison of the two ejectors must be based on the same ejector area ratio. In this section, CPM and CRMC ejectors were compared with the same ejector area ratio. The primary nozzle with throat diameter of 2.0 mm (D2.0) was equipped with the CPM19.0 mixing chamber while the primary nozzle with throat diameter of 1.4 mm (D1.4) was equipped with the CRMC13.4 mixing chamber. Both ejectors provided approximately the same ejector area ratio of 92 as shown in table 5.1. The boiler and evaporator temperatures were maintained constant at 130°C and 7.5°C, respectively. The condenser pressure was varied to determine the critical point of operation. The results are shown in figure 5.2.

Table 5.1 Area ratio of the ejectors

Mixing chamber	Primary nozzle			
	D1.4	D1.7	D2.0	D2.4
CPM13.4 CRMC13.4	91.61 (Area ratio A)	62.13 (Area ratio B)	-	-
CPM19 CRMC19	-	-	90.25 (Area ratio A)	62.67 (Area ratio B)

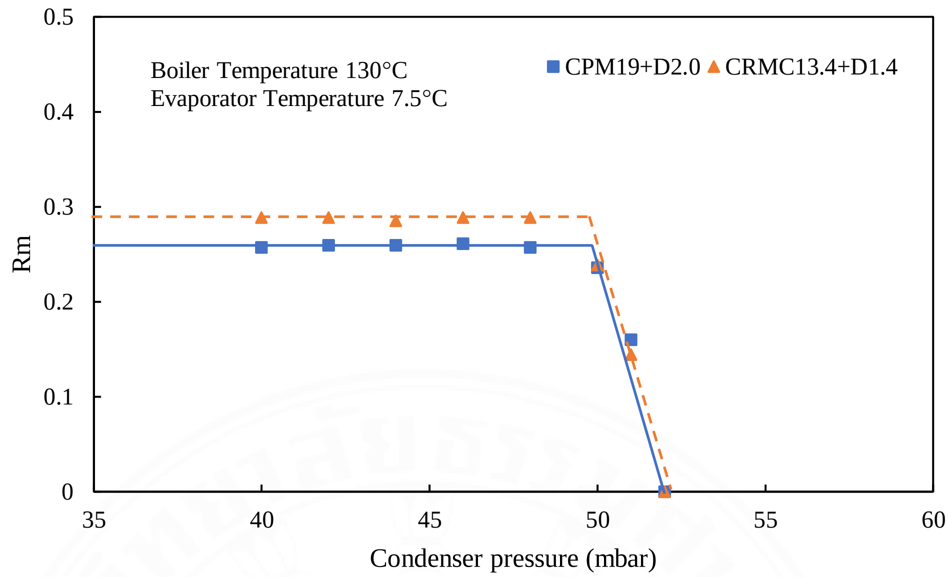

Figure 5.2 Performance of CPM and CRMC ejectors with the same ejector area ratio

It can be seen from figure 5.2 that the CRMC ejector provided a higher entrainment ratio for the choked flow region compared with the CPM ejector, while the critical condenser pressures were almost identical. This is an interesting point which has not been available from any open literature. Therefore, it may be said that CRMC13.4 provides better performance than CPM19.0 under the same ejector area ratio.

5.2.2 Same area ratio via same primary nozzle diameters and same mixing chamber throat diameters

In this section, CPM and CRMC ejectors were compared with the same ejector area ratio. Unlike the previous section, both CPM and CRMC ejectors with the same primary nozzle throat diameter and the same mixing chamber throat diameter were tested. In this test, two CPM ejectors (CPM13.4 and CPM 19) and two CRMC ejectors (CRMC13.4 and CRMC19) were tested with four primary nozzles. The mixing chambers and the primary nozzles were paired in order to achieve the area ratio of approximately 62 and 92 as shown in table 5.1.

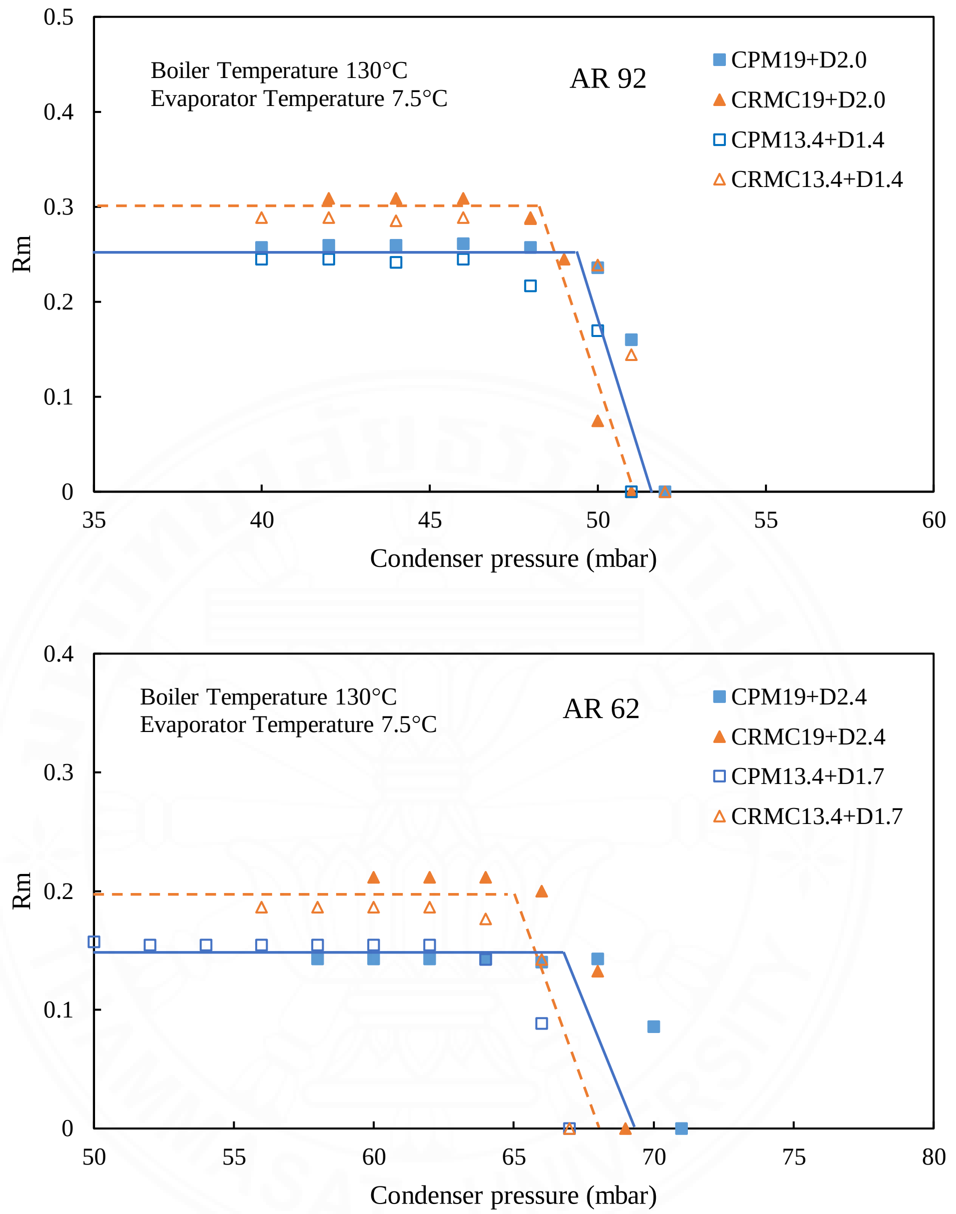

Figure 5.3 Performance of CPM and CRMC ejectors with the same ejector area ratio

From table 5.1, the CPM13.4 and the CRMC13.4 were equipped with primary nozzle D1.4 and D1.7. The area ratios for these ejector specifications were approximately 92 and 62, respectively. The CPM19.0 and CRMC19.0 were equipped with primary nozzles D2.0 and D2.4, which provided area ratios of approximately 92 and 62, respectively. The results obtained from these tests can ensure the performance comparison of CRMC and CPM ejectors at the same area ratio. The results are shown in figure 5.3.

It can be seen from figure 5.3 that, for the same design ejector, when the two ejectors have the same area ratio (even though their geometries were not the same), they provided very similar mass entrainment ratios and critical condenser pressures. When the area ratio changed from 62 to 92, the entrainment ratio increased with a trade-off in the critical condenser pressure as expected.

When comparing the CPM and the CRMC ejectors with the same area ratio, CRMC ejectors provide a significant improvement on the mass entrainment ratio while their critical condenser pressures were similar. This shows that when comparing different design ejectors (CPM and CRMC), they must be tested under the same area ratio.

5.3 Comparative performance of CRMC and CPM ejectors: effect of operating conditions

5.3.1 Effect of the boiler saturation temperature

In this section, CRMC and CPM ejectors were tested under the boiler temperature between 115°C and 140°C while the evaporator temperature was maintained constant at 7.5°C. Four CPM ejectors and four CRMC ejectors were tested. For each particular test case, the mass entrainment ratio and the critical condenser pressure were determined for comparison. Figures 5.4 and 5.5 show plots of the mass entrainment ratio in the choked flow regions versus the critical condenser pressure. In each figure, one CPM ejector and one CRMC ejector with the same area ratio and the mixing chamber throat diameter were compared.

From the figures, it can be seen that in all cases, for the same ejector area ratio, boiler temperature, and evaporator temperature, CRMC ejectors always provided higher entrainment ratio with almost identical critical condenser pressure. It can also be seen that the improvement of the entrainment ratio was more obvious when the boiler temperature was increased. In other words, the advantage of using the CRMC ejector over the CPM ejector was more obvious at relatively high boiler temperatures.

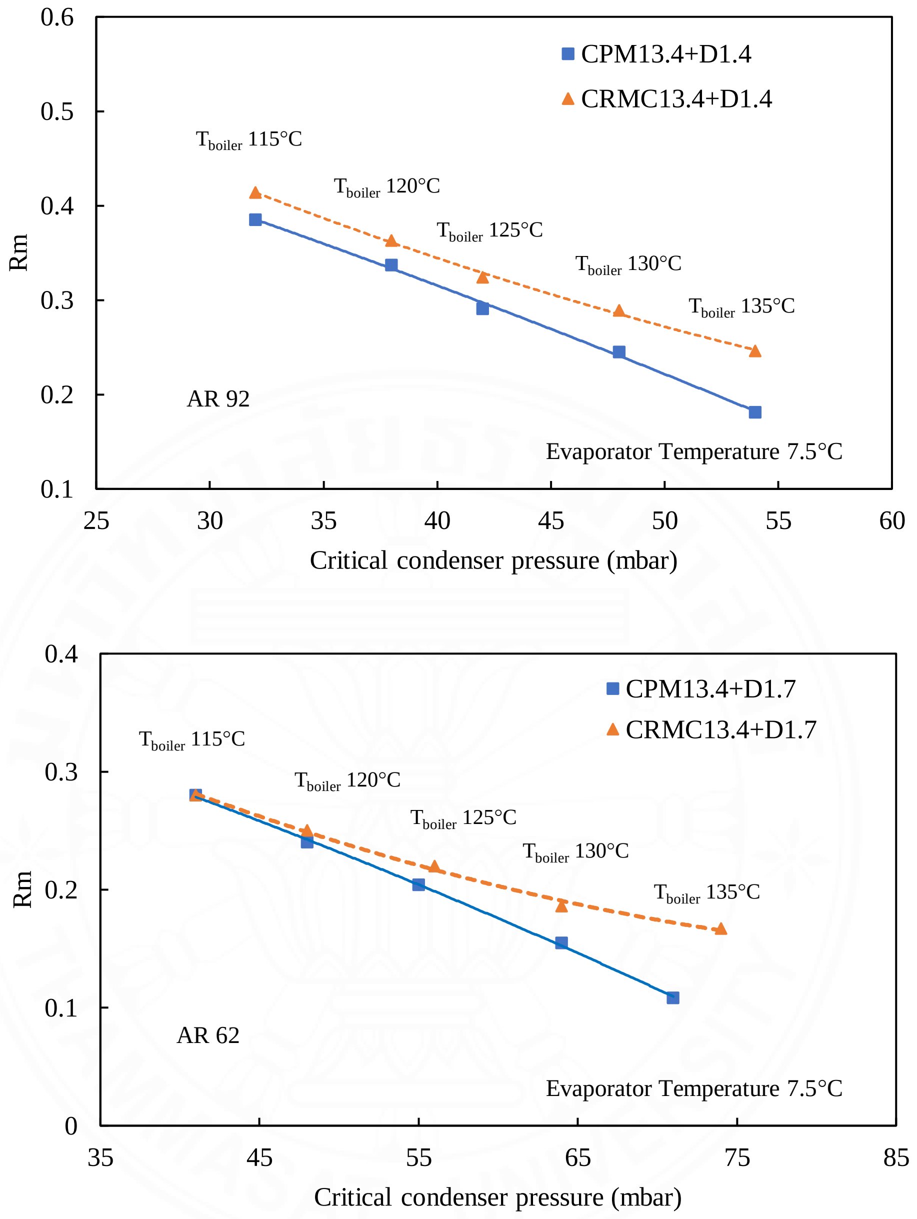

Figure 5.4 Variations of critical performance with boiler saturation temperatures of CPM13.4 and CRMC 13.4 mixing chambers

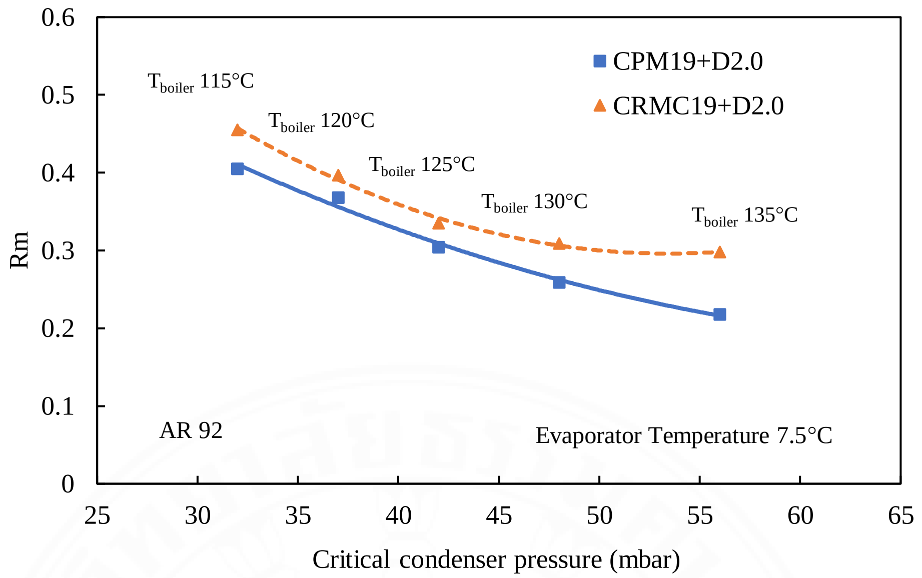

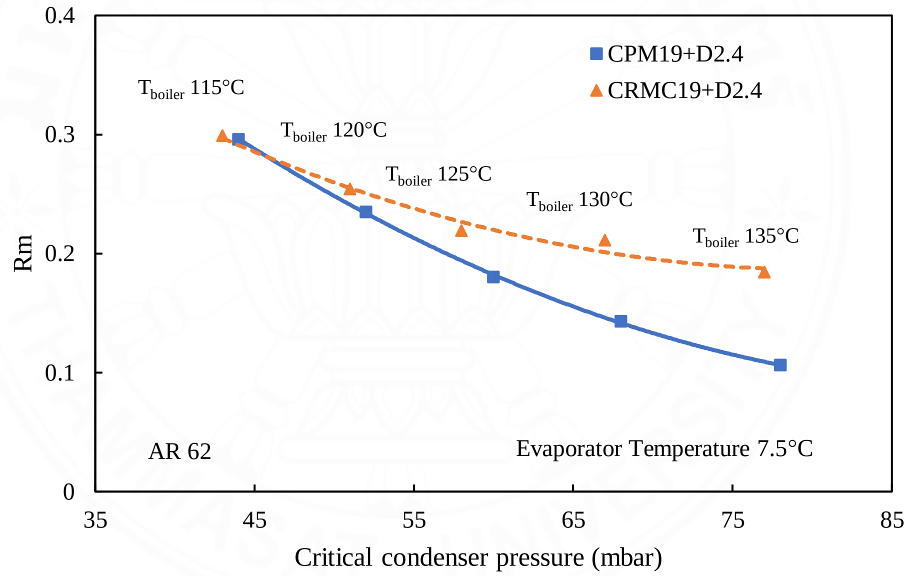

Figure 5.5 Variations of critical performance with boiler saturation temperatures of ejector CPM19 and CRMC19 mixing chambers

Another parameter that is effective for analysing the effect of primary fluid flow condition is the primary fluid expansion coefficient ($C_{primary}$) which was already discussed in chapter 2. The effect of the boiler temperature and the primary expansion coefficient on ejector efficiency (described in chapter 2) is shown in figure 5.6.

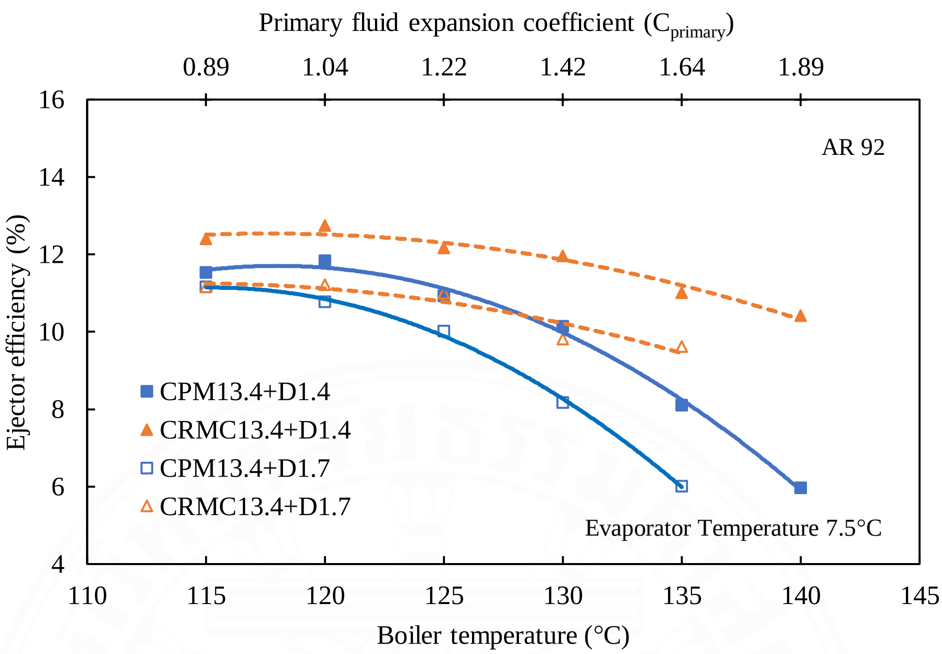

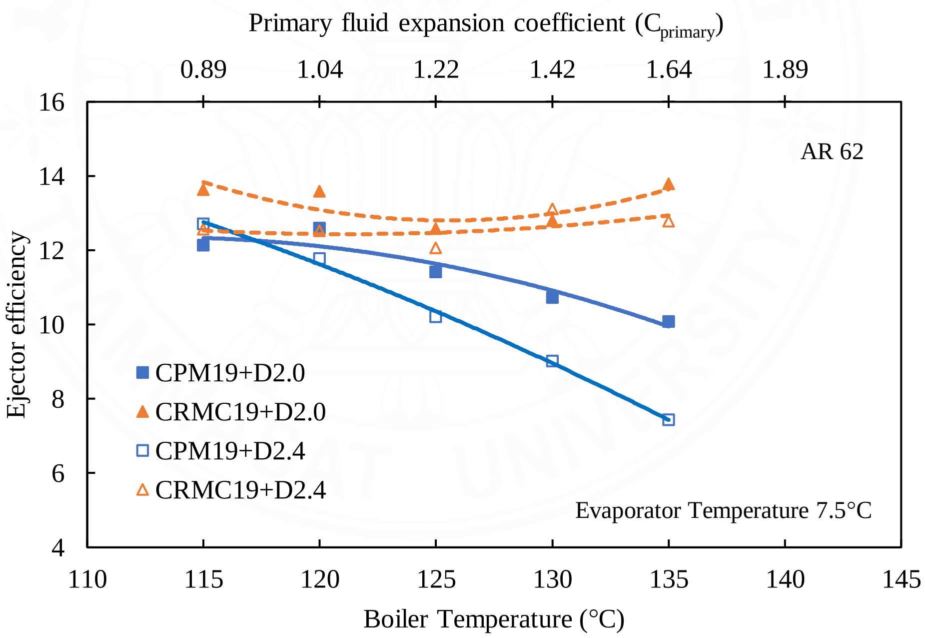

Figure 5.6 Variation of ejector efficiency with boiler temperature and primary fluid expansion coefficient

From the figure, it can be seen that the ejector efficiency for the CRMC ejector is higher than that of the CPM ejector for most of the cases. As the boiler temperature is increased, the ejector efficiency decreased, except for the case of CRMC19 (the efficiency increases with the boiler temperature). It is interesting to see that at boiler temperatures between 115°C and 120°C, at which the primary fluid expansion ratio ($C_{primary}$) has values between 0.9 to 1.04, both the CPM and the CRMC ejectors performed similarly (the performance enhancement of the CRMC ejector is at its minimal). When the primary fluid expansion coefficient value is close to 1 ($C_{primary}\approx 1$), this indicates that the primary fluid expansion is almost at a perfectly expanded state. At a perfect expansion state, the primary fluid's expansion wave experiences no shock train along the jet core as shown in figure 2.6 in Chapter 2. Therefore, the impact of shock on the expansion wave is low due to the flow being closer to isentropic flow. This results in a lower thermodynamic loss and a lower total momentum loss, and the ejector is operated at the most efficient working condition. On the other hand, when the boiler temperature is increased, the primary fluid experiences the under expansion state ($C_{primary}>1$). The primary fluid's expansion wave involves a series of expansion fans which result in further increasing the Mach number combined with the oblique weak shock wave (Sriveerakul et al., 2007b). These expansion fans are closer to the mixing chamber wall which might cause the geometry to play an important role in the entrainment process. This results in a higher ejector efficiency improvement of the CRMC mixing chamber at higher primary fluid expansion coefficient. This effect is exaggerated with the case of CRMC19 mixing chamber in which the ejector efficiency continues to rise with higher primary fluid expansion coefficient.

In this study, the minimum boiler temperature was limited at 115°C. The reason is that at such low boiler temperature, the critical condenser pressure is also low (even lower than the ambient temperature). Therefore, it is not reasonable and practical to operate a refrigeration cycle for such low condenser temperature.

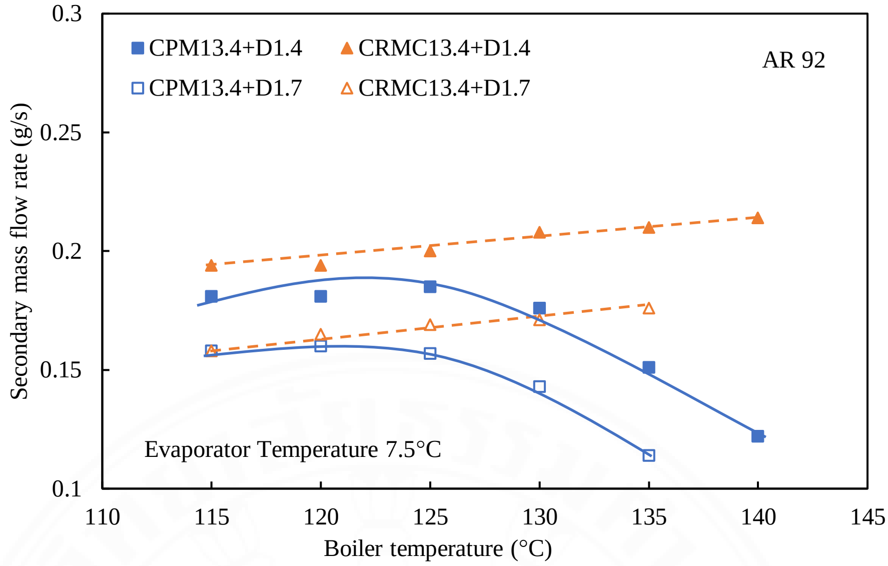

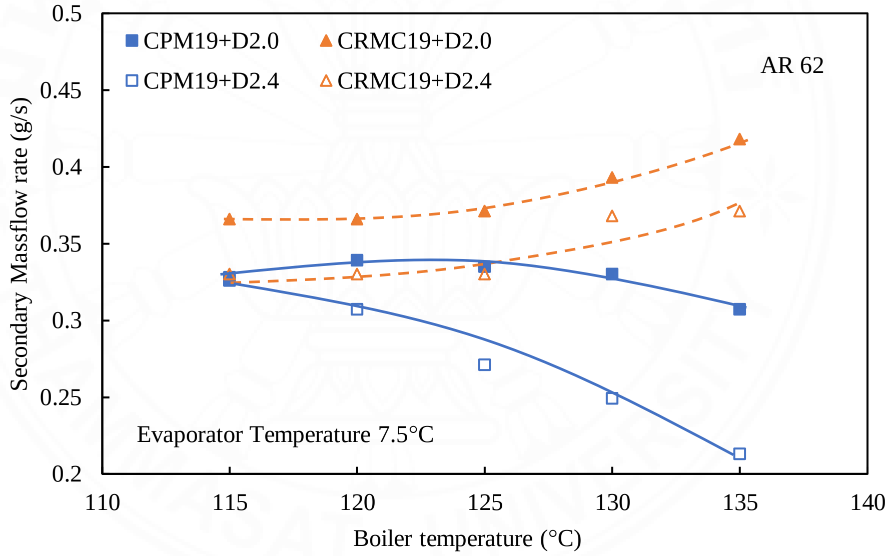

Figure 5.7 Variation of secondary fluid mass flow rate with boiler saturation temperatures

Figure 5.7 shows the variations of the secondary fluid entrained rate with the boiler temperatures. For the CPM ejector, the results agreed well with a previous work by Ruangtrakoon et al. (2011). The secondary fluid entrainment rate produced by the CPM ejector initially increased when boiler temperature increased until it reached a maximum value. Later, if the boiler temperature was increased, the entrained rate decreased. On the other hand, the CRMC ejector always produced a higher secondary entrained rate when the boiler temperature was varied ranging from 115 to 140°C, which shows that there is a significant difference between the two ejector designs in their ability to produce the entrainment process. Even though the primary fluid mass flow rate and the primary nozzle exit velocity were identical (resulting in the same primary stream momentum), the two ejectors produced different phenomenon on the entrainment process.

5.3.2 Effect of the evaporator saturation temperatures

Figure 5.8 shows the experimental results when the boiler saturation temperature was 130°C while the evaporator temperatures were varied from 5°C to 10°C. For all cases, an increase in the evaporator temperature caused the entrainment ratio and critical condenser pressure to be increased. A higher secondary fluid pressure allowed more secondary fluid to be drawn into the mixing chamber. Since the primary mass flow rate was kept constant (due to the fixed boiler saturation temperature), the mass entrainment ratio was increased. For all cases, a higher mass entrainment ratio was always obtained via the CRMC ejector whilst the critical condenser pressure of the two ejectors were similar. The improvement by the CRMC ejector was approximately the same throughout the specified range of the evaporator temperatures. This implies that the CRMC ejector can improve performance in terms of entrainment ratio at any evaporator temperature.

Figure 5.9 shows the effect of the evaporator temperature and the primary fluid expansion coefficient on the ejector efficiency. The ejector efficiency increases with increasing evaporator temperature. As the evaporator temperature increases, the primary fluid expansion coefficient is decreased. The ejector efficiency is higher when the primary fluid expansion coefficient close to 1 ($C_{primary}$≈1). This agrees well with that discussed earlier in section 5.3.1. However, the performance improvement is almost the same at all primary fluid expansion coefficients. This might be because the increase in ejector efficiency as the evaporator temperature increases is mainly due to the higher secondary fluid pressure. The impact of the primary fluid expansion might be less in this case. However, if the evaporator temperature is further increased, the effect of primary fluid expansion might be more pronounced.

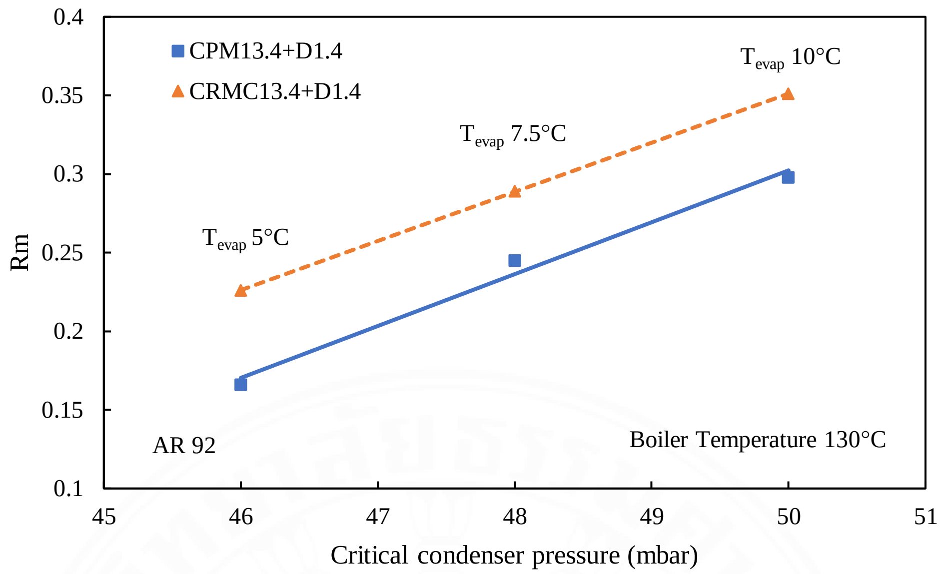

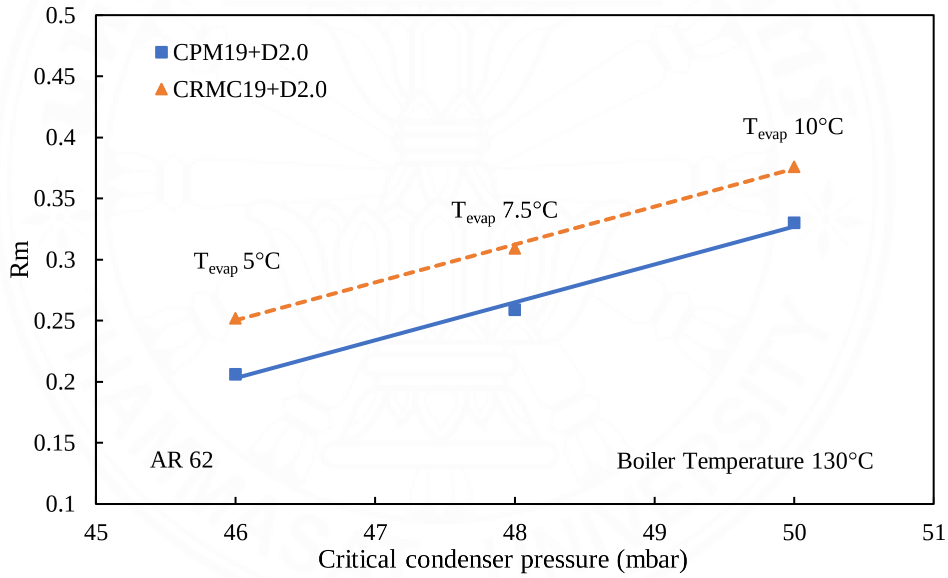

Figure 5.8 Variations of critical performance with evaporation saturation temperatures

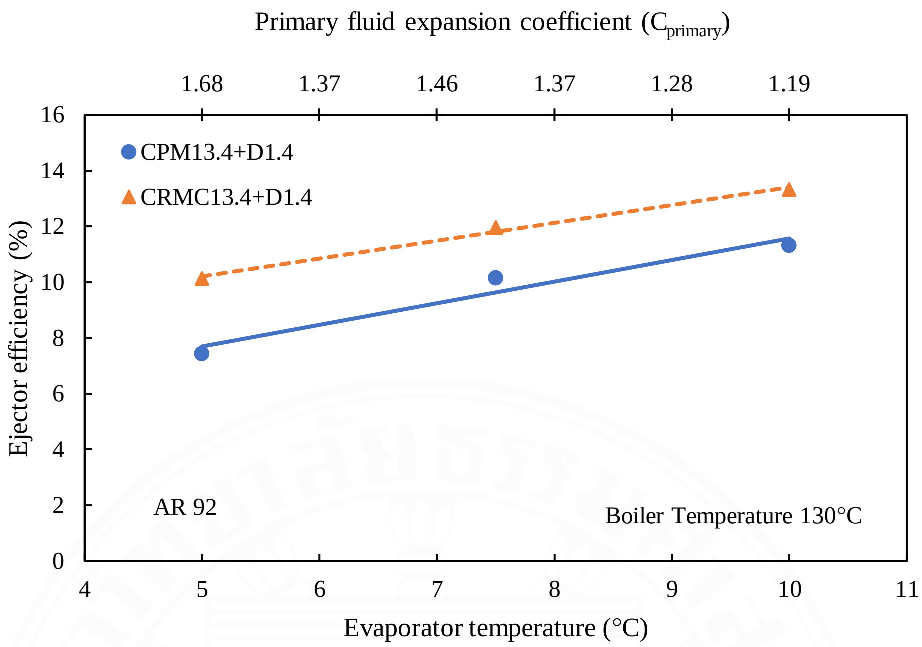

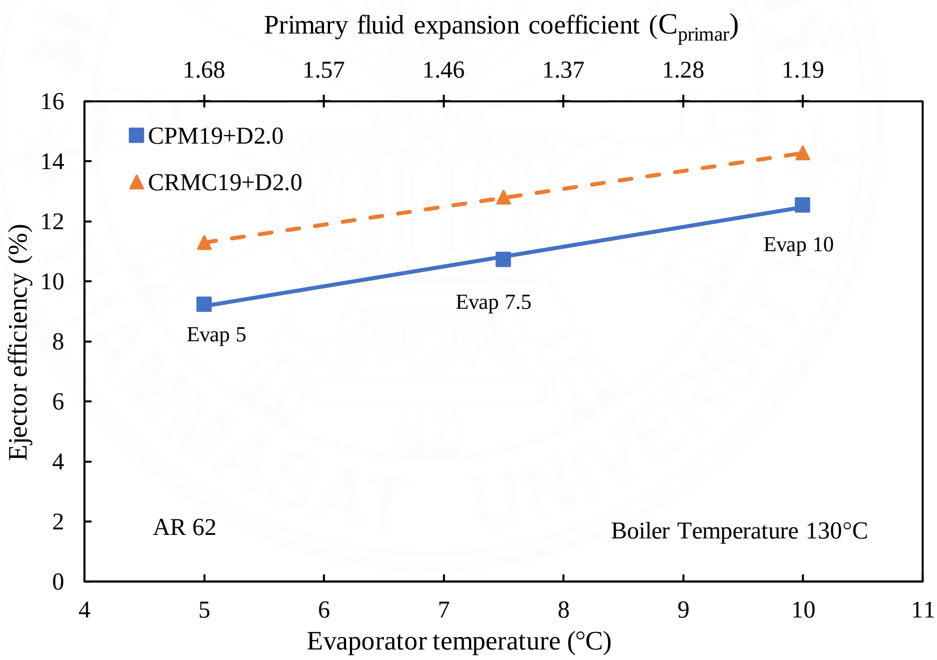

Figure 5.9 Variations of ejector efficiency with evaporator saturation temperatures and primary fluid expansion coefficient

5.3.3 Performance map

Performance maps of the CPM and the CRMC ejectors are shown in figure 5.10. A performance map is a plot of performance at the critical condenser pressure for each operated condition. This map depicts the entire performance of the ejector when working with different working conditions. Regarding the map, the boiler temperature was varied between 115°C and 135°C. The evaporator temperatures were 5°C, 7.5°C, and 10°C, respectively. It can be seen that the performance map of the CRMC ejector shifts up vertically for all cases. This implies that the CRMC ejector provides a higher entrainment ratio when the two ejectors operate with the same working conditions (the boiler temperature, the evaporator temperature, and the critical condenser pressure). Therefore, it can be concluded that, for all cases, the CMRC ejectors provide better performance (higher mass entrainment ratio without sacrificing the critical condenser pressure) compared with the conventional CPM ejectors.

Performance of the CPM and the CRMC are also summarized and tabulated in tables 5.2 and 5.3. These tables show the entrainment ratio, the critical condenser pressure, and ejector efficiency of the CPM and the CRMC ejector at various working conditions. The percentage increase of each parameter obtained for the CRMC ejector over the CPM ejectors is also shown.

For the mixing chamber with throat diameter of 13.4 mm (CRMC13.4 and CPM13.4), the maximum entrainment ratio and the ejector efficiency improvements are 54.63% and 59.90%, respectively, while the average values are 17.62% and 17.99%. For all cases, the critical condenser pressure of the two ejectors is very similar.

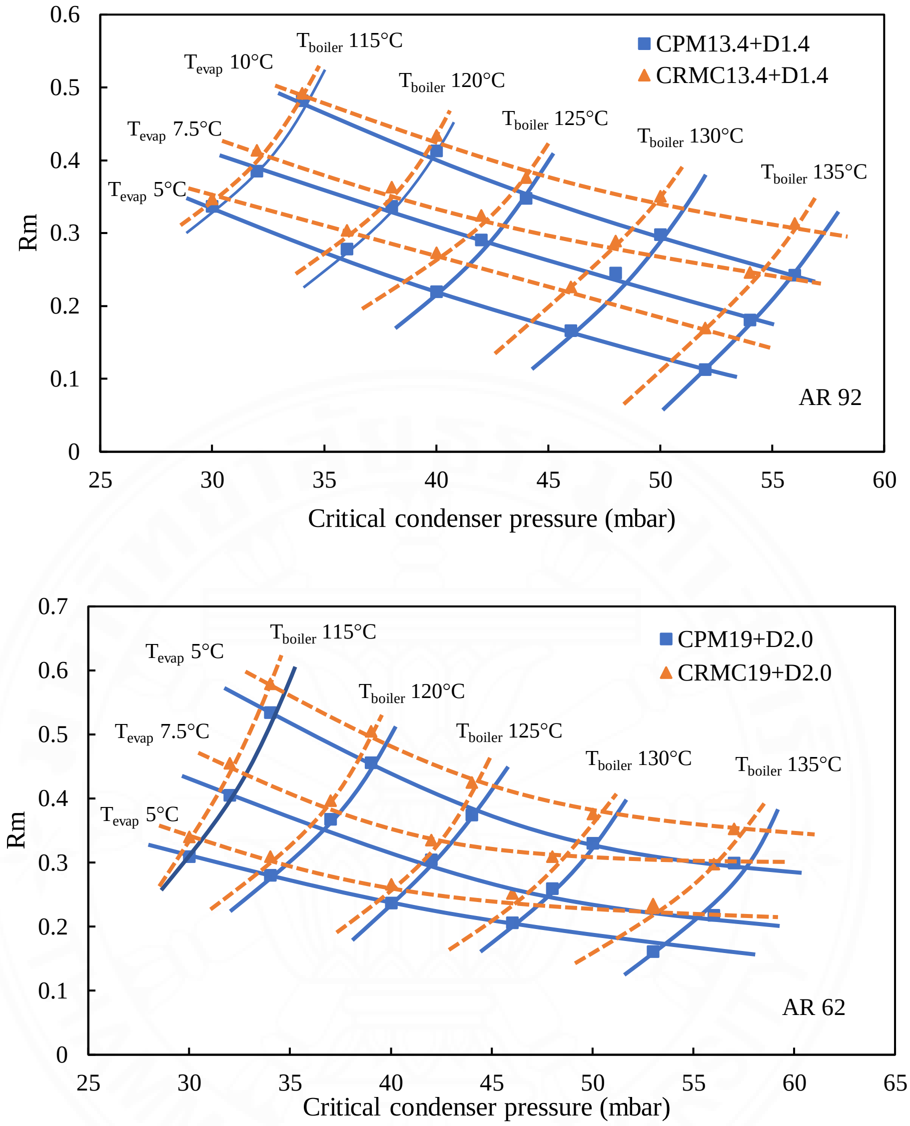

Figure 5.10 Performance map of CPM and CRMC ejector

Table 5.2 Summary of CPM13.4 and CRMC13.4 performance

Nozzle	T_{evap} (°C)	T_{boiler} (°C)	RM		P_{cir} (mbar)		$\eta_{ejector}$ (%)		% increase* (%)		
			CPM	CRMC	CPM	CRMC	CPM	CRMC	RM	P_{cri}	$\eta_{ejector}$
D1.4	5	115	0.337	0.347	30	30	10.98	11.30	2.97	0.00	2.97
		120	0.278	0.304	36	36	10.63	11.63	9.35	0.00	9.35
		125	0.22	0.273	40	40	8.97	11.14	24.09	0.00	24.09
		130	0.166	0.226	46	46	7.44	10.13	36.14	0.00	36.14
		135	0.113	0.17	52	52	5.45	8.20	50.44	0.00	50.44
	7.5	115	0.385	0.414	32	32	11.53	12.40	7.53	0.00	7.53
		120	0.337	0.363	38	38	11.83	12.74	7.72	0.00	7.72
		125	0.291	0.324	42	42	10.93	12.17	11.34	0.00	11.34
		130	0.245	0.289	48	48	10.15	11.97	17.96	0.00	17.96
		135	0.181	0.246	54	54	8.10	11.01	35.91	0.00	35.91
	10	115	0.482	0.492	34	34	13.14	13.41	2.07	0.00	2.07
		120	0.413	0.434	40	40	13.25	13.92	5.08	0.00	5.08
		125	0.348	0.376	44	44	11.97	12.93	8.05	0.00	8.05
		130	0.298	0.351	50	50	11.31	13.32	17.79	0.00	17.79
		135	0.242	0.313	56	56	9.91	12.82	29.34	0.00	29.34
D1.7	7.5	115	0.28	0.28	41	41	11.16	11.16	0.00	0.00	0.00
		120	0.24	0.25	48	48	10.77	11.22	4.17	0.00	4.17
		125	0.204	0.22	55	56	10.01	11.00	7.84	1.82	9.86
		130	0.155	0.186	64	64	8.18	9.81	20.00	0.00	20.00
		135	0.108	0.167	71	74	6.01	9.61	54.63	4.23	59.90
Average percentage increase									17.62	0.30	17.99

*% increase = (CRMC’s value – CPM’s value)/ CPM’s value×100

Table 5.3 Summary of CPM19 and CRMC19 performance

Nozzle	T_{evap} (°C)	T_{boiler} (°C)	RM		P_{cir} (mbar)		$\eta_{ejector}$ (%)		% increase* (%)		
			CPM	CRMC	CPM	CRMC	CPM	CRMC	RM	P_{cri}	$\eta_{ejector}$
D2.0	5	115	0.309	0.34	30	30	10.06	11.07	10.03	0.00	10.03
		120	0.28	0.309	34	34	10.05	11.09	10.36	0.00	10.36
		125	0.237	0.266	40	40	9.67	10.85	12.24	0.00	12.24
		130	0.206	0.252	46	46	9.23	11.29	22.33	0.00	22.33
		135	0.161	0.235	53	53	7.91	11.55	45.96	0.00	45.96
	7.5	115	0.405	0.455	32	32	12.13	13.63	12.35	0.00	12.35
		120	0.368	0.397	37	37	12.59	13.58	7.88	0.00	7.88
		125	0.304	0.335	42	42	11.42	12.58	10.20	0.00	10.20
		130	0.259	0.309	48	48	10.72	12.80	19.31	0.00	19.31
		135	0.218	0.298	56	56	10.08	13.78	36.70	0.00	36.70
	10	115	0.534	0.579	34	34	14.55	15.78	8.43	0.00	8.43
		120	0.456	0.505	39	39	14.22	15.75	10.75	0.00	10.75
		125	0.374	0.425	44	44	12.86	14.61	13.64	0.00	13.64
		130	0.33	0.376	50	50	12.53	14.27	13.94	0.00	13.94
		135	0.299	0.353	57	57	12.49	14.75	18.06	0.00	18.06
D2.4	7.5	115	0.296	0.299	44	43	12.71	12.56	1.01	-2.27	-1.16
		120	0.235	0.254	52	51	11.77	12.53	8.09	-1.92	6.40
		125	0.18	0.219	60	58	10.20	12.06	21.67	-3.33	18.15
		130	0.143	0.211	68	67	9.01	13.11	47.55	-1.47	45.53
		135	0.106	0.184	78	77	7.43	12.77	73.58	-1.28	71.84
Average percentage increase									20.20	-0.51	19.65

*% increase[a] = (CRMC's value – CPM's value)/ CPM's value×100

For the mixing chambers with throat diameter of 19 mm (CRMC19 and CPM19), the maximum entrainment ratio and the ejector the efficiency improvement are 73.58% and 71.84%, respectively, while the average values are 20.20% and 19.65%. In conclusion, it could be said that on the whole, the CRMC ejector always provides superior performance compared with the CPM ejector. In all cases, it can be noted that the performance improvement (mass entrainment ratio and ejector efficiency) of using CRMC ejectors over CPM ejectors increases with the boiler saturation temperature.

It can be seen that at the boiler temperature of 115°C, the improvement is very small. The CRMC ejectors perform very similar to the CPM ejectors. However, at the boiler temperature of 135°C, the CRMC ejectors provide much superior performance over the CPM ejectors. The improvement as high as 70% is possible (average improvement is around 20% for both the mass entrainment ratio and the ejector efficiency). It may be concluded that at relatively low boiler temperature and when the primary fluid expansion coefficient is around unity, the CRMC ejectors and the CPM ejector perform very similarly and either type of ejector can be used. However, when boiler temperature is relatively high (the primary fluid expansion coefficient is greater than one), CRMC ejectors perform much better than CPM ejectors. Therefore, CRMC ejector should be used.

5.4 Comparison between 1-D theory and CRMC theory

As explained earlier, even though the CRMC design theory was intended to mitigate the impact of the compression shock wave on the pressure recovery process, it did not provide an advantage on the critical condenser pressure. It might be because the shock wave was still found somewhere in the mixing chamber of the CRMC ejector. Therefore, the CRMC ejector did not gives advantage to the critical condenser pressure. However, the experiment has proven that at identical area ratio, there is a significant improvement in the mass entrainment ratio via the CRMC ejector when compared with the CPM ejector. As discussed in section 5.2, an improvement in the mass entrainment ratio via the CRMC ejector was the cause of lower primary stream momentum loss due to the jet stream flowing through the curved profile variable area duct. This implies an ejector design based on the CRMC method will produce a lower mixing loss (or a higher mixing chamber efficiency) which is indicated by producing a higher mass entrainment ratio under the same critical condenser pressure.

In this section, a CPM ejector model which is known as a one-dimensional ejector model (1-D theory) which was first proposed by Keenan et al. (1950) is considered. This model was later modified to include loss coefficients in the primary nozzle (η_{nozzle}) and the mixing chamber (η_{mix}) by Ruangtrakoon and Aphornratana (2019). This model, together with the CRMC ejector model proposed by Eames (2002), was compared with the experimental results. Moreover, various mixing chamber efficiencies for the CPM model were employed. The main purpose is to alternatively demonstrate that improvement potential via the CRMC ejector is really caused by a lower momentum loss (higher mixing efficiency) during the momentum transfer process under the same critical condenser pressure.

Figure 5.11 shows the comparison of the results as stated above. It reveals that for the CRMC ejector, the calculated results are much higher than the tested results under the same critical condenser pressure. This confirms that CRMC theory is not close to the real scenarios of the ejector operation. This is because the shock wave is still found in the mixing chamber which is the major reason why the experimental result is far beyond the calculated result under the same critical condenser pressure. More interestingly, the calculated results based on 1-D theory under different mixing efficiency are close to the experimental results from both the CPM and the CRMC ejectors. It can also be seen that the experimental entrainment ratio obtained from the CPM ejector agrees well with that obtained from 1-D theory with mixing efficiency of 90%. Meanwhile, the experimental results obtained from the CRMC ejector agree well with those obtained from 1-D theory with mixing chamber efficiency of around 90% at a relatively low critical condenser pressure and almost 100% at a relatively high critical condenser pressure.

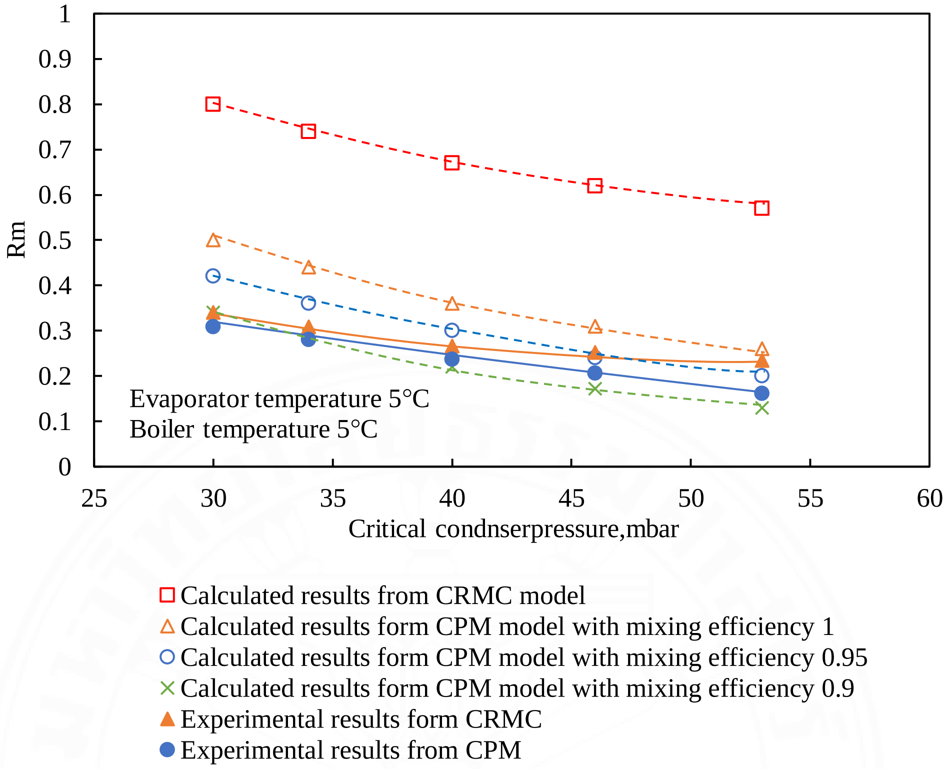

Figure 5.11 Comparison between calculated and experimental results for CPM and CRMC ejectors

It is interesting to see that the experimental mass entrainment ratio obtained from the CRMC ejector is approximately 20% higher than that obtained from CPM ejectors at the critical condenser pressure below 40 mbar. The improvement of the CRMC ejector increases to almost 40% when the condenser pressure is higher than 50 mbar. This implies that the CRMC ejector provides a higher mixing chamber efficiency because the entrainment ratio is well predicted by the 1-D model with mixing chamber efficiency around 95%.

From comparisons of the experimental results obtained from both the CPM and the CRMC ejectors with the calculated values based on 1-D theory, it seems that the experimental entrainment ratio obtained from the CRMC ejector is similar to that calculated from the 1-D model with a higher mixing chamber efficiency. Experimental performance obtained from the CRMC ejector is far from that calculated from the CRMC model. This indicates that the CRMC ejector can enhance the ejector performance because the curved profile variable area duct (CRMC ejector) provides a lower mixing loss (higher mixing chamber efficiency) compared to the conventional conical duct mixing chamber (CPM ejector). Therefore, the authors believe that 1-D theory can be used to predict the critical performance and the ejector throat of both the CPM and the CRMC ejectors. The key parameter to the accuracy of design is the mixing chamber efficiency.

To design a CRMC ejector, the 1-D theory with higher mixing efficiency can be used to calculate the mixing chamber throat diameter. To obtain the curved profile variable area duct, the design method proposed by Eames (2002) may be used. However, the authors believe that any curved profile variable area duct will provide a higher mixing chamber efficiency than that of a CPM ejector with a conventional conical duct. This should be further investigated through both experiments and CFD analysis.

As discussed in this section, ejectors designed based on the CRMC method produce a lower primary fluid momentum loss during the mixing process. This results in a higher mixing chamber efficiency as considered in 1-D design theory by Ruangtrakoon and Aphornratana (2019). The reason is that a curved variable flow area duct results in a gradual change in velocity and pressure. This has caused the momentum loss to be reduced. This demonstrates that the CRMC ejector is key to mitigate the primary momentum loss which yields a better mixing chamber efficiency.

5.5 Conclusion

A comparative performance of the steam ejectors designed based on the CRMC theory with those designed based on CPM theory under identical ejector area ratio was investigated experimentally. The purpose was to demonstrate the improvement potential of the CRMC ejectors over the CPM ejectors. From the tests, it was found that the entrainment ratio produced by the CRMC ejector was always higher than the CPM ejector throughout the range of the specified operating conditions. The entrainment ratio was increased 17.62% and 20.20% on average for mixing chamber throat diameter of 13.4mm and 19mm, respectively. It was also found that the critical condenser pressure of the two ejectors was similar under various operating conditions. The significant new findings from the experiment can be summarized as:

- The compression shock wave might still be present in the flow process of the CRMC ejector. This is in contrast to the design theory of the CRMC ejector. Hence, there is no improvement in the critical condenser pressure.
- The mass entrainment ratio via the CRMC ejector obtained from experiment is much lower than that obtained from design theory under the same critical condenser pressure. However, it is always higher than the CPM ejectors.
- It is possible that the CRMC ejector is a CPM ejector with higher mixing chamber efficiency.
- At relatively low boiler temperature ($C_{primary} \approx 1$), the CRMC and the CPM ejectors perform very similarly, thus either type of ejector can be used. However, when boiler temperature is relatively high ($C_{primary} > 1$) CRMC ejectors perform much better than CPM ejectors. Therefore, CRMC ejectors should be used.

The experimental results have shown that the ejector designed based on the CRMC theory is beneficial. This is a way to improve the overall performance of the steam ejector refrigerator. It is evident from the experiments that an improvement potential via using CRMC ejector is not related to the disappearance of the shock wave since the critical condenser pressure is almost the same as it is for the CPM ejector. However, further investigation to demonstrate the fluid flow inside of CRMC ejector (via CFD simulation) is needed to provide a better understanding of the improvement potential.

CHAPTER 6
COMPUTATIONAL ANALYSIS

In this chapter, an introduction of the computational fluid dynamics (CFD) technique is presented. CFD is employed to simulate the flow characteristics of the two fluid streams (primary and secondary fluid) travelling through the ejector. This is so that their flow phenomenon can be visualized graphically. The aim is to employ CFD for alternatively examining the ejector performance influenced by operating conditions and ejector geometries. In addition, it is also used to predict the ejector performance (in terms of entrainment ratio and critical condenser pressure) at various working conditions. Thus, CFD simulation is recognized as an efficient tool to predict ejector performance and performance assessment. In this work, CFD simulation was alternatively used to explain the reason why the CRMC ejector provides advantage over the CPM ejector. This was due to the limitation of the experiment in which the flow characteristics of the supersonic stream were not visualized accurately. Hence, the detail of developing the CFD modelling is explained as a separate topic in this chapter. The strategy to create the physical model of ejector (geometry with grid elements) and to implement the solver setup are provided.

The CFD model's simulated results obtained from CFD simulation were validated with the experimental data obtained from conducting the experiments to ensure that the model has been developed correctly. During the validation, the mass entrainment ratio and the critical condenser pressure were considered for indicating the accuracy of performance prediction via CFD simulation.

The results obtained from the CFD simulation were used to explain the phenomenon of the experimental result in chapter 5.

6.1 CFD Modelling for steam ejector

In this present work, CFD simulation was employed to simulate the flow behaviour of two fluid streams (primary and secondary fluid) travelling through the ejector. The aim was to use it for predicting the ejector performance (in terms of Rm and critical discharge pressure) and employing the graphic contour obtained from simulation to assess ejector performance at various working conditions. To develop the

CFD modelling for simulation, Ansys Fluent was used. Ansys Fluent provides a package called Workbench for creating the geometry and the mesh modelling (physical model with grid and simulation of the flow behaviour through iteration). In addition, by using Ansys Fluent the prediction of ejector performance could be made and the graphic contour representing the supersonic stream flow behaviour could be established. The procedure for implementing CFD simulation is illustrated by the flow chart shown in figure 6.1.

6.1.1 Assumption of CFD modelling

Normally, to analyse the fluid dynamics problem, all necessary assumptions must be provided. The assumptions of supersonic flow through the steam ejector are provided as follows:

- The flow was assumed to be steady and two–dimensional compressible flow
- The flow was turbulence flow.
- The density of working fluid used was based on ideal gas.
- The flows at all inlets were accelerated from their stagnation state.
- Wall boundary condition of an ejector was set as adiabatic wall which was a stationary and non–slipped surface.

6.1.2 Creating geometries and grid generation

To create the physical model of a steam ejector, DesignModeler was used. The physical dimension of the steam ejector used was taken from an experimental test ejector as illustrated in figure 4.5. Then the mesh was generated in the meshing program provided in the Ansys Workbench.

The physical model of an ejector was constructed based on two-dimensional axis–symmetrical geometry (2–D axis–symmetry), which was axis–symmetrical along the ejector's axis. Only the upper part was adequately constructed when the 2–D axis symmetrical model was chosen. Commonly, the ejector's physical model should be developed based on three dimensional geometry (3–D); however, the work by Pianthong et al. (2007) indicates that using a 2–D axis–symmetry model produced simulated results identical to the case of using a 3–D model. Moreover, using a 3–D model requires much longer time for calculation than using 2–D axis–symmetry (it must require high performance CPU). Their study could be used to guarantee that using 2–D axis–symmetry is adequate to implement CFD simulation for the fluid flow inside the ejector.

A 2–D axis–symmetry model of the ejector was later meshed by the meshing program provided in the Ansys Workbench. The quadrilateral grid element was selected because it is regarded as the most suitable form of grid for supersonic flow application. For one particular case, three different numbers of grids were applied to the physical model. This aimed to prove that the simulated results were independent of the number of grid elements. A dense grid was concentrated on the near wall and the significant area where the shock expansion wave and mixing process were expected to occur. In this present work, the mesh was implemented in an attempt to obtain the wall y+ value of between 10 and 65. The wall y+ value was a non-dimensional distance similar to local Reynolds number, often used in CFD to describe how coarse or fine a mesh is for a particular flow. The use of this value of wall y+ was so that the medium resolution of the mesh could be used, resulting in the reduction of the computational cost. In addition, it was consistent with the case of using the standard wall function as the near wall treatment. The effect of the wall y+ on the simulated results was well demonstrated by Besagni and Inzoli (2017). From the grid independent analysis, the physical models with grid elements of approximately 2,6000 elements were used. This used the reasonable computing time without sacrificing the accuracy of the simulation result. The typical physical model with grid elements (calculation domain) is shown in figure 6.2.

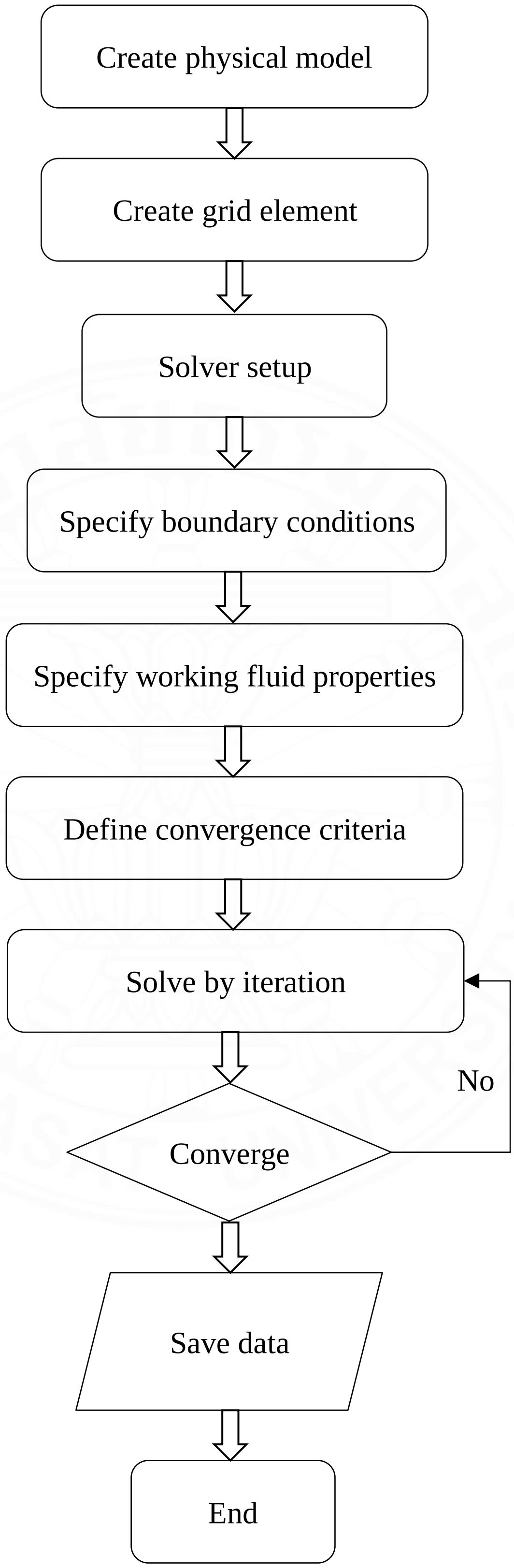

Figure 6.1 Flow chart of implementing the CFD simulation

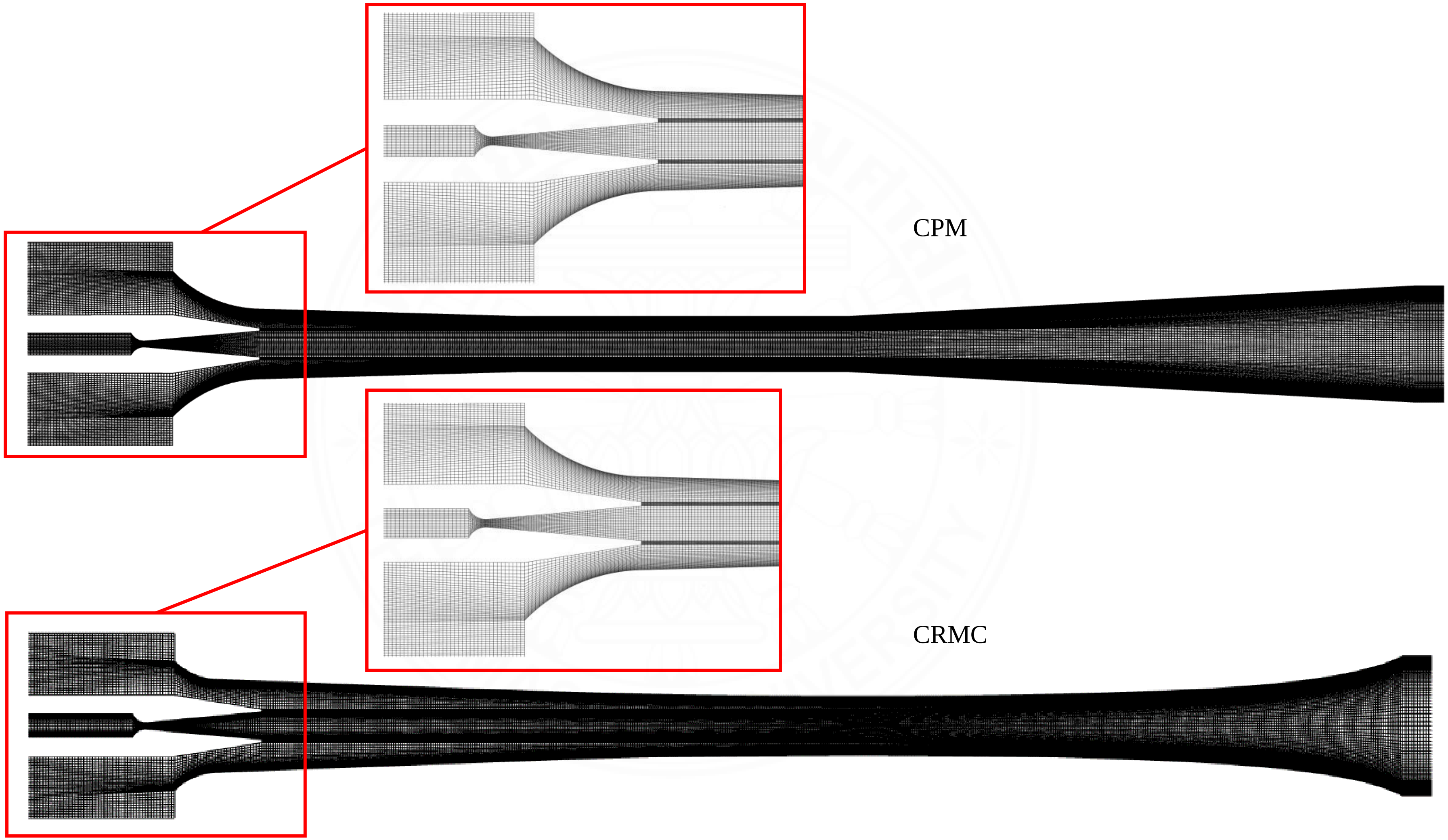

Figure 6.2 Geometries and grid of the CPM and CRMC ejectors

6.1.3 Numerical setting

The flow processes occurring inside the ejector were considered as steady state; two dimensional and adiabatic with a no slip condition; and no work done. The inlet velocity of the primary and secondary fluid and outlet velocity at the ejector discharge were neglected. The fluid flow field inside the ejector was recognized as compressible and turbulent. In such a case, the governing relationships for the three major unknown variables; temperature (T), pressure (P) and the velocity vector (ν); which describe the compressible flow of an isotropic Newtonian fluid, are given by the equations for the conservation of mass (continuity), momentum and energy, in the form of a set of partial differential equations.

Continuity equation:

$$\frac{D\rho}{Dt} + \rho\nabla.\nu = 0 \tag{6.1}$$

Momentum equation:

$$\rho\frac{D\nu}{Dt} = -\nabla P + \nabla.\sigma + \rho g \tag{6.2}$$

Energy equation:

$$\rho\frac{Dh_o}{Dt} = \frac{DP}{Dt} - \nu\Delta P + \nabla.(k\nabla T) + \nabla.(\sigma.\nu) + \rho g.\nu + \rho\dot{q} \tag{6.3}$$

In this present work, Ansys Fluent was employed to solve the 2D axis-symmetrical domain with Reynolds Averaged Navier Stokes (RANS) equations for the turbulent compressible Newtonian fluid flow. The governing equations were discretized as follows. The second order upwind scheme was used for the spatial discretization, in order to limit the numerical diffusion. The turbulence quantities also were evaluated by the second order upwind scheme. Gradients were evaluated by a least-squares approach. After the discretization process of the governing equations, a system of algebraic equations was solved by a “pressure-based coupled solver”. This algorithm solves the continuity, momentum, energy and the necessary equations simultaneously. The formulation of the coupled algorithm requires setting up a Courant-Friedrichs-Lewy (CFL) condition. This condition was needed to prevent the solution from diverging at the first integration steps. A CFL of 0.5 was used for the first 300 steps, and later gradually increased to a value of 5.0.

6.1.4 Turbulence viscosity model and near-wall-treatment

The used of the turbulent viscosity model and near wall treatment usually affects the simulated results. Therefore, the effect of using different turbulence models on the ejector performance was investigated, which was well documented by Besagni and Inzoli (2017). In this present work, the turbulent viscosity model “k -ω-SST” was used to govern turbulent flow characteristics. This turbulence model has been widely used for the flow inside the ejector as supported by previous works, (Besagni et al., 2021; Besagni & Inzoli, 2017; Chandra & Ahmed, 2014; Milazzo et al., 2014; Sriveerakul et al., 2007a). Additionally, the work proposed by Ruangtrakoon et al. (2013) showed that the “k -ω-SST” provided a reasonably accurate result for a steam ejector.

There are many options for modelling the near wall treatment: standard wall function; non-equilibrium wall-function; and enhanced wall treatment. The effect of using different near wall treatments on the ejector performance was implemented by some researchers, (Besagni & Inzoli, 2017; Besagni et al., 2015). Valuable research on the near wall treatment was conducted by Besagni et al. (2015). However, (Ruangtrakoon et al., 2013) showed that for the case of using steam as the working fluid, the standard wall function provided reasonably accurate results in terms of mass entrainment ratio and critical discharge pressure. Therefore, “standard wall function” was selected to combine with the turbulent viscosity model in order to efficiently simulate the flow close to the wall.

6.1.5 Working fluid

Table 6.1 The working fluid properties

Properties	Value
Viscosity, (kg/m.s)	1.34×10^{-5}
Thermal conductivity, (W/m.k)	0.0261
Specific heat, (J/kg.K)	2014
Molecular weight, (kg/kmol)	18.01534

The working fluid used for this present work was steam. The density of the working fluid was assumed as an ideal gas whose density was delivered by the ideal gas equation of state. As the working condition of this present work, the ideal gas assumption was supported by many researchers (Chandra & Ahmed, 2014; Ruangtrakoon et al., 2013; Sriveerakul et al., 2007b). The reason for using an ideal gas assumption was to avoid the difficulty of a real gas equation of state, which requires much longer time for simulation; moreover, it was sometimes difficult to reach a convergence criterion. Other physical properties at atmospheric pressure and temperature of 25°C (which was thermal conductivity, specific heat capacity and viscosity) were used for implementing the simulation. The summary of working fluid properties is tabulated in table 6.1.

6.1.6 Boundary condition

The boundary conditions at the upstream of the calculation domain (primary nozzle inlet face and suction chamber inlet face) were specified by "Pressure – inlet type" while "Pressure–outlet type" was applied to the downstream (diffuser outlet face). These boundary conditions have been proven suitable for supersonic flow fields as supported by previous works (Besagni et al., 2021; Besagni & Inzoli, 2017).

The turbulent intensity of 5% was applied to the inlet face of the calculation domain (inlet face of the primary and secondary fluid). Meanwhile, the turbulent intensity of 10% was applied to the outlet face. The turbulent viscosity ratio of 10 was defined for both inlet and outlet faces. The value of the turbulent intensity and turbulent viscosity ratio recommended for this particular case was supported by Fluent's user guide (Fluent, 2011). However, even though the variation of the turbulent intensity affects the simulated results, it did not provide significant impact on the global ejector performance for this present work (due to providing less impact on the simulated results in term of the mass entrainment ratio and critical discharge pressure). Since this present work aimed to use CFD simulation as a tool for visualising the flow inside the ejector, the results obtained were satisfactory for further implementation.

Because heat loss and gain at wall surfaces has less impact on the ejector performance, all wall surfaces were then set as "adiabatic wall". This is to avoid the complexity of heat transfer equations. Additionally, the wall is also set as no-slip.

6.1.7 Convergence criteria

The simulation is considered to be converged when the following criteria are satisfied:

- Summation of mass flux across the inlet and outlet face is almost zero, which means that the flow is based on the conservation of mass. For this present work, summation of mass flux must be lower than 10^{-7} kg/s.
- Calculation residuals of the significant coefficient must be lower than 10^{-6} for achieving the reasonable results

6.2 Validation of the mass entrainment ratio and critical discharge pressure

To demonstrate the proficiency in predicting the mass entrainment ratio and the critical discharged pressure (condenser pressure) via CFD simulation, many simulation case studies by means of the CRMC and CPM ejector were carried out for validation. The mass entrainment ratio and critical condenser of the two ejectors under identical operating conditions and primary nozzle geometries were considered for validation. The percent error between the CFD results and experimental results under the same working condition were also determined to indicate the accuracy via CFD simulation. The validations were implemented under the boiler temperature of 115ºC to 130ºC while the evaporator was fixed at 5 ºC, 7.5 ºC, and 10 ºC. Validations of the results and percent error are depicted in Tables 6.2 and 6.3.

Table 6.2 shows the comparison of the mass entrainment ratio (Rm) and the critical condenser pressure of the CPM and CRMC ejectors with throat diameter of 13.4 mm under the same boiler and evaporator temperatures. Table 6.3 shows the results obtained from an ejector with mixing chamber with throat diameter of 19 mm. It is seen that there is a slight difference in errors between the CFD results and experimental results. The error of the entrainment ratio is 5.21 to 22.22% depending on the operating boiler temperature and ejector geometry. The error of the critical condenser pressure ranges from 0 to 12.9% depending on the operating boiler temperature and ejector geometry. From table 6.2, the average percentage error of the entrainment ratio and critical condenser pressure are 13.63% and 6.78%, respectively. From table 6.3, the average percentage error of the entrainment ratio and critical condenser pressure are 13.63% and 6.78%, respectively.

The comparison between the CFD and the experimental results of the entrainment ratio and critical condenser pressure at various operating conditions and ejector geometries are shown in figures 6.3 and 6.4, respectively. In figure 6.3, the CFD results are mostly higher than the experimental result. On the other hand, the simulated critical condenser pressure is mostly lower than the experimental result. For both entrainment ratio and critical condenser pressure, the CFD and experimental result are close to each other when the value is low. As the value increases, the CFD results diverge from the experimental result. This mean the simulated result is more accurate at lower critical condenser pressure and entrainment ratio.

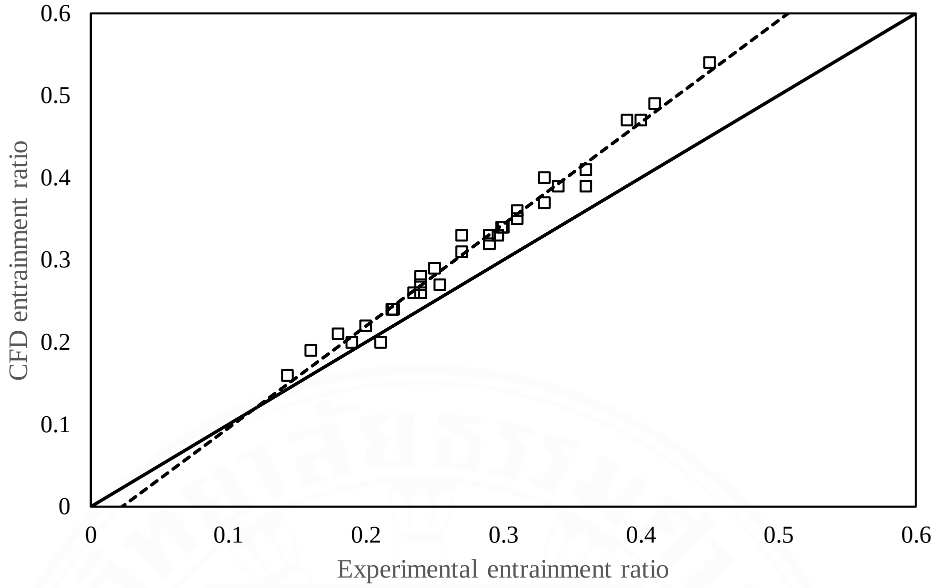

Figure 6.3 Comparison between the CFD and the experimental results of the entrainment ratio at various operating conditions and ejector geometries

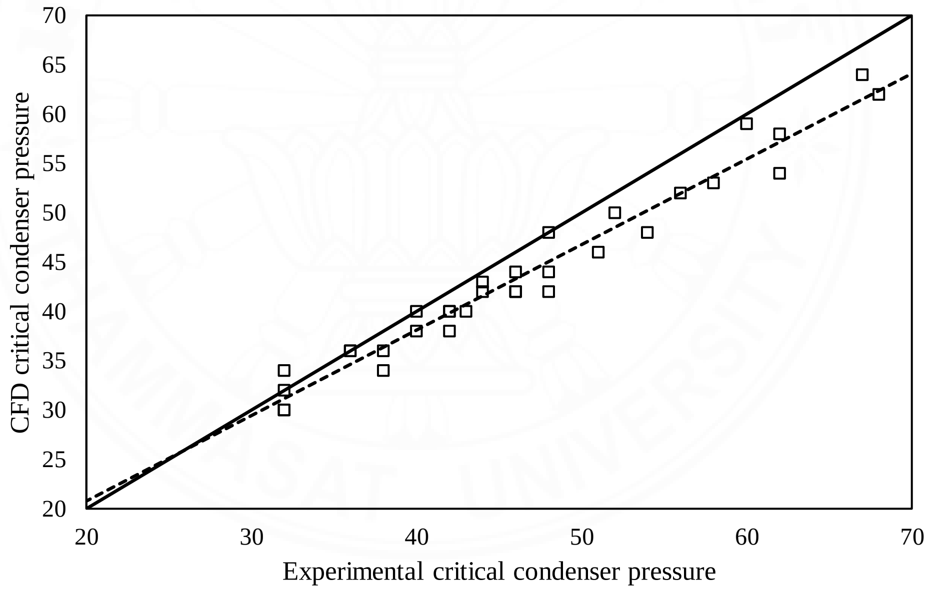

Figure 6.4 Comparison between the CFD and the experimental results of the critical condenser pressure at various operating conditions and ejector geometries

Table 6.2 Validation of experimental and CFD result of ejector with mixing chamber throat diameter of 13.4 mm

Primary nozzle	Mixing Chamber	Boiler Temp.	Entrainment Ratio		% error*	Critical condenser pressure		% error*
			Exp.	CFD		Exp.	CFD	
D1.4	CPM13.4	115	0.39	0.39	14.71	32	30	6.25
		120	0.34	0.37	12.12	38	34	10.53
		125	0.29	0.33	13.79	42	38	9.52
		130	0.25	0.28	16.67	46	42	8.70
	CRMC13.4	115	0.41	0.49	19.51	32	34	6.25
		120	0.36	0.41	13.89	38	36	5.26
		125	0.32	0.36	16.13	44	43	2.27
		130	0.29	0.32	10.34	48	48	0.00
D1.7	CPM13.4	115	0.28	0.31	14.81	40	38	5.00
		120	0.24	0.26	8.33	46	42	8.70
		125	0.2	0.22	10.00	54	48	11.11
		130	0.16	0.19	18.75	62	54	12.90
	CRMC13.4	115	0.28	0.33	22.22	40	40	0.00
		120	0.25	0.27	12.50	48	44	8.33
		125	0.22	0.24	9.09	56	52	7.14
		130	0.19	0.2	5.26	62	58	6.45
Average % error					13.63			6.78

*% error = 100× (CFD result-experimental result)/ experimental result

Table 6.3 Validation of experimental and CFD result of ejector with mixing chamber throat diameter of 19 mm

Primary nozzle	Mixing Chamber	Boiler Temp.	Entrainment Ratio		% error	Critical condenser pressure		% error
			Exp.	CFD		Exp.	CFD	
D2.0	CPM19	115	0.4	0.47	17.50	32	30	6.25
		120	0.36	0.39	8.33	36	36	0.00
		125	0.3	0.34	13.33	42	40	4.76
		130	0.25	0.29	16.00	48	42	12.50
	CRMC19	115	0.45	0.54	20.00	32	32	0.00
		120	0.39	0.47	20.51	36	36	0.00
		125	0.33	0.4	21.21	42	40	4.76
		130	0.31	0.35	12.90	46	44	4.35
D2.4	CPM19	115	0.296	0.33	11.49	44	42	4.55
		120	0.235	0.26	10.64	52	50	3.85
		125	0.18	0.21	16.67	60	59	1.67
		130	0.143	0.16	11.89	68	62	8.82
	CRMC19	115	0.299	0.34	13.71	43	40	6.98
		120	0.254	0.27	6.30	51	46	9.80
		125	0.219	0.24	9.59	58	53	8.62
		130	0.211	0.2	5.21	67	64	4.48
Average % error					13.46			5.09

*% error = 100× (CFD result-experimental result)/ experimental result

The validation has shown that the CFD simulation developed in this present work (both CPM and CRMC ejectors) is implemented accurately because the CFD results predicted by CFD simulation provide a small error compared to the experimental results. However, some errors found during the investigation may come from the following reasons.

- Using an ideal gas assumption to estimate the density of working fluid (steam), it might not be completed. To avoid this problem, the real gas assumption should be applied to the CFD modelling. However, the real gas model usually consists of a very complicated mathematical model which requires a much longer time for simulation. Moreover, in some working conditions where there is a very strong adverse pressure gradient, simulation cannot reach a convergence criteria. This is due to the complexity of the mathematical models. However, it has been proven by some researchers (Ruangtrakoon et al., 2013; Sriveerakul et al., 2007a) that using the ideal gas assumption to simulate the flow inside the steam ejector provides results very close to using the real gas assumption.
- Using the adiabatic wall assumption is one of the causes of prediction error. This is because an adiabatic wall is not possible for the practical use in which there is no heat loss at any ejector's wall surface. However, it has been proven that for the compressible fluid flowing through the conical duct, heat loss at the wall surface has less impact on the flow properties and, therefore, it can be assumed for CFD simulation modelling.
- Using a smooth surface for the internal wall to minimize the friction is also one of the causes of error for ejector performance prediction. It is well known that it is not possible for any surface to be frictionless, even though the internal walls of the experimental ejectors were precisely manufactured. Consequently, it has less impact on the ejector performance's prediction.

The validation has shown that the CFD modelling based on the criteria provided in previous section was developed correctly. Therefore, the flow physics occurring inside the ejector based on the graphical contour, which can be determined from simulation results, can be later used to assess the performance improvement via the CRMC ejector as compared to the CPM ejector.

6.3 CFD result

Since the mixing chambers used in these experiments were produced from transparent casted resin, it was possible to visualize the processes inside. From sight observation of the mixing process within CRMC ejector's mixing chamber as shown in figure 6.5, it was found that there was a condensation ring (condensation shock) of the mixed fluid formed inside. This condensation ring is believed to be a result of a sudden change in static pressure and temperature due to the shock wave taking place (Ben-Dor et al., 2000). These condensation rings (as a result of the condensation shock wave) were always observed from both CPM and CRMC ejectors. It can be said that the compression shock wave is always found in both design methods. However, further study of the behaviour of the fluid flow inside CRMC ejector is needed to verify this hypothesis.

As explained earlier, the ejector based on the CRMC method has proven that a shock wave still exists which is similar to that designed based on the CPM method. Hence, the key improvement of the entrainment ratio via the CRMC ejector does not come from the complete elimination of the shock wave as intended by the design concept. When comparing the CPM ejectors with the CRMC ejectors under the same ejector area ratio, the major improvement via the CRMC ejector was the improvement of the entrainment performance while the critical condenser pressure remains very similar. Dong et al. (2020) and Ariafar et al. (2014) stated that the shear-mixing layer development is a key to produce different secondary mass flow rate. Herein, the primary jet stream is believed to be the significant parameter to create the shear-mixing process. When the boiler temperature and the primary nozzle used are identical for a particular comparison, at the nozzle exit of the two ejectors the primary stream momentums are similar. This means there are other parameters which are key to produce different entrained rates.

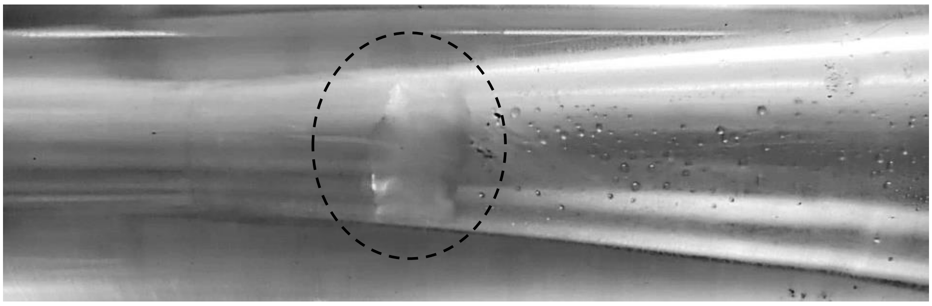

Figure 6.5 Condensation ring of water inside the mixing chamber

To support the above explanation, Computational Fluid Dynamics (CFD) simulation was also implemented. From the CFD simulation, the typical graphical contours of the Mach numbers of CRMC ejector are shown in figure 6.6. The fill contour of Mach number of the CRMC ejector is similar to that of the CPM ejector (figure 2.5). This indicates that the shock wave might also be present in the CRMC ejector. This can clearly be seen when the two ejectors under identical working condition are compared as shown in figure 6.7. The mixing chambers are CPM19 and CRMC19 and the primary nozzle is D2.0. The working conditions of both CPM and CRMC are identical at the boiler temperature of 130°C, evaporator temperature of 7.5°C, and critical condenser pressure of 28 mbar. At this working condition, the ejectors operate at a choke flow condition.

It can be seen from figures 6.7a and 6.7b that the compression shock wave is still found in both ejectors. The appearance of the shock wave of the two ejectors can be indicated by the plots of the static pressure along the ejector's axis as depicted in figure 6.7c. It is seen from figure 6.7c that the position where the static pressure change suddenly is found in both ejectors as indicated by point a and b in figure 6.7c. A sudden change in the static pressure within the short distance means the shock wave is occurring. This can confirm that the shock wave is still found in both ejectors which agrees with the photograph taken from the experiment (figure 6.5) and the fill contour of the Mach number (figure 6.6).

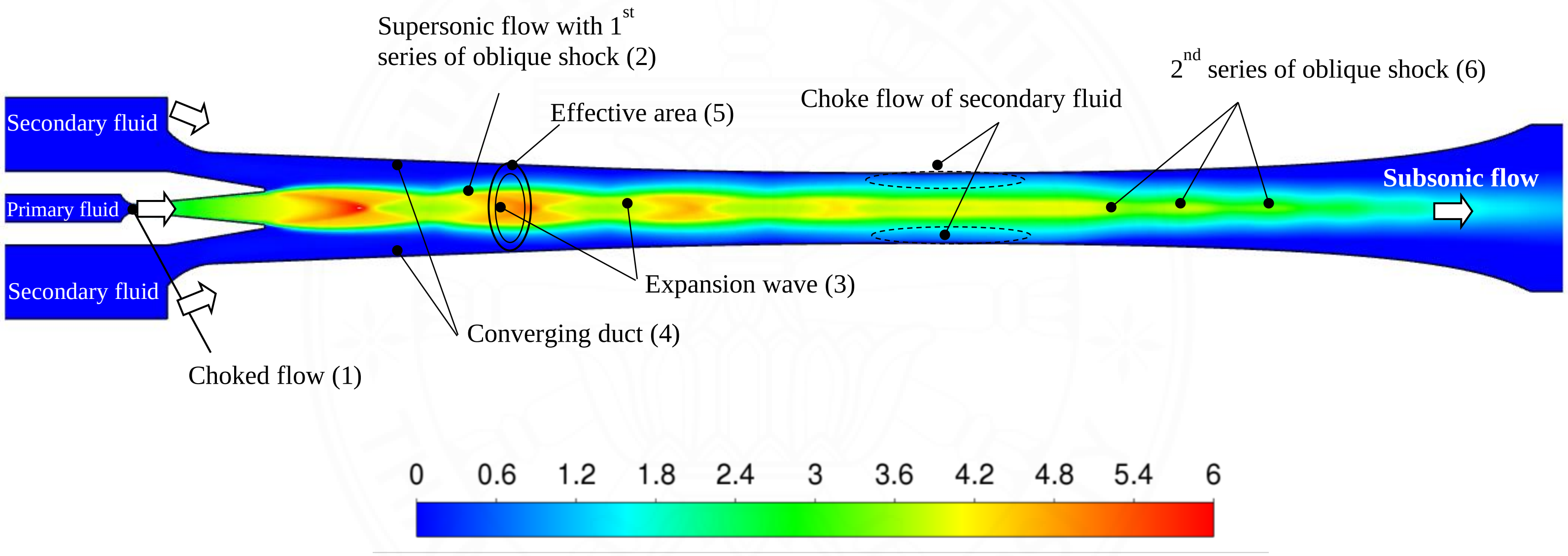

Figure 6.6 The typical filled contour of Mach number of the CRMC ejector

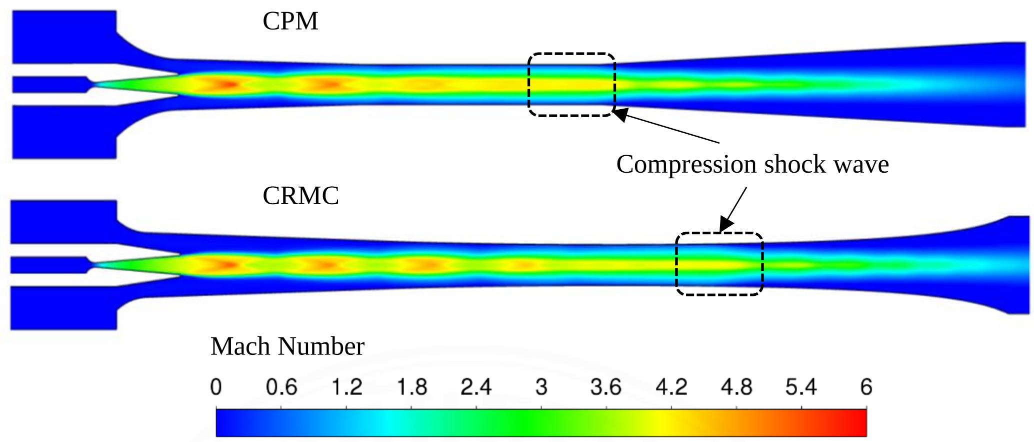

a) The contour of Mach number

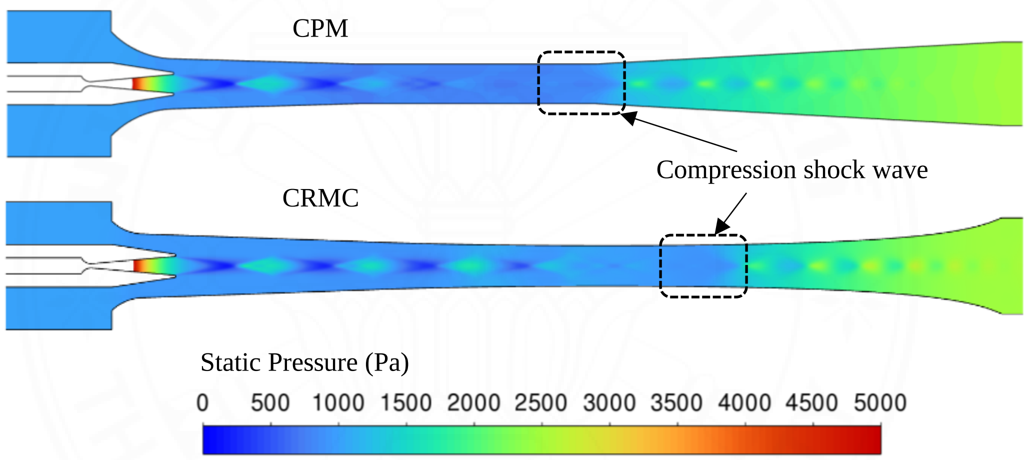

b) The contour of static pressure

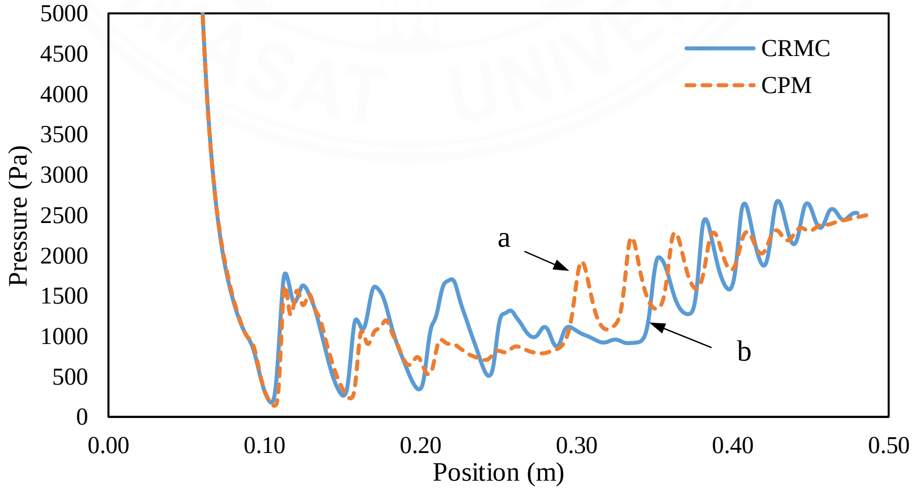

c) Static pressure along ejector axis

Figure 6.7 CFD results based on the CPM and CRMC ejector

To provide more explanation for performance improvement via the CRMC ejector, the contour of Mach number for the primary fluid's e jet core (expansion wave) is later used to discuss as shown in figure 6.8. The mixing chambers are CPM19 and CRMC19 with the primary nozzle D2.0. The working condition is at boiler temperature of 130°C, evaporator temperature of 7.5°C, and condenser pressure of 28 mbar. This can indicate the sonic and supersonic zone throughout the ejectors which is useful for indicating the shear-mixing layer development. It can be seen from figure 6.8 that the first loops of the expansion wave of the CRMC and CPM ejectors are similar since the primary fluid working conditions of the two ejectors are similar. It is obvious that for the CRMC ejector, the shear mixing layer and the mixing length are longer than that for the CPM ejector. This means that velocity of the jet stream at the same distance of the two ejectors is different. The primary stream velocity of the CRMC ejector is higher than that of the CPM ejector. This is because a primary momentum loss is reduced which causes a longer mixing length (or longer jet core). Thus, the CRMC ejector has a higher potential to entrain more secondary fluid. It is interesting that even if the total mass flow rate (primary and secondary fluid) of the mixed fluid stream produced by the CRMC ejector is higher, its mixing length is still longer than the CPM ejector which is normally shorter as proposed by several researchers based on the CPM ejector (Ruangtrakoon et al., 2013; Sriveerakul et al., 2007b). A longer mixing length yields a longer contact area between the two fluid streams which results in producing a higher shear force. This results in producing a higher secondary fluid entrained rate.

Figure 6.9 shows the contour of primary fluid jet core Mach number at various boiler temperatures. It is also seen from the contour in figure 6.9 that a series of the expansion wave formed inside the CRMC ejector begins to be different from that formed inside the CPM ejector when the shear-mixing layer is developed for a certain distance from the nozzle's exit. More interestingly, it is also seen that the difference in the series of the expansion wave between the two ejectors is more obvious when the boiler temperature is increased. This indicates that an ability to produce a lower primary momentum loss of the CRMC ejector is more obvious at a quite high boiler temperature.

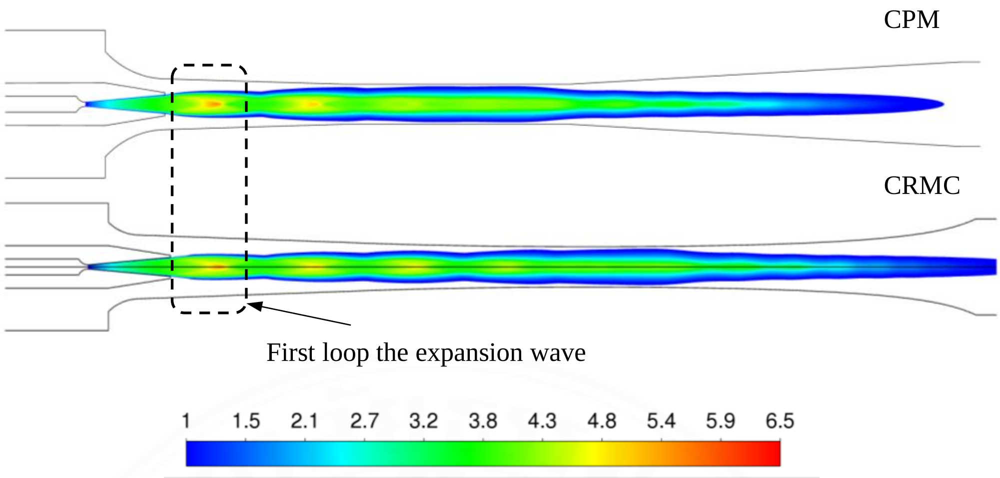

Figure 6.8 The graphic contour of Mach number representing the flow inside of the CRMC and CPM ejector under the same working condition

Figure 6.10 shows the path line of the fluid flow inside the ejector. It can be seen that the flow separation (represent by the green zone) occurs for both the CPM and the CRMC ejector. Flow separation for the CPM ejector at boiler temperature 115°C to 125°C is represented by free space between the ejector wall and the secondary fluid path line. The flow separation occurs when the flow of the boundary layer relative to the wall surface has stopped and reversed direction. The flow separation of the CPM ejector occurs at the position at which the flow leaves the constant area section (mixing chamber's throat) and enters the diverging duct section (subsonic diffuser). The separation points of the CPM ejector are all the same at this position. This indicates that the flow separation of the CPM ejector is due to the widening of the flow area at the sub sonic diffuser which creates an adverse pressure gradient. This results in momentum loss of the flow inside the ejector. On the other hand, for the CRMC ejector, the flow separation also occurs, but the separation points are further away from the primary nozzle. It might be said that the CRMC design can delay the separation which results in less momentum loss and higher entrainment ratio.

As the boiler temperature increases, the flow separation of CPM is larger; this might be caused by a higher flow velocity. This might explain the phenomenon at which the secondary mass flow rate of the CPM ejector decreases with higher boiler temperature as shown in figure 5.7. The larger separation region causes more loss which results in lower entrainment ratio. In contrast, for the CRMC ejector, the flow separation occurs mainly at the ejector outlet (subsonic diffuser outlet). The separation point moves upstream as the boiler temperature is increased from 115 to 135°C. Since the flow separation is reduced, the reduction of momentum loss is less. This might be the reason that the secondary fluid entrainment rate of the CRMC ejector becomes higher as the boiler temperature increases as shown in figure 5.7.

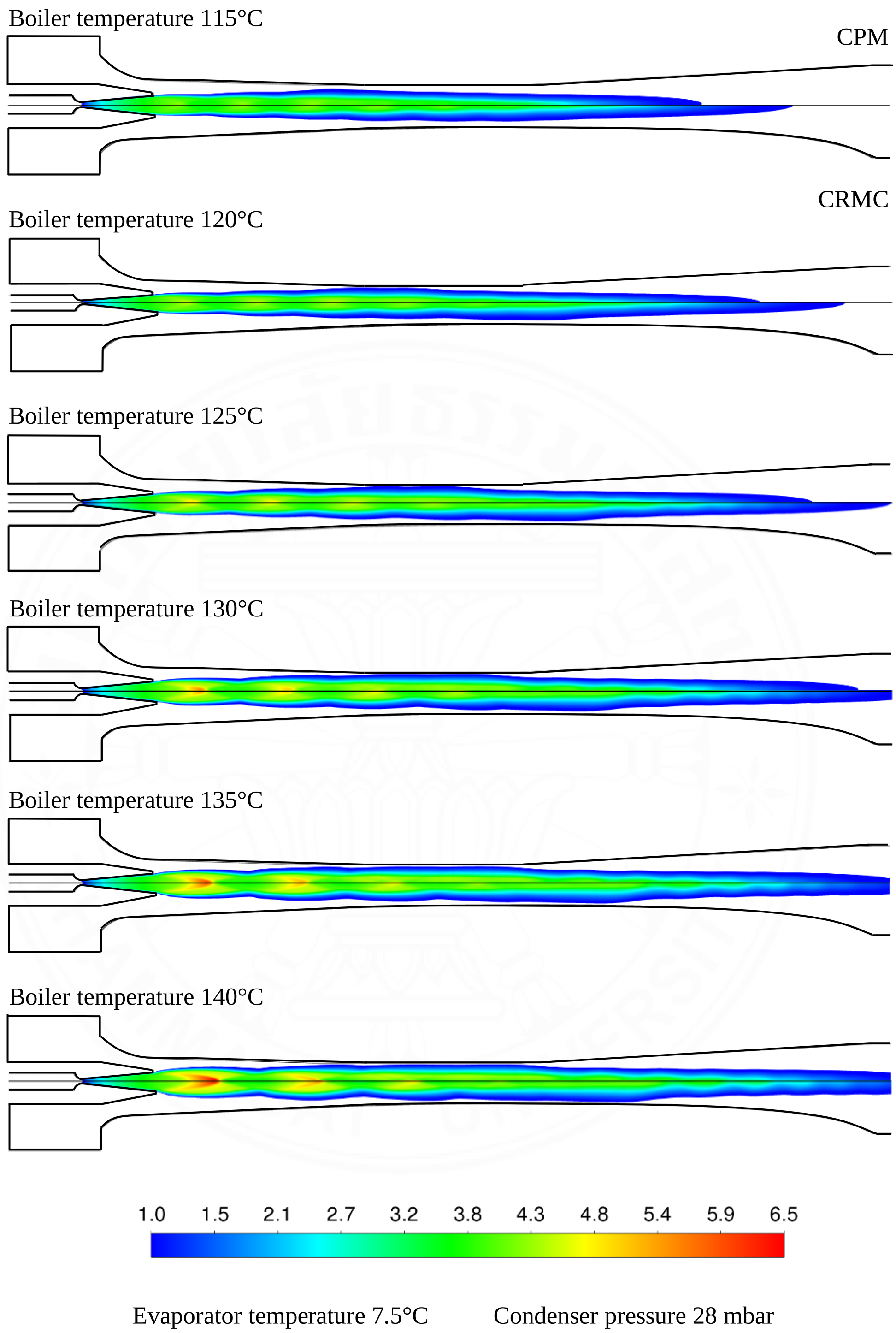

Figure 6.9 The graphic contour of Mach number representing the flow inside CRMC and CPM ejectors under different boiler saturation temperatures

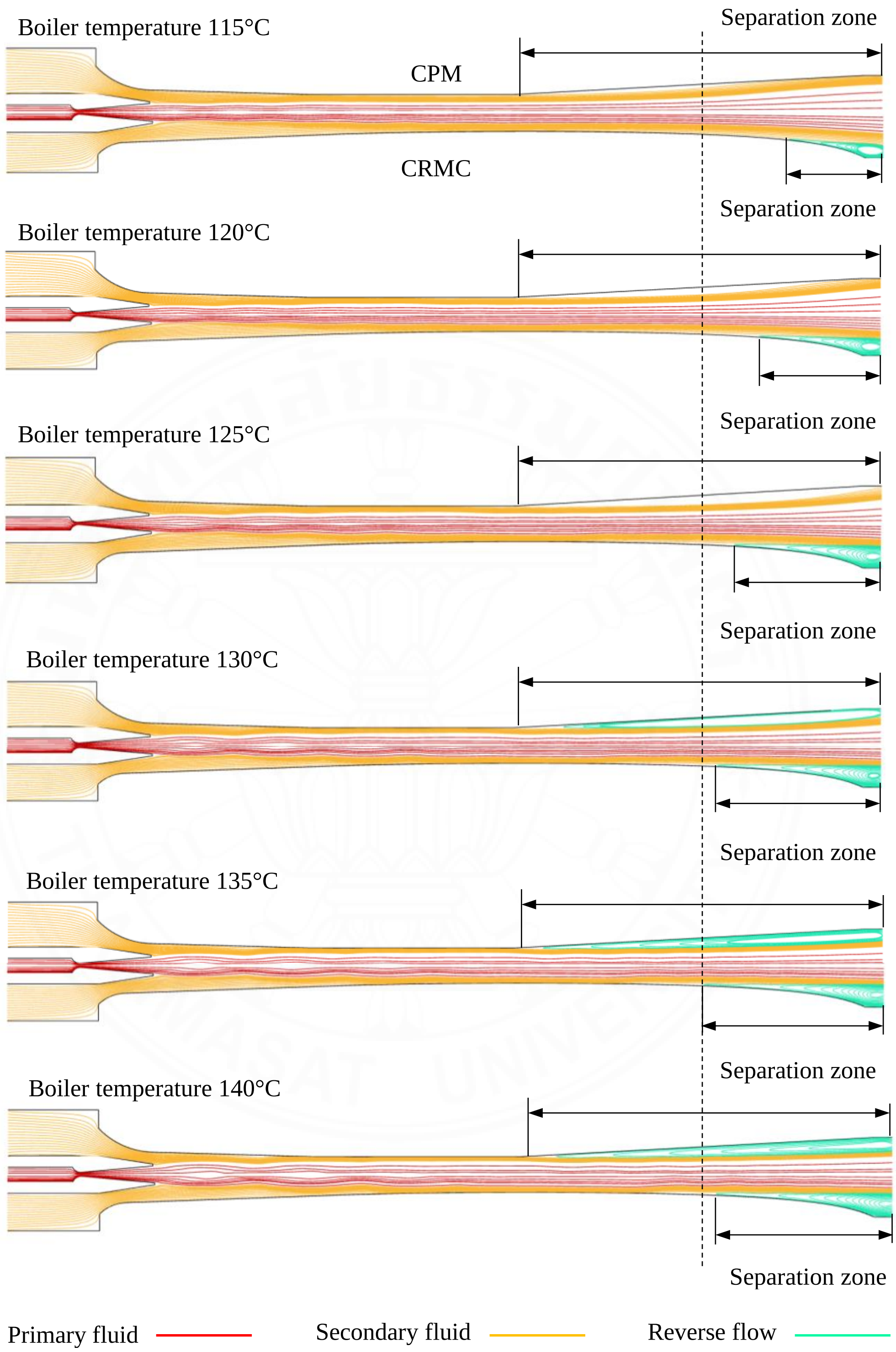

Figure 6.10 The graphic path line representing the flow inside CRMC and CPM ejectors under different boiler saturation temperatures

6.4 Conclusion

In this chapter, the CFD simulation setup developed was applied to simulate the flow behaviour inside the steam ejector. The strategy to develop the CFD model was presented. The criteria to create the physical model with grid elements (calculation domain) was explained. The solver setup and the method to define the mathematical models for CFD modelling were proposed. The simulated CFD results were compared with the experimental results for validation. The CFD results showed good agreement with the experimental results with the average percentage error of approximately 13% for the entrainment ratio and approximately 6% for the critical condenser pressure. This shows that the CFD simulated technique could be used for predicting the performance and the flow phenomenon inside the ejector.

Then by using the CFD technique, the filled contour of Mach number and the flow path line along with the plot of pressure inside the ejector were used to analyse and explain the process inside the mixing chamber of both the CPM and the CRMC ejectors. The shock wave was still present in the CRMC ejector which is opposite to that suggested in theory. The main reason of improvement of the CRMC ejector was due to the less momentum loss of the flow. For the CPM ejector, at the subsonic diffuser inlet where the flow area changes from a constant area duct to a diverging duct, flow separation was found. The flow separation causes the momentum loss and leads to lower entrainment ratio. It is thought that the flow separation might be the key parameter that causes the CRMC ejector to be superior over the CPM ejector.

CHAPTER 7
CONCLUSION

The main aim of this dissertation was to provide performance comparison between the conventional CPM ejectors and the CRMC ejectors on performance of steam ejector refrigeration system. The experimental steam ejector refrigerator with maximum cooling capacity of 1 kW, was designed, constructed, and tested. The CPM and CRMC ejectors were tested and compared at various operating conditions with mainly identical ejector area ratio.

Four mixing chambers, CPM13.4, CRMC13.4, CPM19 and CRMC19, were used. Mixing chambers CPM13.4 and CRMC 13.4 had throat diameters of 13.4 mm, and CPM19 and CRMC19 had throat diameters of 19 mm. Four primary nozzles, D1.4, D1.7, D2.0 and D2.4, were used. The CPM and CRMC ejectors were tested and compared on the steam ejector refrigerator under various working conditions. The boiler saturation temperatures were 115 to 130°C. The evaporator saturation temperatures were 5 to 10°C. The experimental results were discussed. CFD analysis was also employed. The simulation results provided useful explanations.

At first, the CPM and CRMC ejectors were designed with the same boiler and evaporator saturation temperature. They used the same primary nozzle. The mixing chamber of the CRMC ejector had throat diameter of 13.4 mm (CRMC13.4) while the CPM ejector had throat diameter of 19.0 mm (CPM19). Therefore, they had different ejector area ratios. The test results showed that the CRMC ejector provided a lower mass entrainment ratio but with a higher critical condenser pressure. This is very normal when two ejectors with different area ratios are compared. This cannot be used to prove that the CRMC ejector is better. To say which ejector is better, the mass entrainment ratio or the critical condenser must be higher while the other remains the same or both increase. For this reason, the CPM and CRMC ejector must be tested when the same area ratio.

Four CPM ejectors and four CRMC ejectors were tested. The area ratios were 91.61 and 62.13. When the two ejectors (CPM and CMC) were tested with the same area ratio, they always provided very similar critical condenser pressure. However, the CRMC always provided higher mass entrainment ratio with average value of around

19%. The improvement ranged from 0 to 70% depended on the operating condition. Therefore, it can be said that the CRMC ejector always provided superior performance compared with the CPM ejector.

From the experimental results, the CRMC ejector could improve performance in terms of entrainment ratio with the identical critical condenser pressure when compared with the CPM ejector. This result contrasts with the CRMC theory which aims to eliminate the shock wave inside the mixing chamber. Since the shock wave results in a loss in stagnation pressure, the CRMC ejector should provide an improvement in the critical condenser pressure. Moreover, as the mixing chambers were made from transparent resin, sight observation of the mixing process inside was possible. A condensation shock was found for both ejectors. This indicates that a shock wave was induced in both ejectors.

To clarify the mixing process within both ejectors, CFD analysis was employed. The contour of Mach number, static pressure, and plot of static pressure along the ejector axis showed the evidence of shock waves inside both the CRMC and CPM ejectors. This confirmed that the CRMC design method cannot eliminate the shock wave from the flow process. However, the CRMC still improved a higher entrainment ratio. This can be explained by the contour of Mach number of the primary fluid jet core. It showed that the jet core of the CRMC ejector was longer than the jet core of the CPM ejector. This means less momentum loss for the CRMC ejector.

It was concluded that the CRMC ejector always outperformed the CPM ejector in terms of the mass entrainment ratio while the critical condenser pressure was similar. Shock waves were found in both type of ejectors. This was in contrast to what was proposed by Eames (2002). If the shock was completely eliminated from the CRMC ejector, a much higher critical condenser pressure should be obtained. The results of the studies are summarized as follows:

- The compression shock wave was still found in the flow process of CRMC ejector. This was in contrast to the design theory of the CRMC ejector.

  Hence, there was no improvement in the critical condenser pressure.

- The key improvement via the CRMC was a lower loss in momentum during the mixing process which results in higher potential to draw more secondary entrained rate. This might be due to the curved profile variable area duct CRMC ejector.

- The mass entrainment ratio via the CRMC ejector obtained from experiments was much lower than that obtained from the design theory under the same critical condenser pressure. However, it was always higher than the CPM ejectors.
- It is possible that the CRMC ejector was a CPM ejector with higher mixing chamber efficiency.

The result of this study shows that the CRMC design method can be used to improve the performance of the ejector even though the shock wave is still present in the ejector. The improvement is mainly due to the smooth curved profile. It implies that the conventional 1-D theory can still be used to design the ejector but instead of dividing the mixing chamber into constant area throat and conical diverging duct, the smooth curved profile can be used to reduce loss of the flow. However, the curve used for the mixing chamber profile should be further studied to optimize the performance. With help of the CFD technique, it can be seen that flow separation is present in the CRMC ejector. If this flow separation can be minimized or eliminated, the performance will be better.

REFERENCES

Alsafi, M. (2017). *Constant Rate of Momentum Change Ejector: simulation, experiments and flow visualisation* University of Southern Queensland].

Aphornratana, S. (1995). *Theoretical and experimental investigation of a combined ejector-absorption refrigerator* University of Sheffield, Department of Mechanical and Process Engineering].

Aphornratana, S., & Eames, I. W. (1997). A small capacity steam-ejector refrigerator: experimental investigation of a system using ejector with movable primary nozzle. *International journal of refrigeration*, *20*(5), 352-358.

Ariafar, K., Buttsworth, D., Sharifi, N., & Malpress, R. (2014). Ejector primary nozzle steam condensation: Area ratio effects and mixing layer development. *Applied thermal engineering*, *71*(1), 519-527.

Ben-Dor, G., Igra, O., & Elperin, T. (2000). *Handbook of shock waves, three volume set*. Elsevier.

Besagni, G., Cristiani, N., Croci, L., Guédon, G. R., & Inzoli, F. (2021). Computational fluid-dynamics modelling of supersonic ejectors: Screening of modelling approaches, comprehensive validation and assessment of ejector component efficiencies. *Applied thermal engineering*, *186*, 116431.

Besagni, G., & Inzoli, F. (2017). Computational fluid-dynamics modeling of supersonic ejectors: Screening of turbulence modeling approaches. *Applied thermal engineering*, *117*, 122-144.

Besagni, G., Mereu, R., Chiesa, P., & Inzoli, F. (2015). An Integrated Lumped Parameter-CFD approach for off-design ejector performance evaluation. *Energy Conversion and Management*, *105*, 697-715.

Bian, Q. (2020). Waste heat: the dominating root cause of current global warming. *Environmental Systems Research*, *9*(1), 1-11.

Bumrungthaichaichan, E., Ruangtrakoon, N., & Thongtip, T. (2022). Performance investigation for CRMC and CPM ejectors applied in refrigeration under equivalent ejector geometry by CFD simulation. *Energy Reports*, *8*, 12598-12617. https://doi.org/https://doi.org/10.1016/j.egyr.2022.09.042

Çengel, Y. A., & Boles, M. A. (1994). *Property Tables, Figures, and Charts to Accompany Thermodynamics: An Engineering Approarch*. McGraw-Hill.

Chandra, V. V., & Ahmed, M. R. (2014). Experimental and computational studies on a steam jet refrigeration system with constant area and variable area ejectors. *Energy Conversion and Management*, *79*, 377-386.

Chen, J., Havtun, H., & Palm, B. (2014). Investigation of ejectors in refrigeration system: Optimum performance evaluation and ejector area ratios perspectives. *Applied thermal engineering*, *64*(1-2), 182-191.

Chunnanond, K., & Aphornratana, S. (2004). An experimental investigation of a steam ejector refrigerator: the analysis of the pressure profile along the ejector. *Applied thermal engineering*, *24*(2-3), 311-322.

Dong, J., Hu, Q., Yu, M., Han, Z., Cui, W., Liang, D., Ma, H., & Pan, X. (2020). Numerical investigation on the influence of mixing chamber length on steam ejector performance. *Applied thermal engineering*, *174*, 115204.

Eames, I., Aphornratana, S., & Haider, H. (1995). A theoretical and experimental study of a small-scale steam jet refrigerator. *International journal of refrigeration*, *18*(6), 378-386.

Eames, I., Wu, S., Worall, M., & Aphornratana, S. (1999). An experimental investigation of steam ejectors for applications in jet-pump refrigerators powered by low-grade heat. *Proceedings of the Institution of Mechanical Engineers, Part A: Journal of Power and Energy*, *213*(5), 351-361.

Eames, I. W. (2002). A new prescription for the design of supersonic jet-pumps: the constant rate of momentum change method. *Applied thermal engineering*, *22*(2), 121-131.

Eames, I. W., Milazzo, A., Paganini, D., & Livi, M. (2013). The design, manufacture and testing of a jet-pump chiller for air conditioning and industrial application. *Applied thermal engineering*, *58*(1-2), 234-240.

Elbel, S., & Hrnjak, P. (2008). Experimental validation of a prototype ejector designed to reduce throttling losses encountered in transcritical R744 system operation. *International journal of refrigeration*, *31*(3), 411-422.

Fluent, A. (2011). Fluent 14.0 user's guide. *Ansys Fluent Inc*.

Flügel, G. (1941). *The Design of Jet Pumps*.

Hoggarth, M. (1970). The design and performance of high-pressure injectors as gas jet boosters. *Proceedings of the Institution of Mechanical Engineers*, *185*(1), 755-766.

Huang, B., Chang, J., Wang, C., & Petrenko, V. (1999). A 1-D analysis of ejector performance. *International journal of refrigeration*, *22*(5), 354-364.

Keenan, J., & Neumann, E. (1942). A simple air ejector.

Keenan, J., Neumann, E., & Lustwerk, P. (1950). An investigation of ejector design by analysis and experiment.

Kranakis, E. F. (1982). The French connection: Giffard's injector and the nature of heat. *Technology and Culture*, *23*(1), 3-38.

Kumar, V., Singhal, G., & Subbarao, P. (2013). Study of supersonic flow in a constant rate of momentum change (CRMC) ejector with frictional effects. *Applied thermal engineering*, *60*(1-2), 61-71.

Liu, J., Wang, L., Jia, L., & Wang, X. (2017). The influence of the area ratio on ejector efficiencies in the MED-TVC desalination system. *Desalination*, *413*, 168-175.

Macintire, H. J., & Hutchinson, F. W. (1950). *Refrigeration engineering*. Wiley.

Mazzelli, F., & Milazzo, A. (2015). Performance analysis of a supersonic ejector cycle working with R245fa. *International journal of refrigeration*, *49*, 79-92.

Milazzo, A., Rocchetti, A., & Eames, I. W. (2014). Theoretical and experimental activity on ejector refrigeration. *Energy Procedia*, *45*, 1245-1254.

Munday, J. T., & Bagster, D. F. (1977). A new ejector theory applied to steam jet refrigeration. *Industrial & Engineering Chemistry Process Design and Development*, *16*(4), 442-449.

Pianthong, K., Seehanam, W., Behnia, M., Sriveerakul, T., & Aphornratana, S. (2007). Investigation and improvement of ejector refrigeration system using computational fluid dynamics technique. *Energy Conversion and Management*, *48*(9), 2556-2564.

Ruangtrakoon, N., & Aphornratana, S. (2019). Design of steam ejector in a refrigeration application based on thermodynamic performance analysis. *Sustainable Energy Technologies and Assessments*, *31*, 369-382.

Ruangtrakoon, N., Aphornratana, S., & Sriveerakul, T. (2011). Experimental studies of a steam jet refrigeration cycle: effect of the primary nozzle geometries to system performance. *Experimental thermal and fluid science*, *35*(4), 676-683.

Ruangtrakoon, N., Thongtip, T., Aphornratana, S., & Sriveerakul, T. (2013). CFD simulation on the effect of primary nozzle geometries for a steam ejector in refrigeration cycle. *International Journal of Thermal Sciences*, *63*, 133-145.

Shigeru, M., Kousuke, K., Junji, N., Md Tawhidul Islam, K., Toshiaki, S., & Heuy Dong, K. (2012). Effects of supersonic nozzle geometry on characteristics of shock wave structure. *Open Journal of Fluid Dynamics*, *2012*.

Sriveerakul, T., Aphornratana, S., & Chunnanond, K. (2007a). Performance prediction of steam ejector using computational fluid dynamics: Part 1. Validation of the CFD results. *International Journal of Thermal Sciences*, *46*(8), 812-822.

Sriveerakul, T., Aphornratana, S., & Chunnanond, K. (2007b). Performance prediction of steam ejector using computational fluid dynamics: Part 2. Flow structure of a steam ejector influenced by operating pressures and geometries. *International Journal of Thermal Sciences*, *46*(8), 823-833.

Thongtip, T., & Aphornratana, S. (2021). Impact of primary nozzle area ratio on the performance of ejector refrigeration system. *Applied thermal engineering*, *188*, 116523.

Worall, M. (2001). *An investigation of a jet-pump thermal (ice) storage system powered by low-grade heat* University of Nottingham].

Yapıcı, R., Ersoy, H., Aktoprakoğlu, A., Halkacı, H., & Yiğit, O. (2008). Experimental determination of the optimum performance of ejector refrigeration system depending on ejector area ratio. *International journal of refrigeration*, *31*(7), 1183-1189.

BIOGRAPHY

Name Borirak Kitrattana

Education 2015: Bachelor of Engineering (Mechanical Engineering)
Sirindhorn International Institute of Technology
Thammasat University
2017: Master of Science (Engineering and Technology)
Sirindhorn International Institute of Technology
Thammasat University

Publications

Kitrattana, B., Aphornratana, S., & Thongtip, T. (2021). One dimensional steam ejector model based on real fluid property. *Thermal Science and Engineering Progress*, *25*, 101016.

Kitrattana, B., Aphornratana, S., Thongtip, T., & Ruangtrakoon, N. (2017). Comparison of traditional and CRMC ejector performance used in a steam ejector refrigeration. *Energy Procedia*, *138*, 476-481.

Kitrattana, B., Aphornratana, S., & Thongtip, T. (2017). The performance of steam ejector refrigeration system based on alternative analysis. Energy Procedia, 138, 482-487.